Golder Associates Ltd.

7017 Farrell Road S.E.
Calgary, Alberta, Canada T2H 0T3
Telephone (403) 259-3413
Fax (403) 252-4884

Golder Associates

TITLE:
LABORATORY SIMULATION AND CONSTITUTIVE BEHAVIOUR FOR HYDRAULIC FRACTURE PROPAGATION IN OIL SANDS

Part of Energy, Mines and Resources Cost-Shared Energy Conversion Program and Part of the Program of the Federal Panel on Energy Research & Development (PERD)

Final Report
(Phase 2)

Work on the project was conducted under the auspices of the Canada Centre for Mineral and Energy Technology, Energy, Mines and Resources Canada.

SSC FILE No.: 06SQ.23440-1-9035
CONTRACT FILE No.: 23440-1-9035/01-SQ
CANMET SCIENTIFIC AUTHORITY: Dr. A.E.D. GEORGE

Distribution:
- 3 copies - Canada Centre for Mineral and Energy Technology (CANMET), Ottawa, Ontario
- 2 copies - Esso Resources Canada Ltd., Calgary, Alberta
- 2 copies - Shell Canada Ltd., Calgary, Alberta
- 2 copies - Alberta Oil Sands Technology and Research Authority (AOSTRA), Calgary, Alberta
- 2 copies - Golder Associates Ltd., Calgary, Alberta

MICROMEDIA

145 pp

June, 1992 **912-2055**

TABLE OF CONTENTS

EXECUTIVE SUMMARY i

SOMMAIRE EXCUTIF ii

1.0 INTRODUCTION 1
1.1 Background 1
1.2 Review of Phase 1 Work 2
1.2.1 Characteristics of Phase 1 Test Materials 2
1.2.2 Large Scale Fracture Tests 3
1.3 Objectives of the Phase 2 Study 5
1.4 Project Funding 6

2.0 TEST MATERIALS, EQUIPMENT AND PROCEDURES 7
2.1 Test Materials 7
2.2 Test Equipment 8
2.3 Sample Preparation 10
2.4 Test Procedures 11
2.5 Sample Excavation and Sampling 14

3.0 FRACTURE TESTS 16
3.1 Fracture Test No. 1 16
3.2 Fracture Test No. 2 18
3.3 Fracture Test No. 3 20
3.4 Fracture Test No. 4 22
3.5 Fracture Test No. 5 23

4.0 NUMERICAL SIMULATION OF FRACTURE TESTS 25
4.1 Method of Analysis 25
4.2 Modelling Procedure 26
4.3 Discussion of Results 29

5.0 ASSOCIATED TESTS 31
5.1 Interpretation of Pore Pressure Parameter B Tests 31
5.2 Magnetic Resonance Imaging 32

6.0 DISCUSSION 34

7.0 CONCLUSIONS AND RECOMMENDATIONS 38

TABLE OF CONTENTS

LIST OF TABLES

3.1 - Summary of Hydraulic Fracture Test Program (Phase 1 and 2)
3.2 - Results of Hydraulic Fracture Test Program (Phase 1 and 2)

LIST OF FIGURES

2.1 - Large Triaxial Stress Chamber
2.2 - Pressure Control Board
2.3 - Cross Section of Injection Well at Mid-Height of Sample
2.4 - Constant Flow Pump
2.5 - Injection Well Detail
2.6 - Photograph of Large Triaxial Chamber
2.7 - Pluviation of Sand Into Stress Chamber
2.8 - Instrumentation Detail for Fracture Simulations
3.1 - Fracture Test No. 2 - Sample Dimensions
3.2 - Fracture Test No. 2 - Response of Fluid Pressure Transducers
3.3 - Fracture Test No. 2 - Pattern of Fluorescent Dye in Sample
3.4 - Fracture Test No. 3 - Sample Dimensions
3.5 - Fracture Test No. 3 - Response of Fluid Pressure Transducers
3.6 - Fracture Test No. 3 - Pattern of Fluorescent Dye in Sample
3.7 - Fracture Test No. 4 - Sample Dimensions
3.8 - Fracture Test No. 4 - Response of Fluid Pressure Transducers
3.9 - Fracture Test No. 4 - Pattern of Fluorescent Dye in Sample
3.10- Fracture Test No. 5 - Sample Dimensions
3.11- Fracture Test No. 5 - Response of Fluid Pressure Transducers
3.12- Fracture Test No. 5 - Pattern of Fluorescent Dye in Sample
4.1 - Finite Difference Grid
4.2 - Locations for Monitoring Pore Pressure Development
4.3 - Plot of Maximum Unbalanced Nodal Force Against Time Step
4.4 - Extent of Yielding at End of Fluid Injection
4.5 - Distribution of Pore Pressures at End of Fluid Injection
4.6 - Displacement Vectors at End of Fluid Injection
4.7 - Principal Stress Vectors at End of Fluid Injection
4.8 - Extent of Yielding at End of Numerical Simulation
4.9 - Distribution of Fluorescent Dye in Laboratory Sample
4.10- Plot of Pore Pressure Development (Numerical versus Laboratory)
5.1 - Location of Samples for MRI
5.2 - MRI Imaging Sections
5.3 - MRI of Sample 2Frac3-6
5.4 - MRI of Sample 2Frac3-10
5.5 - MRI of Sample 2Frac4-1

TABLE OF CONTENTS

LIST OF APPENDICES

I - Permeability Tests
II - Sub-Fracture Pressure Injection Tests
III - Steady State Fracture Tests
IV - Data File Used In Numerical Simulation

EXECUTIVE SUMMARY

The bitumen contained within the oil sands reservoirs of Alberta is highly viscous and will not flow readily at formation temperatures. Bitumen production from deeply buried oil sands formations requires mobilizing the bitumen by in situ stimulation techniques. The most common method for reducing the viscosity of the bitumen so it can be pumped to the surface involves injecting pressurized steam into the reservoir. The flow of the steam into the reservoir is inhibited by the low permeability of the oil sands formation. In order to achieve economic injection rates the formation must fracture or fail.

The mechanics of hydraulic fracture in oil sands reservoirs is complicated by highly non-linear and inelastic geotechnical behaviour exhibited by unconsolidated clastic sediments. A significant obstacle to the development and use of fracture models has been the lack of reliable verification data. Verification data is normally inferred from in situ tests. However, the boundary conditions in field tests are not well defined because the in situ stress field is unknown and the geology may be complex. Spatial variations in mechanical, physical and thermal properties of the geological strata may occur over the length of a fracture. Due to these uncertainties, field results alone are not adequate to evaluate a fracture model.

This report documents the second phase of a joint industry laboratory testing project carried out to enhance the mathematical formulations of models by providing data to calibrate and verify the models currently employed for fracture analysis. The design of the testing was to study the propagation of leak off dominated fractures. A series of laboratory injection simulations on homogeneous sand were carried out in a large triaxial stress chamber. The test sand was saturated with a highly viscous liquid, and injected with the same liquid, but dyed for differentiation. Single phase fluid flow models can therefore be used for analysis of the test data. Constant pressure (below the minimum effective confining stress applied to the sample) injectivity tests, permeability tests as well as steady state fracture tests (sample injected with "undyed" liquid at constant flow rate) were carried out prior to the fracture tests. Specimens taken from the large scale fracture sample were examined using Magnetic Resonance Imaging to study the pattern of fracture in more detail.

The results of the testing have demonstrated that the manner in which the fluid is transported through the sample depends on the injection rate and boundary conditions. The data appears to indicate that shear failure occurred at the injection rates used in the laboratory program. Numerical simulation of one of the fracture tests gave a close match to the laboratory results. This analysis also indicates the behaviour of the sample is consistent with shear deformations and failure during injection. This report provides recommendations regarding future testing to further delineate failure mechanisms associated with hydraulic fracture of uncemented sands.

SOMMAIRE EXÉCUTIF

Le bitume contenu dans les dépôts de sable bitumineux de l'Alberta est hautement visqueux et ne s'écoulera pas de lui-même à la température ambiante des formations. La production de bitume de formations profondes de sable bitumineux requirt une mise en circulation du bitume par des techniques de stimulation in situ. La méthode la plus commune pour réduire la viscosité du bitume, de façon à ce qu'il puisse être pompé vers la surface, implique l'injection de vapeur à haute pression dans le dépôt. L'écoulement de la vapeur dans le réservoir est contré par la faible perméabilité de la formation de sable bitumineux. De façon à obtenir des taux d'injection qui soient économiques, la formation doit être fracturée.

Le processus de fracturation hydraulique dans les dépôts de sable bitumineux est rendu plus complexe par le comportement géotechnique hautement non-linéaire et inélastique, propre aux sédiments détritiques non consolidés. Un obstacle de taille au developpement et à l'usage de modèles de fracturation fut le manque de données fiables pour opérer leur vérification. Les données de vérification sont généralement déduites des essais in situ. Cependant les conditions limites des essais de chantier ne sont pas très bien définies puisque le champ de contraintes en place demeure inconnu et que la géologie du site peut être complexe. Des variations spatiales dans les propriétés mécaniques, physiques et thermales des horizons stratigraphiques peuvent se produire le long d'une fracture donnée. Suite à ces incertitudes, les résultats de chantier à eux seuls ne sont pas suffisants pour évaluer un modèle de fracturation.

Ce rapport présente les résultats de la duexieme phase d'un projet conjoint entre l`industrie et un laboratoire d`essîi, destiné à supporter les formulations mathématiques de modèles, en fournissant des données permettant de calibrer et de vérifier les modèles actuellement utilisés dans le cas de la fracturation hydraulique. Le but du programme d`essai consistait en l`étude de la propagation de fractures avec dmoninance de perte de fluide. Une série de simulations d`injection en laboratoire, réalisées sur un sable homogène, ont été effectuées dans une enceinte triaxiale de grandes dimensions. La sable utilisé a été saturé avec un liquide à haute viscosité et injecté avec le même liquide lequel a été coloré pour fins de différenciation. Des modèles d`écoulement à phase unique pouvaient par conséquent être utilisés pour l`analyse des données d`essai. Des essais d`injection à pression constante (inférieure au niveau de la contrainte de confinement effective minimum appliquée à

l`échantillon), des essais de perméabilité, de même que des essais de fracturation à l`état stable (échantillon injecté avec un liquide incolore selon un débit constant) ont été réalisés avant les essais de fracturation. Des échantillons de sol obtenus de l`essai de fracturation à grande échelle ont été examinés par procédé d imagerie par résonnance magnétique pour évaluer le patron de fracturation de façon détaillée.

Les résultats des essais ont démontré que la façon selon laquelle de fluide migre au sein de l`échantillon dépend du taux d`injection et des conditions limites. Les doninées semblent indiquer qu`une rupture par cisaillement se produit pour la fourchette de taux d`injection considérés dans le programme de laboratoire. Une simulation numérique d`un des essais de fracturation a fourni une bonne correspondance avec des résultats de laboratoire. Cette analyse indique également que le comportement de l`échantillon est consistant avec les déformations et le mode de rupture par cisaillement notés au cours de l`injection. Ce rapport fournit des recommandations touchant de futurs travaux afin de définir d`advantage les mécanismes de rupture associés à la fracturation hydraulique des sables non cimentés.

1.0 INTRODUCTION

1.1 Background

The economical viability of an oil sands reservoir can be directly affected by the ability of the operators to create effective fracture patterns in the reservoir production zone. Fracture design in uncemented reservoirs is a relatively new technology, in the early stages of development. Improvements in hydraulic fracture technology are likely to have significant economic benefit by reducing production costs through such measures as more efficient well patterns and more efficient stimulation procedures.

To fracture an oil sands reservoir, injection fluid is forced rapidly into the oil sands matrix causing individual grains to slide relative to each other to accommodate the induced mechanical strain. These structural changes to the oil sands matrix are generally highly non-linear and inelastic. The associated volume change significantly alters the in situ stress field in the fracture zone and therefore controls the initiation, propagation and orientation of fractures. As a result, the mechanics of hydraulic fracturing in uncemented sands is complex and consideration must be given to the mechanical behaviour of the oil sands.

This report describes the second phase of a project to gain a better understanding of the fundamental mechanisms of fracturing of uncemented sand formations. The project is based on carrying out hydraulic fracturing in a large scale triaxial stress chamber. A laboratory test of this nature allows the major factors controlling the fracture process to be measured or controlled. It is also possible to trace the fracture propagation by careful examination of the specimen after the test. Therefore, such tests provide the necessary information required to develop new mathematical and numerical models, and to validate existing models. Field data for

the same purpose is subject to much larger uncertainties with regard to most of the measurements made.

1.2 Review of Phase 1 Work

Phase 1 of the Joint Industry/CANMET funded project to study hydraulic fracture propagation in oil sands through large scale laboratory tests was carried out over the period of April 1990 to March 1991. The purposes of the Phase 1 study was to provide a preliminary indication of the mechanism of hydraulic fracturing under conditions of high leak off. The results of the Phase 1 work are detailed in a report prepared by Golder Associates Ltd. entitled "Laboratory Simulation and Constitutive Behaviour for Hydraulic Fracture Propagation in Oil Sands - Phase 1" dated July, 1991 (Supply and Services Canada File No. 06SQ.23440-9-9263). The major aspects of the Phase 1 study are summarized below.

1.2.1 Characteristics of Phase 1 Test Materials

Oil sands reservoirs in Alberta are commonly fractured using water or steam. The relatively low viscosity of these fluids leads to formation leak off even at high injection rates. Because the leak off phenomenon in oil sands which contains two separate liquid phases (bitumen and water) is very difficult to model analytically, the Phase 1 program focused on large scale laboratory simulations on samples where the pore and injected fluids were the same.

Calculations based on poroelastic theory were carried out to give a general indication of the effect of fluid and sand properties on the injection rate required to propagate a radial fracture in the triaxial stress chamber. The formulations assumed the volume of fluid stored in the fracture was small relative to the volume of fluid leaked off into the formation. Details of the formulations are given in the

Phase 1 report. On the basis of these calculations, the fluid flow characteristics of the sand and pore/injection liquid were chosen for the fracture tests.

It was important that the sand used in the large scale fracture tests undergo the same geomechanical response as in situ oil sands during fluid injection. Oil sands exhibit high shear dilatancy and post-peak softening behaviour during triaxial compression under the low effective confining stresses such as those associated with hydraulic fracture. Small scale triaxial stress testing indicated that dense, uniform quartz sand samples prepared in the laboratory show very similar behaviour when compared to undisturbed oil sands tested at in situ stresses even though the stress level of the in situ sample is very much higher. It was therefore appropriate to use a quartz sand in the laboratory to investigate the fundamental fracture mechanisms in the field.

In the large scale fracture tests, the injected fluid was coloured with a fluorescent dye so that the fracture and the zone of leak off could be traced when the sample was excavated. Small scale testing carried out at the beginning of Phase 1 indicated that fluorescent dye did not alter the viscosity of the injection fluid and would not diffuse into the resident pore fluid over the time required to excavate the sample after the test.

Small scale laboratory testing was carried out to provide constitutive parameters for stress-strain behaviour and flow characteristics for the material tested in the large chamber.

1.2.2 Large Scale Fracture Tests

The Phase 1 program included experiments for propagation of 6 horizontal fractures (i.e. the initial minor principal stress is vertical) in which the fracture location is

dictated by the radial symmetry of the test apparatus. A seventh test was carried out with the initial minor principal stress horizontal so the effect of varying the initial stress conditions could be investigated. Constant pressure (below the minimum effective confining stress applied to the sample) injectivity tests, permeability tests as well as drained/undrained loading tests were carried out prior to the fracture tests.

The data from the Phase 1 large scale fracture simulations appeared to indicate that different mechanisms occur depending on the injection rate used in the test. The exact mechanisms were not identified, but the different dyed patterns observed in the tests suggested that different mechanisms occurred. In general the penetration of dye into the sample during the fracture tests was greater than the amount of flow that would occur through the interconnected pore space in the sand. Therefore, it was assumed that the sand was locally in a failure stress state (fractured) during injection causing the development of more permeable flow paths.

Two possible mechanisms of failure were described in the Phase 1 report which could account for the patterns of dye found in the sand after fluid injection:

1. Tensile Failure or Parting. Tensile parting will occur when the rate of fluid injection into an uncemented sand mass exceeds the rate of flow that can occur through the interconnected pores in the sand. If the fluid pressure at this injection rate is greater than the total minor principal stress there can be tensile stress in the sand matrix. Since an uncemented sand will not support such stresses, the sand grains will be forced apart and a parting will propagate through the sand.

2. Shear Failure. Shear failure occurs when the shear forces at a sand grain contact exceeds the shear resistance at the contact. Increases in the pore

fluid pressure from fluid injection into the sand mass results in a decrease in the normal forces at contacts between sand grains and therefore a reduction in shear resistance. When the shear resistance falls below the shear force, the sand grains slide relative to one another. In dense sands the shear sliding results in a less densely packed array of sand grains. The volume of the void spaces in the sand mass is increased (this is termed shear dilation) and the sand is therefore more permeable along shear surfaces.

Tensile and shear failure mechanisms may not occur independently of one another. The dye patterns observed in Phase 1 testing appeared to show evidence of both tensile parting and shear failure. The failure process appeared to depend on the injection rate and boundary conditions. For example, the pattern of dye found in samples which had significant friction between the ends of the sample and the top loading plate and chamber base was more extensive. In general, the dye pattern was also more extensive in samples where higher injection rates were used.

1.3 Objectives of the Phase 2 Study

The major objective of the study is to provide a better understanding of the mechanisms of hydraulic fracture formation and propagation in oil sands through laboratory simulations of the fracturing process in a large triaxial stress chamber. Phase 1 of the study provided a preliminary indication of the mechanisms of hydraulic fracturing under conditions of high leak off. The purpose of the Phase 2 study was to further understand the role these mechanisms have in the hydraulic fracturing phenomenon in uncemented sands by building on the data obtained during the initial phase of study.

The objective of Phase 2 large scale fracture tests was to determine the effect of fluid injection rate on fracture propagation. The results of these tests would

determine whether fracture processes and patterns are consistent with those predicted by leak off dominated fracture models. Phase 1 test conditions, such as initial stress conditions, pore fluid properties, etc., were used in Phase 2 testing to minimize the number variables which could control the initiation and propagation of fractures. This helped to relate the results of the Phase 1 study to those of Phase 2.

The ultimate goal of this work is to provide the basis for developing a framework to evaluate, verify and refine analytical models for fracturing of uncemented sands. It is recognized that this objective will require an intimate and fundamental understanding of the physical processes of hydraulic fracture which will evolve through comprehensive program of large scale laboratory simulations. The present phase of work represents an initial stage of this program in which basic processes are identified and characterized.

1.4 Project Funding

The project documented in this report has been jointly funded by the following companies and government agencies:

- Canada Centre for Mineral and Energy Technology (CANMET)
- Alberta Oil Sands Technology and Research Authority (AOSTRA)
- Shell Canada Ltd
- Esso Resources Canada Ltd.
- Golder Associates Ltd.

2.0 TEST MATERIALS, EQUIPMENT AND PROCEDURES

This section describes the properties of the sand and fluid used in the large scale laboratory simulations of hydraulic fracture. The test apparatus is also described together with the sample preparation, test, sample excavation, and sampling procedures. Many aspects of the materials, equipment and procedures adopted for this phase of study were developed in Phase 1 and were described in detail in the Phase 1 report prepared by Golder Associates Ltd. entitled "Laboratory Simulation and Constitutive Behaviour for Hydraulic Fracture Propagation in Oil Sands - Phase 1" dated July, 1991 (Supply and Services Canada File No. 06SQ.23440-9-9263). This section will provide a brief summary of the pertinent information from Phase 1 and will detail changes adopted for the Phase 2 study.

2.1 Test Materials

The materials used in Phase 2 large scale hydraulic fracture tests can be characterized as follows:

Sand

- commercial name: Lane Mtn. 125
- uniformly graded, sub-angular, D_{50} = 0.07 mm
- quartz mineralogy
- specific gravity of grains = 2.65
- exhibits strain softening post-peak behaviour when sheared in dense state
- strongly dilatant when sheared in dense state
- permeability to water = 4.56 x 10^{-3} cm/s (from small scale tests)
- permeability to 1.49 Pa-s fluid = 5.39 darcys (from small scale tests)

Pore/Injection Fluid

- commercial name: Invert liquid sugar
- clear and colourless
- fully soluble in water
- treated with enzymes to prevent crystallization

- viscosity at 20° C = 1.60 Pa-s (100% concentration)
- viscosity at 20° C = 1.49 Pa-s (95% liquid sugar + 5% water)
- specific gravity of (95% liquid sugar + 5% water) = 1.36

Fluorescent Dye

- commercial name: SPECTRAGLOW WD-801
- blue water dye
- intensely fluorescent under black light
- negligible diffusion of dye in sand samples saturated with liquid sugar

2.2 Test Equipment

The large scale hydraulic fracture tests were carried out in the triaxial stress chamber shown in Figure 2.1. The apparatus accommodates samples 1.4 m in diameter and up to 1 m high. Principal stresses of up to 1000 kPa can be applied independently through a circumferential (σ_h) and upper (σ_v) cavity as illustrated in the figure. The pore fluid pressure is applied to the sample through drainage ports in the base of chamber and through ports in top loading plate. A manually controlled system (Figure 2.2), fed by a pressurized air supply, is used to impose a variety of stress conditions on the test sample using 130 litre capacity air-over-water cells (one cell each for σ_h, σ_v, and pore fluid pressure) and pressure regulators. Constant stress conditions are achieved by pressure regulators. Horizontal stresses are transmitted to the sample through a latex rubber membrane, as in triaxial testing, while vertical stresses are applied through a steel plate.

The injection well is situated in the centre of the sample cavity and extends the full height of the sample. For each test the well is located and the sand sample placed around it. The well was a hollow steel pipe with an inside diameter of 25.4 mm and an outside diameter of 33.5 mm. The well is perforated at mid-sample height over an interval of 50.0 mm with 8 rows of 3.5 mm diameter holes (Figure 2.3). The perforated zone is protected against sand infiltration by a 230 mesh screen. The

injection well passes through the loading plate, the upper pressure cavity and the chamber top lid and is connected with 12.7 mm copper tubing to the injection pump. The injection well is vented through the base of the chamber with 12.7 mm copper tubing.

The injection pump unit (Figure 2.4) consists of the following major components:

- an AC hydraulic power unit (hydraulic pump, electric motor, fluid tank, set relief valve and check valve);
- a 9.4 litre pressure accumulator;
- a pressure compensated temperature stabilized flow control valve with compensator stroke adjustment;
- a 6.4 cm diameter, 30.5 cm stroke hydraulic cylinder

The hydraulic power unit drives oil through the flow control valve and into the hydraulic cylinder to drive a metal piston. The piston provides an interface between the hydraulic oil and the injection fluid which is pumped into the sample through the injection well. A LVDT was attached to the piston rod of the hydraulic cylinder to measure volume of fluid pumped into the sample during a test. The injection pump unit was designed to deliver a constant flow rate (0 to 200 ml/sec) independent of load or flow resistance up to a maximum 3500 kPa. This is accomplished by the flow control valve and the pressure accumulator.

Prior to the fracture simulations the injection pump unit was tested by rapidly cycling the output pressure between 0 kPa and 3500 kPa and recording the displacement of the LVDT (i.e. flow rate). A linear relationship between displacement and time was attained. This confirmed that the flow rate was independent of flow resistance over the working range of the pump.

Instrumentation was embedded in the sample to measure pore fluid changes during the fracture tests. A transducer was also mounted outside the well at the point of injection to track the injection pressure in the sample close to the well during the test. The transducer was placed outside the well to negate measuring head losses as the fluid passes through the perforations and well screen. Transducers were also used to measure the pressures in the horizontal and vertical stress cavities, pressure of the fluid entering the top of the injection well, and the pressure at the injection well vent. Pore fluid pressures, vertical stress, radial stress, injection pressures, and injection flow rate were recorded electronically using an IBM based computer data acquisition system located adjacent to the stress chamber (Figure 2.6).

2.3 Sample Preparation

Samples were prepared by pluviation of dry sand from a hopper directly above the chamber (Figure 2.7). The hopper is exactly the same diameter as the sample and equally high so that one complete sample can be formed without reloading. The equal diameters result in essentially one dimensional pluviation conditions. The base plate of the hopper is perforated with 5.2 mm diameter holes on 63 mm centres (approximately 400 holes). Pluviation was initiated and terminated by moving a shutter plate installed directly below the base plate of the hopper.

Prior to pluviation the injection well was installed and instrumentation for measuring pore fluid pressure changes were suspended at strategic points in the sample. The instrumentation was placed on three levels, two above the injection zone and one below. Details of the instrument placement is given in Figure 2.8.

The configuration of the drainage boundaries at the base and at the top of the sample consisted of the following:

- a layer of gravel
- geotextile (filter cloth)
- a layer of POLYNET (geonet consisting of two sets of polyethylene strands forming a diamond shape)
- a layer of high density polyethylene (HDPE), 40 mil perforated with 6.4 mm diameter holes
- geotextile (filter cloth)
- a layer of gravel (uniformly graded, sub-rounded, D_{50} = 3 mm)

Gravel layers provided uniform distribution of pore fluid and back pressure at the bottom drainage interface. Use of the filter cloth was to prevent migration of sand into the gravel and drainage tubing. The geonet and HDPE were used to reduce friction at the ends of the sample. The friction angle between the geonet and HDPE was measured to be approximately 8 degrees. These boundary conditions at the top and bottom of the sample were designed to provide a uniform stress distribution in the sample.

Once the sample was deposited, the top surface of the sample was levelled by smoothing the small hummocks on the sand surface with a wood plank. The chamber was then assembled. An isotropic confining stress of 450 kPa was applied to the sample. The top of the sample was subjected to a negative 70 kPa (vacuum) pressure. The viscous pore fluid was injected at room temperature under a driving pressure of 400 kPa through the bottom drainage ports.

2.4 Test Procedures

The test procedure for carrying out a large scale hydraulic fracture test is summarized below.

After the sample was saturated and the applied stresses relaxed back to atmospheric pressure, the test procedure was as follows:

1. The data acquisition system was started and initial reading of the instruments was taken to provide a zero reference level.

2. Vertical and horizontal confining stresses were applied in equal increments of 25 kPa to the test sample to a stress of 450 kPa. The sample was then permitted to consolidate under these isotropic stress increments for 1 to 2 days. This time was to ensure that excess pore fluid pressures which were generated due to the consolidation process could dissipate. The pore fluid pressure was increased to 200 kPa in increments of 25 kPa. After this step was completed, the pore fluid pressure in the sample was not permitted to fall below 200 kPa until excavation of the sample began (step 10)

3. A pore pressure parameter B test was performed. The B parameter is a ratio of the undrained pore fluid pressure response of the sample to a change in isotropic total stress. The isotropic total stress increase used in the test was 100 kPa.

4. The horizontal stress applied to the sample was increased to 600 kPa to give a K_o value of 2.0 (ie. σ_H = 600 kPa, σ_V = 400 kPa, u = 200 kPa).

5. A series of constant head permeability tests was performed. In each test a constant head was maintained across the sample and the volume of pore fluid flowing per unit time (q) was measured. The piezometers embedded in the sample were used to measure the hydraulic gradient (h/l). Permeability was calculated using Darcy's law:

$$k = ql/Ah$$

The difference in pressure between points of intake and discharge for the tests was 40 kPa, 80 kPa and 160 kPa. The pore fluid pressure between each test was allowed to dissipate to equilibrium conditions (200 kPa pore fluid pressure). Flow rate versus time plots for each test were made.

6. A series of sub-fracture pressure injectivity tests were carried out. The injection well was pressurized rapidly from 200 to 240 kPa. The flow rate of fluid entering the sample through the injection well was plotted with time. When the flow rate became constant with time the injection pressure was instantaneously increased to 280 kPa. After the flow rate became constant with time the injection pressure was increased to 360 kPa. Flow was permitted across the top and bottom drainage boundaries. The drainage boundaries were connected to the same pressure source.

7. A steady state hydraulic fracture test was carried out. The test was carried out at constant injection rate and injection pressure with time was measured. Flow was permitted across the top and bottom drainage boundaries. The drainage boundaries were connected to the same pressure source.

8. The injection well was primed with dyed injection fluid under a pressure of 195 kPa.

9. A fracture test was carried out. The test was carried out at constant injection rate (injection pressure measured with time). Flow was permitted across the top and bottom drainage boundaries. The drainage boundaries were connected to the same pressure source.

10 After injection, the sample was allowed to reach equilibrium based on readings of the internal instrumentation. After equilibrium conditions were attained, the system was depressurized slowly under undrained conditions.

After the test was completed the computer logged data was stored on permanent data discs. The data was then processed and plots of each pressure transducer versus time were produced.

2.5 Sample Excavation and Sampling

Once the chamber lid and upper loading plate were removed the upper drainage boundary was placed under black light and checked for the presence of fluorescent dye. The drainage boundary (gravel, filter cloth, etc.) was then carefully removed and the top of the sample was exposed. A wooden platform was then erected around the chamber and the black light unit was affixed above the chamber. The sample was then excavated in horizontal lifts, normally 2 to 4 cm in thickness, under black light using small spatulas and scoops. When the lift was completely excavated, locations of fluorescent dye were marked with black string. The black light was then turned off and under normal light, signs indicating the test number, orientation of the sample (0, 90, 180, 270 degrees), and depth of the lift as well as a meter stick were placed on the surface of the sample. A photograph of the sample surface was then taken with a camera located directly above the chamber. The procedure was then repeated for each lift until the lower drainage boundary was reached. The time required to excavate a particular sample varied from 2 to 5 days depending on the complexity of the pattern of dye.

Thin walled tube samples were extracted from the sample at various depths. These samples were retained for small scale testing.

The photographs showing the locations of the dye were digitized. Each photograph was orientated on the grid of an electronic tablet using the angle markers placed on the sample surface. The meter stick on the surface of the sample was used to scale each photograph. The cross hairs of the input cursor of the digitizer were used to target and record in Cartesian coordinates the dye locations. Patches of dye on the photographs were digitized on grid points. Digitized data were then plotted in three dimensions. Areas in the sample where the dye was concentrated appear as clouds of points on the plot. The plotting program allows rotation of the three dimensional axes so that the orientation of surfaces can be observed. Hard copies of each plot showing the dye surfaces from several viewing angles were made.

3.0 FRACTURE TESTS

A total of 5 hydraulic fracture tests were carried out during Phase 2 of this project, as summarized on Table 3.1. The results of testing from Phase 1 are also included in the table. Initial stress conditions, injection rates are also shown. The results of these large scale fracture simulations are presented in this section. Instrument response data is given as plots of the channel output in engineering units versus time. The instruments which are embedded in the fracture sample are identified by numbers which indicate their positions as follows:

XXX - YZ

where:

XXX is the angular position of the instrument in degrees

Y is the vertical position of the instrument
1 = 25 cm above injection point
2 = 10 cm above injection point
3 = 10 cm below injection point

Z is the radial position of the instrument
i = 0.25 x radius

As discussed in the previous section, locations of fluorescent dye are plotted as point clouds in "three dimensional" plots.

3.1 Fracture Test No. 1

The undrained isotropic loading test carried out on this sample gave a pore pressure parameter B value of 0.83. The results of the three constant head permeability tests carried out on this sample are given in Appendix I. Included are flow rate versus time and cumulative flow volume versus time plots. These constant head tests gave

permeability values of 2.8, 4.0 and 3.2 darcys for pressure heads of 40, 80 and 160 kPa maintained across the sample, respectively.

During the sub-fracture pressure injection tests the piezometers in the sample indicated pore fluid pressures that were very similar to that of the injection pressure (Appendix II). These abnormally high pressure readings were indicative of partial plugging of the drainage boundaries of the sample. Additional permeability tests carried out on the sample confirmed that the head loss across the top boundary far exceeded the head loss across the sample. Given the poor drainage conditions across the top boundary of the sample, it was decided to forego the fracture test. It would be very difficult to interpret and analyze the fracture test result because of these uncertain sample boundary conditions. Instead of performing a fracture test on this sample, this test was used to assess the homogeneity of the sand pack.

Approximately 500 ml of liquid sugar coloured with fluorescent dye was injected into the centre of the sample under a constant pressure of 280 kPa (80 kPa above resident pore fluid pressure). During excavation of the sample under black light, the dye was present as a concentric halo around the injection zone. The dye was found within a zone of sand with an average radius of approximately 5 cm from the well over a vertical distance of about 10 cm. No evidence of preferred flow paths caused by non-uniform packing of the sand during sample preparation was apparent.

The upper and lower drainage boundaries of the samples were found to be contaminated with sand when the apparatus was disassembled. In particular, the perforations in the HDPE layers were completely plugged with sand, resulting in a significant barrier to flow. It would appear that sand had "washed" through the metal screens that had been used to separate the sample from the drainage during the saturation of the sample and permeability tests. To prevent this occurrence in

subsequent tests the screens were replaced with filter cloth as outlined in Section 2.3.

3.2 Fracture Test No. 2

The sample dimensions and position of internal instrumentation for Fracture Sample 2 are shown in Figure 3.1. The K_o value for this test was 2.0 ((ie. σ_H = 600 kPa, σ_V = 400 kPa, u = 200 kPa).

The pore pressure parameter B of this sample was 0.5. This value is lower than the 0.83 measured in Test 1. The significance of the B value results are discussed in Section 5.1.

The results of three separate permeability tests carried out on this sample are given in Appendix I. The permeability of the sample was found to range between 3.9 and 4.3 darcys.

The results of the sub-fracture pressure injection tests carried out on this sample are given in Appendix II. In each test (injection pressures of 240 kPa, 280 kPa and 360 kPa), the flow rate decreases rapidly after the onset of injection and reaches steady state flow (constant flow) conditions 30 to 60 seconds after the injection pressure was applied. The internal piezometers, located at a radial distance of 17 cm from the injection point, show little change in pore fluid pressure.

A total of 4 steady state hydraulic fracture tests were carried out on this sample. The tests were carried out at constant injection rates of 0.28 ml/s, 0.40 ml/s, 1.00 ml/s and 0.25 ml/s. Approximately 850 ml of undyed fluid was injected during each test. The results of the tests are given in Appendix 3. The following observations are noted:

1. Injection pressure increases rapidly during the initial stages of injection, the peak injection pressure exceeds the minimum confining stress in three of the tests (q = 0.28, 0.40 and 1.00 ml/s). For these three tests the peak injection pressure increases as the flow rate is increased. The last test carried out at 0.25 ml/s displays a peak injection pressure slightly lower than the minimum confining stress.

2. For each test, the injection pressure levels off soon after injection was initiated. The first three tests show some variation in injection pressure with time, the injection pressure is essentially constant with time during the final test.

3. Piezometers embedded in the sample display a pressure increase in response to each injection rate. The response increases as the injection rate is increased and decreases with distance from the injection zone.

The results of the constant rate fracture test using dyed fluid are given in Figures 3.2 and 3.3. In this test 200 ml of dyed liquid sugar was injected into the test sample in 500 seconds (0.4 ml/s). The peak injection pressure exceeded the minimum confining stress by about 220 kPa. The injection pressure increases rapidly with time over the first 200 seconds of injection, then decreases with time for the remainder of the test, and is almost constant at the end of the 500 second injection period. It is noted, that the injection pressure curve is similar to the initial portion of the steady state fracture test carried out at the sample injection rate (Appendix III). The piezometers in the sample closest to the injection zone show a slight pore fluid pressure increase of 10 to 20 kPa during the test. Fluorescent dye was not found more than a few centimetres from the well screen, Figure 3.3.

Test 2 results indicate that it is possible to sustain pore fluid pressures in a sand mass which exceed the minimum confining stress for several hundred seconds without causing a tensile parting to propagate.

3.3 Fracture Test No. 3

The sample dimensions and position of internal instrumentation for Fracture Sample 3 are shown in Figure 3.4. The K_o value for this test was 2.0 ((ie. σ_H = 600 kPa, σ_V = 400 kPa, u = 200 kPa).

Permeability tests carried out after the sample was saturated yielded permeability values of 5.6 and 5.4 darcys. Permeability test results are contained in Appendix I. A pore pressure parameter B test carried out on this sample gave a value of 0.5.

The results of sub-fracture pressure injection tests are given in Appendix II. Two separate tests were carried out following the same test procedure to determine if the test results were repeatable. Both tests gave essentially the same results. As in Fracture Test 2, the flow rate was found to decrease rapidly after the onset of injection and reached steady state flow (constant flow) conditions shortly after the injection pressure was applied.

Steady state fracture tests were carried out at constant flow rates of 1.0, 3.0, 10 and 30.0 ml/s. A total of 850 ml of undyed liquid was injected into the sample in each test The test carried out at 3.0 ml/s was repeated prior to performing the fracture test with dyed fluid. The results of these tests are given in Appendix III. The results of these steady-state fracture tests differ significantly from those carried out on the previous sample. For tests carried out on the previous sample (Fracture Test 2), the peak injection pressure increased as the flow rate was increased. This trend is not present for this sample. In fact the peak injection pressure for the test

carried out at 3 ml/s is higher than a subsequent test carried out at 30 ml/s, even through the injection rate has increased by an order of magnitude. However, when the 3 ml/s test was repeated the peak injection pressure is much lower, the same phenomenon was noted for testing on the Fracture Sample 2. These observations tend to suggest that some disruption of the sand matrix near the injection zone occurs when these tests are carried out. The effect appears to be more pronounced at higher injection rates. Piezometers embedded in the sample display a pressure increase in response to each injection rate. Unlike the tests carried out on fracture Test 2 there was no direct relationship between injection rate and the magnitude of pore pressure response measured by the piezometers. This is also evidence of changes in sand structure caused by previous injection tests.

The results of Fracture Test 3 are given in Figures 3.5 and 3.6. In this test 200 ml of dyed liquid sugar was injected into the test sample in 6.7 seconds (30 ml/s). Two important aspects of the test are noted:

1. The peak injection pressure did not exceed the minimum confining stress applied to the sample.

2. The fluorescent dye was found in a thick zone of sand originating at the well (zone of injection) and extending up and away from the well into the sample.

Based on the dye distribution in the sample and the low peak injection pressure, it does not appear that tensile parting was generated in this test.

3.4 Fracture Test No. 4

Fracture Test 4 was carried out under the same stress conditions and injection rate utilized for Test 5. The sample dimensions and position of internal instrumentation for Fracture Sample 4 are shown in Figure 3.7. The purpose of the test was to determine if the results of the previous fracture test were affected by sub-fracture pressure injection tests and steady state fracture tests carried out before the fracture test with dyed fluid. No steady state fracture tests were carried out on this sample. Two permeability tests were carried out along with a single sub-fracture pressure injection test (240 kPa injection pressure). These tests allow the overall flow conditions in the sample as well as flow conditions around the zone of injection to be assessed and evaluated in terms of previous tests.

Permeability tests carried out after the sample was saturated gave permeability values of 4.8 and 4.6 darcys. Permeability test results are contained in Appendix I. A pore pressure parameter B test carried out on this sample gave a value of 0.5.

The results of a single sub-fracture pressure injection test carried out at 240 kPa is given in Appendix II. The results of this test are consistent with previous tests carried out on previous fracture samples.

The results of Fracture Test 4 are given in Figures 3.8 and 3.9. In this test 250 ml of dyed liquid sugar was injected into the test sample in 8.3 seconds (30 ml/s). The results of Test 4 differ significantly from Test 3 which was carried out at the same injection rate. The magnitude of the pore fluid pressure increase measured in the sample immediately adjacent to the injection zone in Test 4 (Figure 3.8) was greater than that measured in Test 3 for the same period of flow. The distribution of dye in the sample was found to be more extensive in Test 4 (Figure 3.9). Dye was found to extend out and up from the injection zone. In the upper portion of the

sample the dye was concentrated on discrete surfaces. These surfaces were near horizontal near the centre of the sample and the surfaces turned downward toward the edges of the sample.

The difference in the injection pressure response and the pattern of dye in Tests 3 and 4 may be due to the stress path followed by each sample prior to the injection of dye. Fracture sample 3 was subjected to sub-fracture injection and steady state fracture tests during which several litres of fluid was injected into the sample at pressures up to 400 kPa above the minimum confining stress. Shear and compressive strains developed during these injection tests may have significantly altered the stresses and resulting fluid flow in the vicinity of the injection zone.

3.5 Fracture Test No. 5

The sample dimensions and position of internal instrumentation for Fracture Sample 5 are shown in Figure 3.10. The K_o value for this test was 2.0 ((ie. σ_H = 600 kPa, σ_V = 400 kPa, u = 200 kPa).

The pore pressure parameter B of this sample was 0.5. The results of two separate permeability tests carried out on this sample are given in Appendix I. The permeability of the sample was found to range between 5.9 and 6.4 darcys. The results of the sub-fracture pressure injection test carried out at an injection pressure of 240 kPa is given in Appendix II. These results indicate that fluid flow characteristics of Fracture Sample 5 were consistent with previous samples tested in the laboratory program.

In Fracture Test 5 approximately 260 ml of fluid was injected into the sample at 200 ml/s. The results of the test are given in Figures 3.11 and 3.12. Two aspects of the test are worth noting:

1. The piezometer at the top of the injection well peaks at about 2000 kPa and decreases rapidly after the well is shut in. This piezometer is located immediately downstream of the shut in valve. The piezometer in the centre of the sample (just outside the well screen) peaks at 608 kPa several seconds later. It would appear that there is significant pressure gradient in the tubing at this pumping rate. When the piezometer at the top of the well peaks at 2000 kPa the piezometer in the sample is only at about 300 kPa. After the well is shut in, the pressure at the top of the well drops while the pressure at the centre of the sample continues to rise, eventually the pressure in the well equalizes and the two instruments give equivalent readings.

2. The pattern of dye in the sample is consistent with previous tests where the dominant mode of failure was shearing of the sand in the vicinity of the injection zone. It should be noted that in the upper portion of the sample where dye was found, the dye was concentrated in thin zones of sand similar to that found in sample 4. However, the length of these surfaces was only about 5 cm.

The above results suggest that at the time the well was shut in the pressure at the zone of injection was less than the minimum confining stress and therefore tensile parting was unlikely to have taken place during the injection period. After the well was shut in, fluid would continue to flow into the sample as the excess pressure in the well dissipated, but the flow was no longer constant. In fact, the rate of flow during this time period was much slower than the original injection rate and was decreasing with time as the pressure driving the fluid dissipated. Under these conditions it seems unlikely significant tensile parting in the sample would occur even when the pressure in the sample reaches 600 kPa (200 kPa above the minimum confining stress).

4.0 NUMERICAL SIMULATION OF FRACTURE TESTS

Numerical simulation of one of the laboratory hydraulic fracture tests was carried out to examine the geomechanical behaviour of the uncemented sand under conditions associated with the fluid injection process. The purpose of the analysis was to determine whether injection and sample pore pressures as well as pattern of dye observed in the test samples were consistant with shear failure propagation. The analysis was intended to be an initial estimation of whether shear failure was a viable concept. Fracture Test 4 was examined because it had not been subjected to steady state fracture tests prior to injection of the dye. As a result the stress path experienced by the sample prior to the fracture test was relatively simple and more easily modelled. The mechanical characteristics of the sand as measured in the Phase I laboratory program were incorporated in the analyses.

4.1 Method of Analysis

Fast Lagrangian Analysis of Continua (FLAC) is a two-dimensional explicit finite difference code which simulates the behaviour of soil, rock or other materials which may undergo plastic flow when their yield limit is reached. It is based upon a "Lagrangian" calculation scheme which is well suited for modelling large distortions.

FLAC has seven built-in material models, ranging from the "null" model which represents holes in the grid to the shear and volumetric yielding models which include strain hardening/softening behaviour and represent non-linear, irreversible shear failure and compaction.

Structures such as well casings, tunnel liners, rock bolts, yielding props or sheet piling which interact with the surrounding rock or soil may be modelled with the structural element logic. It is possible to examine the stabilizing effects of

supported excavations, or to examine the effects of soil or rock instability on surface structures.

FLAC models the full coupling between a deformable porous solid and a viscous fluid flowing within the pore space. The fluid may be assumed to obey either the isotropic or anisotropic form of Darcy's law, and is considered to be deformable. Non-steady flow is modelled, with steady flow treated as an asymptotic case. The flow model can also be run independently from the mechanical calculation, and both confined and unconfined flow can be simulated.

4.2 Modelling Procedure

Modelling was carried out by dividing the sample inside the chamber into 50 zones horizontally and 50 zones vertically (total of 2500 elements) as shown on Figure 4.1. Axisymmetrical condition was used and therefore only half of the chamber was studied.

Large scale Fracture Test 4 was selected for analysis because the amount of supplementary testing carried out on this sample was not as extensive as those carried out on the other samples and, therefore, the stress history of the sample could be modelled more easily. The properties of the sand and the fluid used in the analysis were obtained from Phase I of the laboratory program. The sand was assumed to be linear elastic with strain softening behaviour and was assumed to satisfy the Mohr-Coulomb failure criterion.

The properties of the sand used in the analysis are summarized as follows:

Shear Modulus	16,420 kPa
Bulk Modulus	27,369 kPa
Poisson's ratio	0.25
Dry Density	1485 kg/m^3
Saturated Density	2000 kg/m^3
Specific Gravity of Grains	2.65
Porosity	0.48
Peak Friction Angle	38°
Residual Friction Angle	30°
Cohesion and Tension	0
Peak Dilation Angle	30°
Residual Dilation Angle	5°
Permeability to 1.49 Pa-s viscosity liquid	4 x 10^{-6} cm/s

The fluid properties used in the analysis were as follows:

Density	1330 kg/m^3
Bulk Modulus	333 MPa

The modelling procedure used in the analysis of Fracture Test 4 was as follows:

1) External stresses (σ_{xx} = 600 kPa and σ_{yy} = 400 kPa) were applied to the sample. Pore pressures inside the sample were held constant at 200 kPa.

2) The vertical axis of symmetry was fixed from horizontal movement and the bottom horizontal boundary was fixed from vertical movement.

3) Drainage was allowed on the top and bottom horizontal boundaries.

4) The simulation was brought to equilibrium through a series of time steps. The maximum unbalanced nodal force and the displacements at the boundary of the sample were monitored for each time step. In an explicit dynamic code like FLAC, the model is stepped through time (calculation time, not real time), allowing the kinetic energy of the mesh to damp out, thus providing the static solution.

5) All the displacements during consolidation were reset to zero and the pore pressures inside the sample were allowed to change.

6) A constant flow rate of 30 ml/s was applied for a period of 8.3 sec at the injection zone as indicated on Figure 4.1.

7) FLAC couples flow and mechanical calculation until equilibrium is reached. Each fluid step corresponds to a real period of time. By default, FLAC alternates between one mechanical step and one fluid step. At the beginning of a coupled problem, many mechanical steps should be used for each fluid step to keep the solution in equilibrium. In this study, 200 mechanical steps were used for every fluid step. The unbalanced nodal force was monitored for each fluid step to ensure this value was less than 1% of initial maximum value.

8) After the discharge was applied for a period of 8.3 sec (equivalent to injecting 250 ml of fluid into the sample), flow into the sample was turned off and the dissipation of pore pressures was monitored. The locations for monitoring the pore pressures are shown on Figure 4.2.

9) Data files which contained all the commands necessary for the modelling procedures are attached to Appendix IV for reference.

4.3 Discussion of Results

Figure 4.3 shows a plot of maximum unbalanced nodal force against time step during the simulation. It can be seen that when the solution reaches equilibrium, the maximum unbalanced nodal force approaches a value less than 1% of those at the beginning of the time step.

Figure 4.4 shows the extent of yielding at 8.3 sec after flow is injected into the sample. General yielding occurs around the injection point and at 45° about the upper half of the sample, out to half the radius. Yielding also occurs near the outer boundary in the lower portion of the sample.

The distribution of pore pressures, displacement vectors and principal stress vectors are presented on Figures 4.5 to 4.7 respectively. At the end of consolidation, pore pressures are constant at 200 kPa at every point inside the sample. It was found that everywhere in the sample the stress state was quite close to yield. After flow is injected into the sample, the pore pressure contours indicated that the pore pressure on the upper half of the sample are slightly higher than those at the lower half.

The extent of yielding at the end of simulation is presented on Figure 4.8. Figure 4.9 shows the extent of the observed yielding from the laboratory test. An examination of Figures 4.4, 4.8 and 4.9 suggests that the extent of yielding produced from the numerical simulation is similar to that found during the laboratory simulation.

Pore pressure development at four locations inside the sample during the numerical simulation are plotted against laboratory results on Figure 4.10. It can be seen that

the pore pressures predicted from the numerical simulation match that found from the laboratory tests.

The majority of the parameters used as input for this initial numerical analysis were measured values. However, two parameters (bulk modulus of the fluid and the relationship between shear dilation and permeability) were estimated. These parameters should be quantified through small scale laboratory testing so that more rigorous analyses can be carried out. This initial analysis demonstrates that the pattern of dye found in the sample and the response of piezometers at the well screen and in the sample are consistent with shear failure of the laboratory sample during injection.

5.0 ASSOCIATED TESTS

5.1 Interpretation of Pore Pressure Parameter B Tests

Undrained isotropic loading tests were carried out on each large scale fracture sample. The purpose of these tests was to measure pore pressure parameter B which is commonly used in small scale tests to assess the saturation of the test samples. The B value is a measure of the undrained pore fluid pressure response of the sample to change in isotropic stress. The greater the increase in pore pressure, the greater the sand skeleton compressibility. For most reconstituted sands the B parameter is usually close to one because the sand structure is more compressible than the pore fluid and therefore the load is taken almost entirely by the fluid.

The B value measured in Test 1 was 0.83. Tests 2 through 5 yielded B values of 0.50. The pore pressure response is affected by the volume increase of the drainage lines which separate the test chamber from the upstream and downstream back pressure valves and by the presence of air in the sample, drainage filters or lines. It is noted that the drainage boundaries in Test 1 were partially plugged during the test and as a result the compliance of the tubing and ports peripheral to the sample would have a lesser effect on the pore pressure response during the undrained loading. In the remaining tests (Tests 2 through 5) the sample boundaries were clear and the B value was significantly lower. These results indicate that the B value is significantly affected by the compliance of the testing apparatus and therefore the B parameter is not a good indicator of sample saturation for these very large samples.

5.2 Magnetic Resonance Imaging

Thin walled tube samples taken from two of the large scale fracture test samples were examined using a magnetic resonance imaging (MRI) spectrometer. The MRI spectrometer is a nondestructive analysis tool capable of differentiating among various solids and fluids within core samples. These tests were carried out at the Petroleum Recovery Institute (PRI) Imaging Centre in Calgary.

The samples subject to MRI testing were taken from Fracture Sample 3 at depths of 28 cm and 39 cm from the top of the sample (14 cm and 3 cm above the injection zone, respectively) and from Fracture Sample 4 at a depth of 46 cm (approximately level with the injection zone). The samples measured 4.5 cm in diameter by 7.5 cm long. Each sample was taken at the interface between zones of sand which appeared visually under black light to contain fluorescent dye and native undyed sand, Figure 5.1. The zones of dyed sand are encompassed by black string in Figure 5.1. These sampling locations were selected to provide an indication of how the dyed fluid was transported through the sand during the injection process.

The MRI process permits sectioning of the sample for inspection of the interior of the sample. Figure 5.2 shows the series of sections through the samples taken from the large scale fracture tests. A total of 8 equally spaced sections were taken through each sample perpendicular to the sample axis (transverse, vertical slices). An additional 8 equally spaced sections were taken parallel to the sample axis, 4 vertical (longitudinal, vertical slices) and 4 horizontal (longitudinal, horizontal slices). These sections give a sense of the distribution of dyed fluid in the samples in three dimensions.

The series of images through the fracture samples are shown in Figures 5.3 to 5.8. The orientation of each particular MRI sample with respect to the large scale

fracture sample from which it was taken (Figure 5.1) is shown on each set of images. It should be noted that resolution of the imaging probehead used to examine the samples was not capable of distinguishing the pore network from the sand grains. However, the zones of the sample which contain dyed fluid can be easily distinguished by colour from native sand on each section. The portion of the sample which contains dyed fluid appears on the MRI image as blue in colour.

The surface of contact between the dyed and undyed sand varies from image to image. In general, the contact between the two materials is very irregular. This heterogeneity is indicative of flow along discontinuities such as shear surfaces or partings.

6.0 DISCUSSION

The data from 5 large scale fracture tests were presented in this report. In 4 of the 5 tests fluid coloured with fluorescent dye was in injected at a constant flow rate. These fracture tests were similar to those carried out in Phase 1 of the study. In the remaining test, the dyed fluid was injected under constant pressure. The purpose of this test was to examine the homogeneity of the packing of the large scale sand sample.

In Fracture Test 1, 500 ml of dyed fluid was injected at a constant pressure of 280 kPa. The objective of the test was to determine if packing and saturation procedures effect the results of the large scale fracture tests. Of particular interest was whether the sand preparation procedures could result in zones of different porosity in the sand that could provide a preferential flow path for injection of fluid into the sample during the fracture tests. The pressure used in the test was 80 kPa above the pore fluid pressure in the sample and 120 kPa below the minimum confining stress applied to the sample. If the packing of the sample was nonuniform in the vicinity of the injection well, flow would be expected to concentrate in the high porosity sand zones. Under these conditions the pattern of dye in the sample would be irregular delineating the more permeable zones. The actual pattern of dye found in the sample after the test was uniform around the injection zone and preferential flow channels were not present.

Fracture Tests 2 through 5 were carried at fluid injection rates ranging from 0.4 ml/s to 200 ml/s. The initial stress conditions of the samples were identical (σ_H = 600 kPa, σ_V = 400 kPa and u = 200 kPa). Samples 2 and 3 were subjected to extensive fluid injection testing prior to injection of the dyed fluid. Samples 4 and 5 were subjected only to a single constant pressure fluid injection test at a pressure of 160 kPa below the minimum applied external stress.

Fundamentally there are two mechanisms of failure that are possible in uncemented sands when subjected to fluid injection: tensile failure (or parting) and shear failure. The data obtained from the Phase 2 appears to indicate evidence of shear failure of the specimen at all fluid injection rates that were investigated. This evidence of the shear failure mechanism includes the following:

1. In three of the large scale fracture tests (Fracture Tests 2, 4 and 5) the peak injection pressure exceeded the minimum confining stress on the sample. In each case the dye did not propagate along a horizontal surface to the edge of the sample (a horizontal fracture would be expected since the horizontal to vertical effective stress ratio in each test was 2.0). This data suggests that the fracture observed in the tests were dominated by the influence of the dilation of the sand. Expansion of the initial fracture cavity resulted in shear strains in the sand surrounding the fracture. These shear strains in turn cause a tendency to dilation of the sand. However, as the sand is constrained by the surrounding material and is limited in its potential for expansion, there is a relatively large increase in the effective confining stress on the sand surrounding the fracture. As a result the large injection pressures are offset by large local stresses in the sand matrix (which exceed the minimum confining stress on the sample) and limits the propagation of the fracture.

2. In Fracture test 3 the dye was able to penetrate the sample an appreciable distance even though the peak injection pressure was less than the confining stress on the sample. It is noted that this sample was subjected to several steady state fracture tests prior to injection of the dye. In each of these tests, the peak injection pressure exceeded the minimum confining stress. As noted previously, the peak injection pressure for the test carried out at 3 ml/s is higher than a subsequent

test carried out at 30 ml/s, even though the injection rate has increased by an order of magnitude. However, when the 3 ml/s test was repeated the peak injection pressure is much lower. These observations tend to suggest that some disruption of the sand matrix occurs when these tests are carried out. These results suggest a shear failure zone may have developed in the sample during the steady state fracture tests creating a preferred pathway for the dye. The pressure required to impregnate this zone with a relatively small amount of dye would be less due to the reduced strength, enhanced permeability, and redistribution of stress in the sheared zone.

3. A numerical simulation of Fracture Test 4 using the computer program FLAC which handles strain-softening and dilatant sand behaviour gave a close match to the laboratory results. The fluid pressures at the injection zone and at points within the sample measured during the test were consistent with those produced in the numerical simulation. In addition, the pattern of dye found in the sample after the test is similar the shear failure zone predicted by the model.

4. An examination of samples taken near the fracture zone of two samples using MRI analysis shows the contact between the native sand and the sand invaded by the dyed fluid was very irregular. This heterogeneity may be representative of flow along discontinuities such as shear surfaces or partings.

In general, the propagation of dye into the fracture samples in Phase 2 tests were less than that observed in Phase 1 tests even though the injection rates were lower in Phase 2 and the total amount of dyed fluid injected in Phase 2 tests was greater. It is noted that for the first 6 tests of Phase 1, friction between the ends of the

sample and the rigid chamber lid/base used to transmit vertical load restricted lateral deformation adjacent to these surfaces. Analyses carried out by Boone (1991, personal communication) have shown that this boundary condition will result in low stresses in the centre portion of the sample. This may account for the more distributed dye pattern observed in these samples (Table 3.2). It should also be noted that Phase 2 fracture samples were subjected to more extensive testing prior to the fracture tests. As discussed previously, these tests may also account for the difference in the distribution of dye observed in the tests of each phase.

The numerical simulation carried out in this study has shown that when the fracture samples were subjected to effective confining stresses corresponding to a K_o value of 2.0, the stresses in the samples were very close to shear failure envelope. It is noted that the amount of shear failure, caused by increases in pore fluid pressure, should be more extensive in these samples than in samples that are subjected to smaller stress differences. The pattern of dye and the pore fluid pressure response in the sample at the injection point as well as at other points within the sample would be expected to be different if a different K_o value were used in the tests.

7.0 CONCLUSIONS AND RECOMMENDATIONS

The data from the large scale fracture simulations carried out in the Phase 2 study have provided more insight into the mechanisms of fracture in uncemented sands. Shearing has been identified as one failure mechanism affecting the fracture process. However, the results of Phase 1 and Phase 2 testing clearly indicate that the failure process depends on the injection rate and boundary conditions. The role shear failure has on fracture propagation at higher injection rates has not been examined.

Further large scale fracture tests and pertinent numerical modelling is necessary to fully understand the hydraulic fracturing phenomenon in uncemented sands. Additional numerical modelling, similar to that performed in this study, should be carried out to assess both Phase 1 and Phase 2 test results and to develop test parameters for future large scale laboratory tests. This modelling should include the assessment of factors such as stress inhomogeneities and leak off and fabric inhomogeneities.

Based on the tests reported in Phase 1 and Phase 2 of this study, the next phases of the study should include tests to examine the effect fluid injection rate has on fracture propagation. The object of these tests would be to determine if fracture processes and patterns observed in the first two phases of tests occur at higher injection rates. The same volume of fluid would be injected into the sample at higher rates. The stresses applied to the sample would be the same for each test.

It would be useful to carry out a series of tests to examine the effect of initial stress conditions on fracture propagation. The purpose of these tests would be to determine if the mode of oil sands failure during fluid injection changes when the orientation of applied stresses change. A series of tests would be carried out at

constant injection rate, the stress difference applied to the sample would be varied in each test. The relationship between fracture patterns and K_o values would be examined to assess the relative influence tensile and shear failure mechanisms have on fracture propagation.

Once the failure mechanisms controlling fracture propagation in sand where the injection fluid and pore fluid are the same is understood, a set of tests to study the effect of injection of a different fluid from the pore fluid to induce the hydraulic fracture should be carried out. In the field it is common to inject steam into oil sands which are saturated with bitumen and water. The injection fluid is thus less viscous than the pore fluid. In addition, the injection fluid may or may not be miscible with the pore fluid.

GOLDER ASSOCIATES LTD.

PROFESSIONAL ENGINEER ALBERTA K.M. KOSAR

K.M. Kosar, P. Eng.

PERMIT TO PRACTICE
GOLDER ASSOCIATES LTD.
Signature
Date June 3/92
PERMIT NUMBER: P 5122
The Association of Professional Engineers, Geologists and Geophysicists of Alberta

Table 3.1 Summary of Hydraulic Fracture Test Program (Phase 1 and 2)

Phase of Study	Test No.	Vertical Stress (kPa)	Horizontal Stress (kPa)	Pore Fluid Pressure (kPa)	Kv	Injection of Dye		Displacement Tests		
						Rate (mL/s)	Volume (mL)	Permeability Tests	Injectivity Tests	Diffusivity Tests
1	1	400	600	—	—	96.0	927	not performed	not performed	not performed
1	2	Test aborted due to fitting leak								
1	3	480	496	400	2.2	93.5	907	not performed	not performed	not performed
1	4	400	600	200	2.0	20.0	80	not performed	not performed	not performed
1	5	400	600	200	2.0	5.0	20	not performed	not performed	not performed
1	6	400	600	200	2.0	5.0	18	1.5	200 kPa* 200 kPa**	not performed
1	7	400	600	200	2.0	10.0	40	4.4	200 kPa**	not performed
1	8	600	400	200	0.5	10.0	40	2.8	200 kPa**	not performed
2	1	400	600	200	2.0	constant pressure of 280 kPa	600	4.0 2.8 3.2	240 kPa 280 kPa 360 kPa	not performed
2	2	400	600	200	2.0	0.4	200	3.9 4.3 4.3	240 kPa 280 kPa 360 kPa	0.28 ml/s 0.40 ml/s 1.00 ml/s 0.25 ml/s
2	3	400	600	200	2.0	30	200	5.8 5.4	240 kPa 280 kPa 360 kPa	1.0 ml/s 3.0 ml/s 10.0 ml/s 30.0 ml/s 3.0 ml/s
2	4	400	600	200	2.0	30	250	4.9 4.6	240 kPa	not performed
2	5	400	600	200	2.0	200	280	5.9 6.4	240 kPa	not performed

Notes: * Initial pore fluid pressure in sample = 35 kPa
** Initial pore fluid pressure in sample = 0 kPa

Table 3.2 Results of Hydraulic Fracture Test Program (Phase 1 and 2)

Phase of Study	Test No.	Top and Bottom Boundary Conditions	Location of Piezometer at Injection Zone	Injection Zone		Pattern of Dye in Sample
				Pmax (kPa)	(dP/dt)max (kPa/s)	
1	1	Frictional	Inside Well			
1	2	Test Aborted due to fitting leak				
1	3	Frictional	Inside Well			
1	4	Frictional	Inside Well	< 900	175	distributed
1	5	Frictional	Outside Well	240	10	distributed
1	6	Frictional	Outside Well	232	9	---------
1	7	Low Friction	Outside Well	425	56	compact
1	8	Low Friction	Outside Well	320	30	distributed
2	1	Low Friction	Outside Well	---	--	---------
2	2	Low Friction	Outside Well	620	2	compact
2	3	Low Friction	Outside Well	380	27	compact
2	4	Low Friction	Outside Well	550	42	distributed (discrete surfaces)
2	5	Low Friction	Outside Well	608	97	compact (discrete surfaces)

LARGE TRIAXIAL STRESS CHAMBER

Figure 2.1

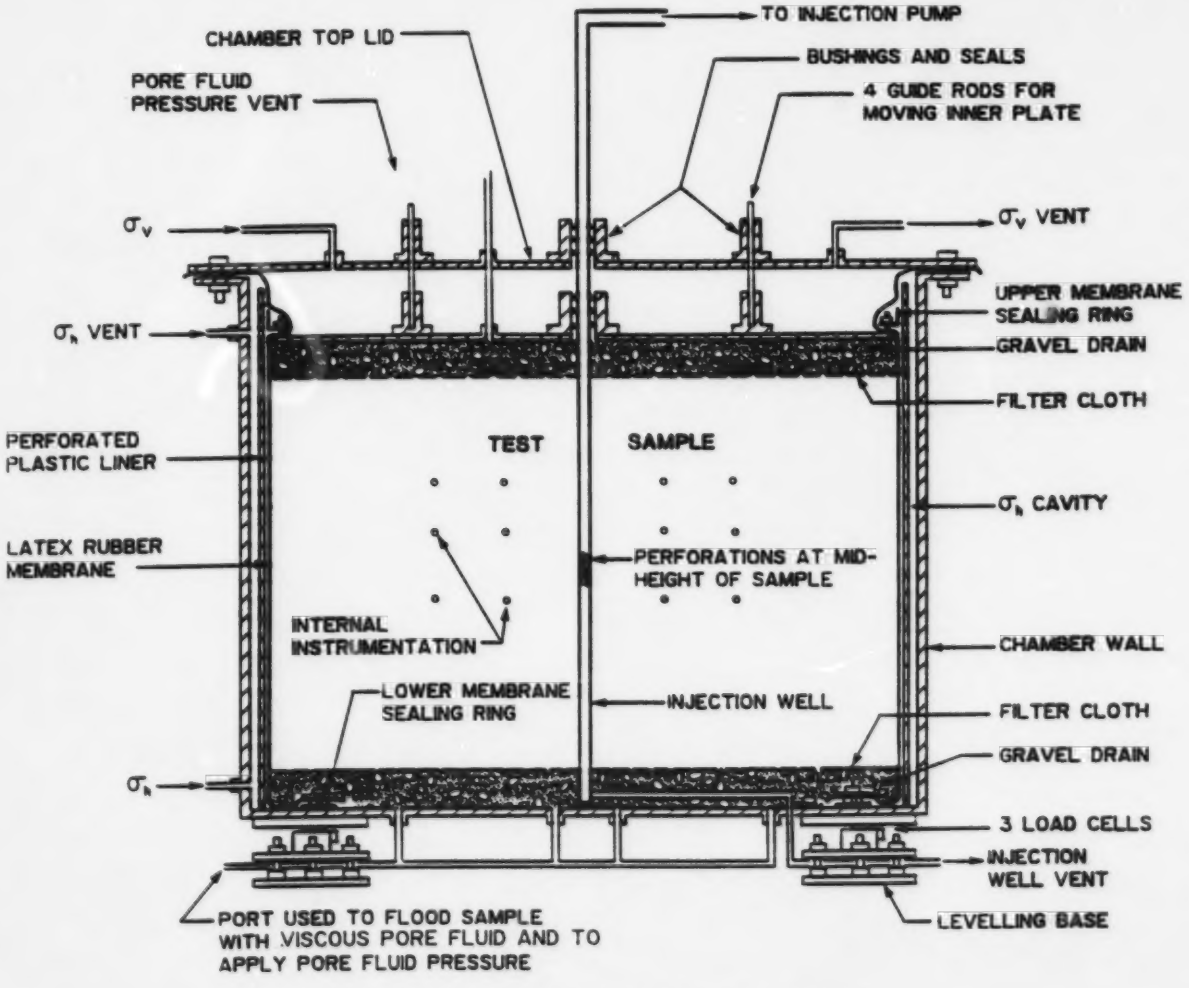

NOTE: SCHEMATIC ONLY - SOME DETAIL NOT SHOWN

PROJECT No. 912-2055 DRAWN RR REVIEWED KMK DATE APR 91

PRESSURE CONTROL BOARD	Figure 2.2

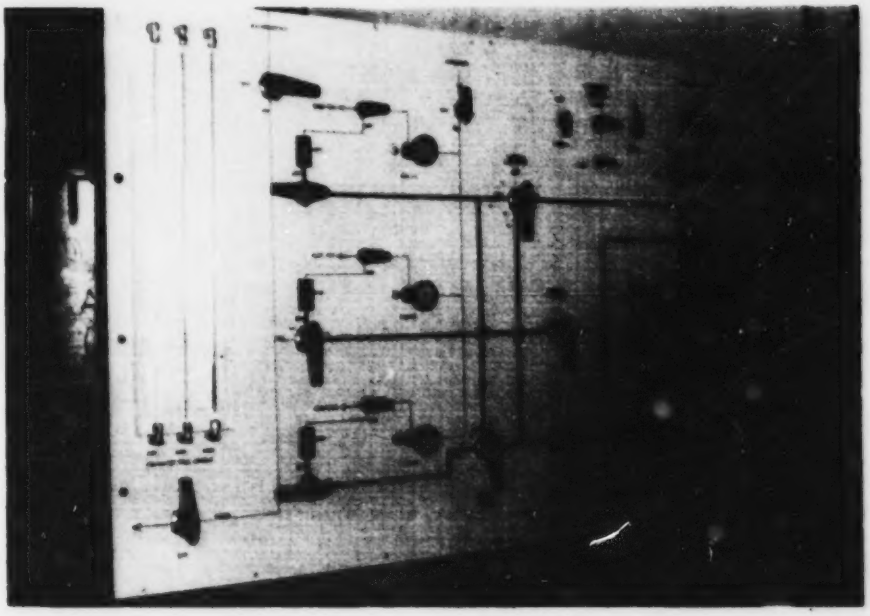

PROJECT No. 912-2055 DRAWN CG REVIEWED _____ DATE APR 91

CROSS SECTION OF INJECTION WELL AT MID-HEIGHT OF SAMPLE

Figure 2.3

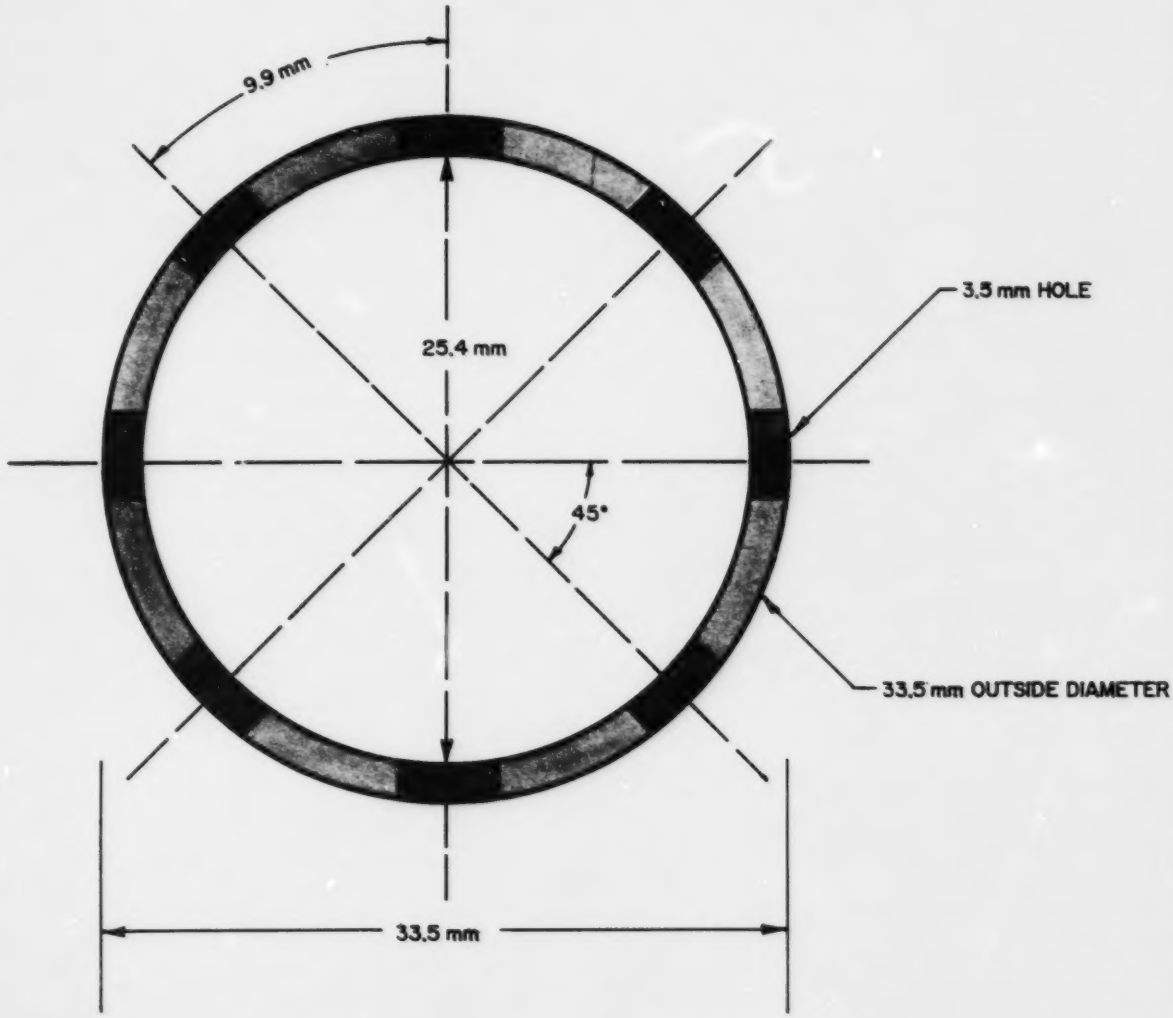

8 ROWS ON 6.4 mm CENTERS

PROJECT No. 912-2055 DRAWN CG REVIEWED KHK DATE JUNE 90

CONSTANT FLOW PUMP	Figure 2.4

PROJECT No. 912-2055 DRAWN CG REVIEWED _____ DATE APR 91

INJECTION WELL DETAIL	Figure 2.5

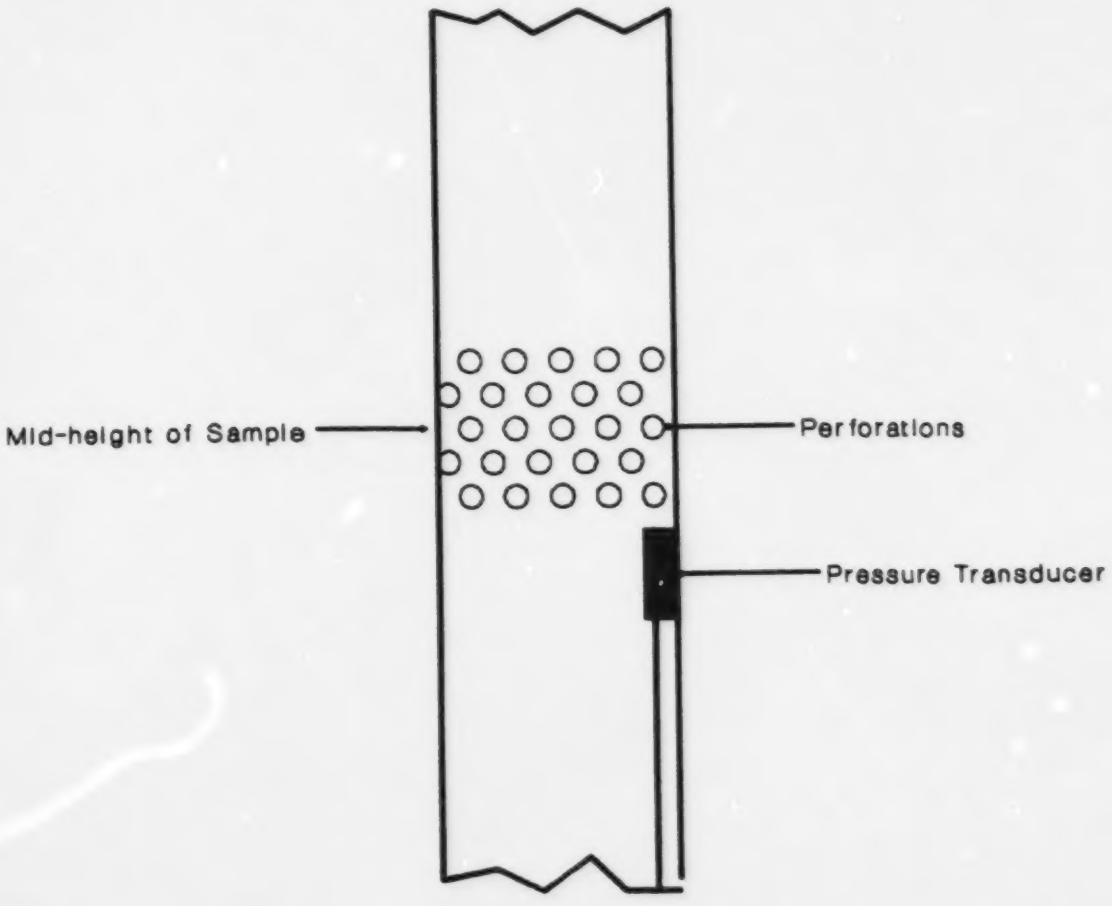

PROJECT No. 912-2055 DRAWN CG REVIEWED KMK DATE JUNE 90

Golder Associates

PHOTOGRAPH OF LARGE TRIAXIAL CHAMBER

Figure 2.6

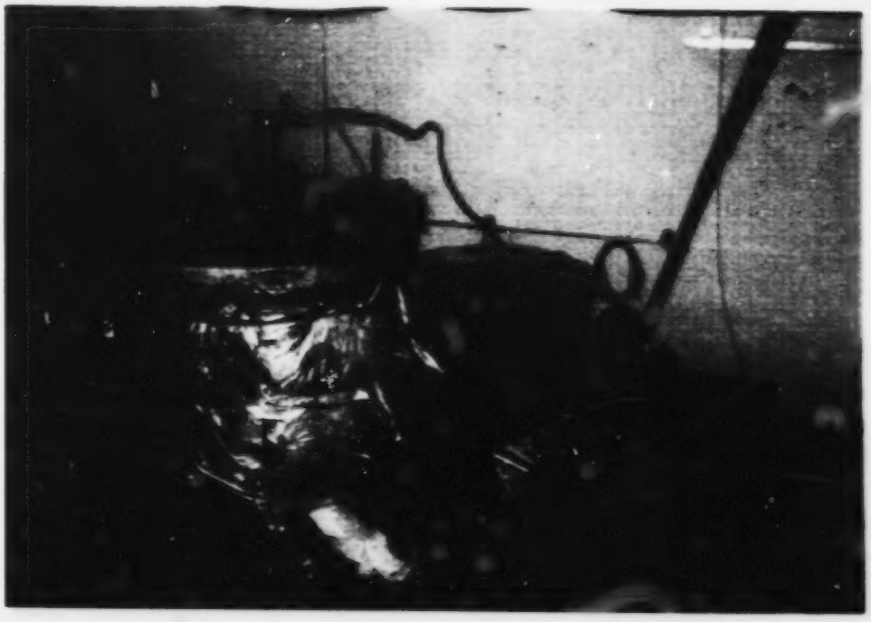

PROJECT No. 912-2055 DRAWN CG REVIEWED DATE APR 91

PLUVIATION OF SAND INTO STRESS CHAMBER

Figure 2.7

THE SAND IS LOADED IN A HOPPER WHICH IS ERECTED DIRECTLY OVER THE TRIAXIAL CHAMBER.

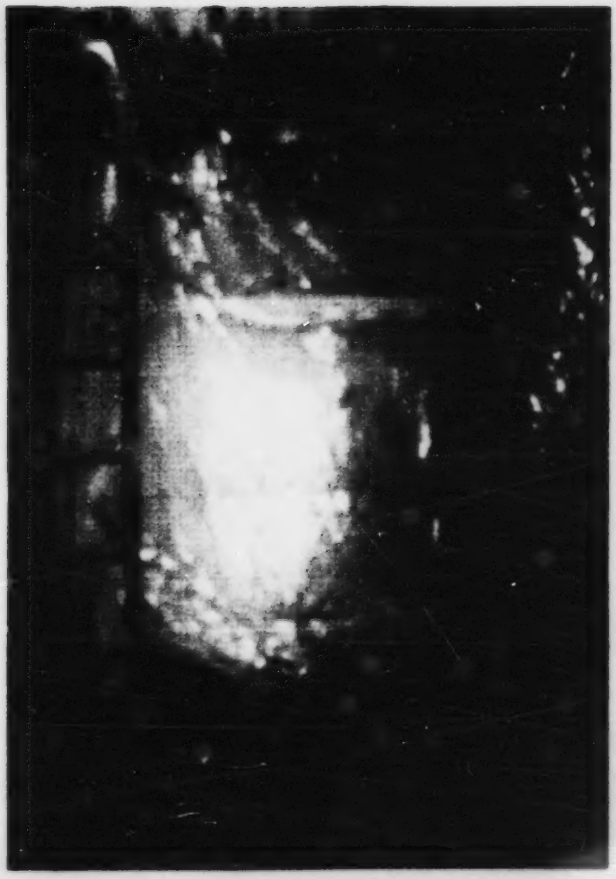

THE SAND IS PLUVIATED INTO THE CHAMBER SLOWLY TO PRODUCE A DENSE, HOMOGENEOUS SAMPLE. A PLASTIC CURTAIN AROUND THE CHAMBER DURING PLUVIATION LIMITS THE AMOUNT OF AIRBORNE PARTICLES IN THE LABORATORY.

PROJECT No. 912-2055 DRAWN CG REVIEWED DATE APR 91

PROJECT No. 912-2055 DRAWN CG REVIEWED [illegible] DATE JUNE 90

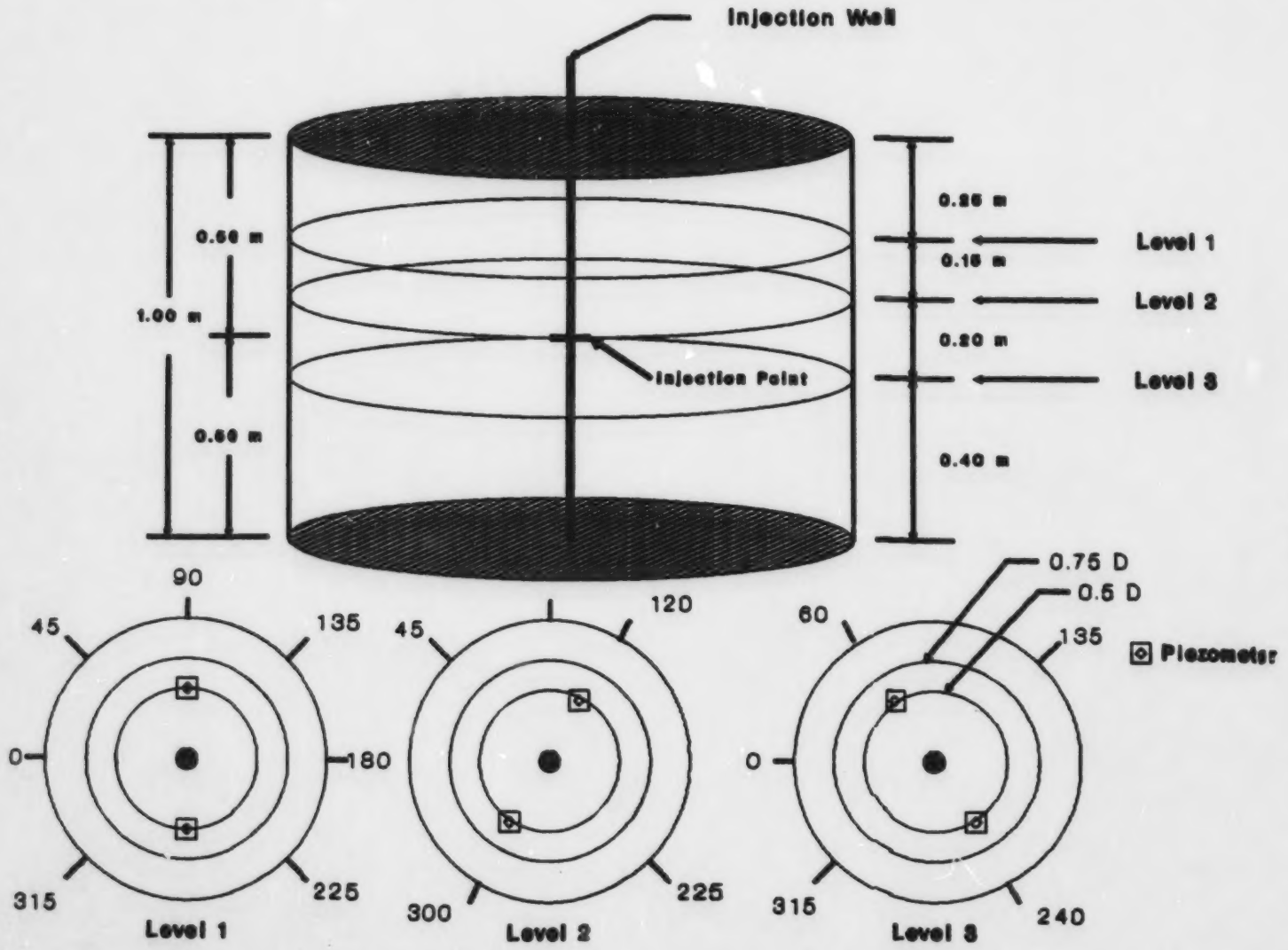

INSTRUMENTATION DETAIL FOR FRACTURE SIMULATIONS

Figure 2.8

Golder Associates

PROJECT No. 912-2055 DRAWN RR REVIEWED KMK DATE APR 92

Fracture Test No. 2 - Sample Dimensions

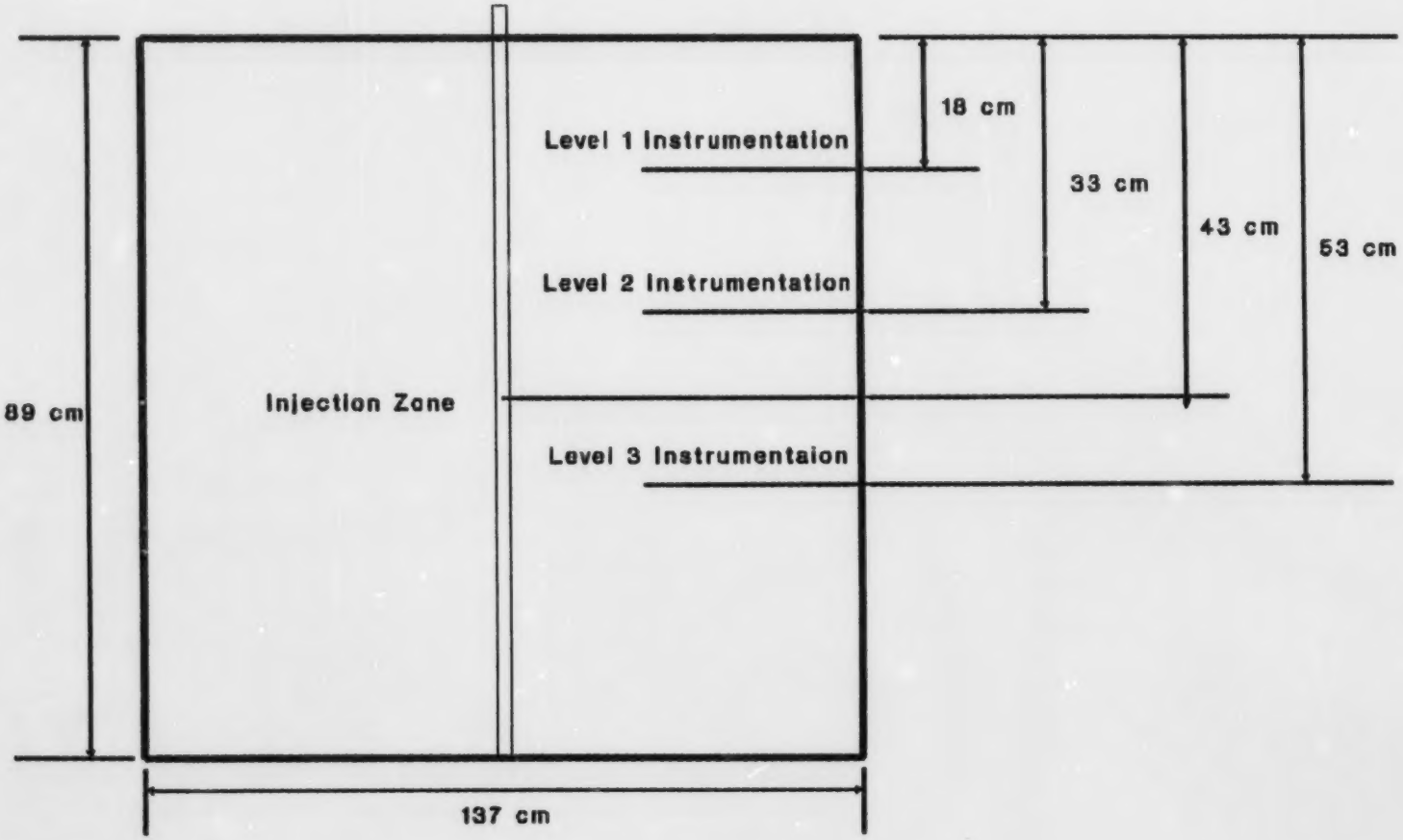

Golder Associates

FRACTURE TEST No. 2
SAMPLE DIMENSIONS

Figure 3.1

FRACTURE TEST No. 2
RESPONSE OF FLUID PRESSURE TRANSDUCERS

Figure 3.2

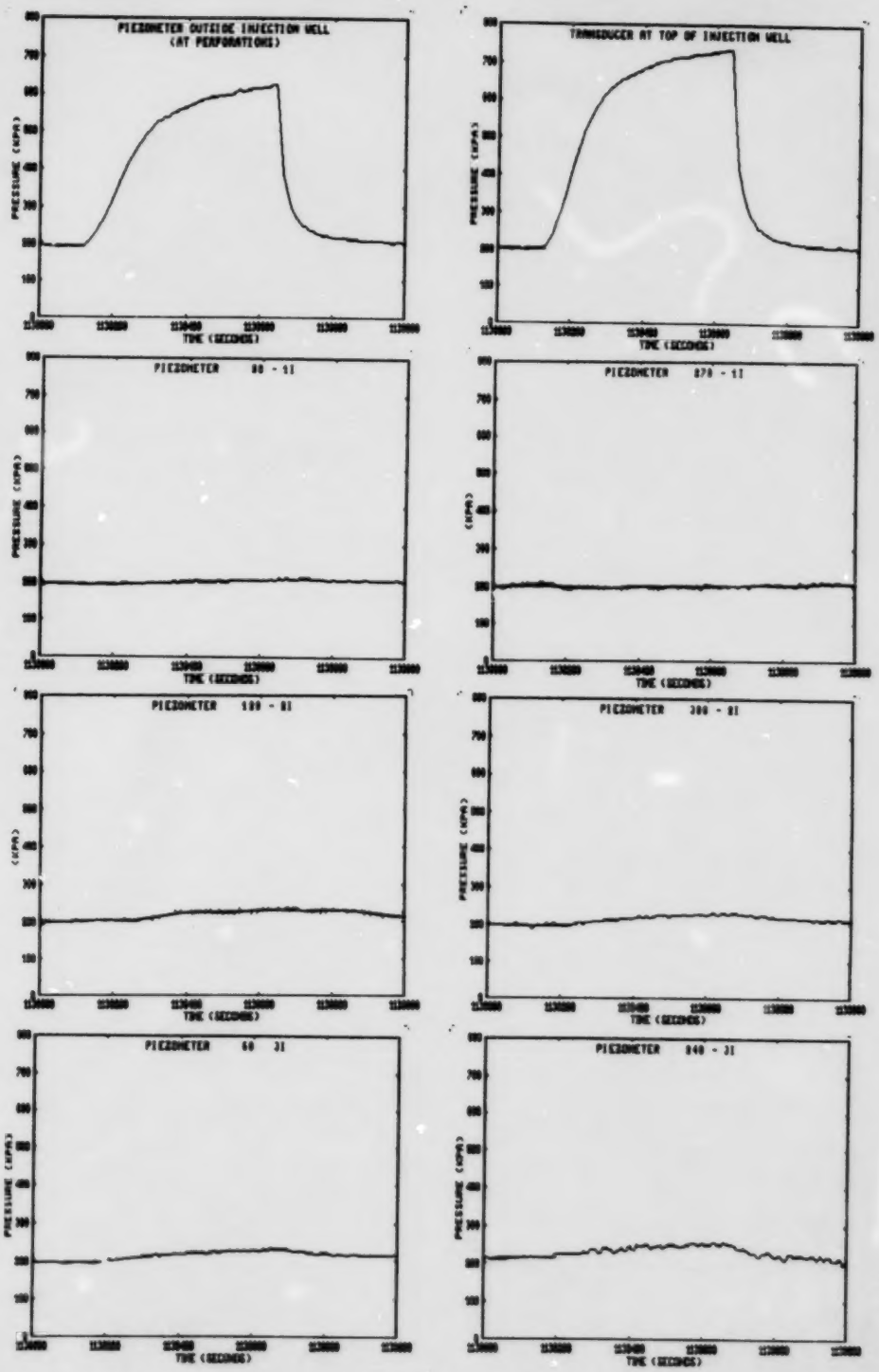

PROJECT No. 912-2055 DRAWN RR REVIEWED KMK DATE APR 92

FRACTURE TEST No. 2
PATTERN OF FLUORESCENT DYE IN SAMPLE

Figure 3.3

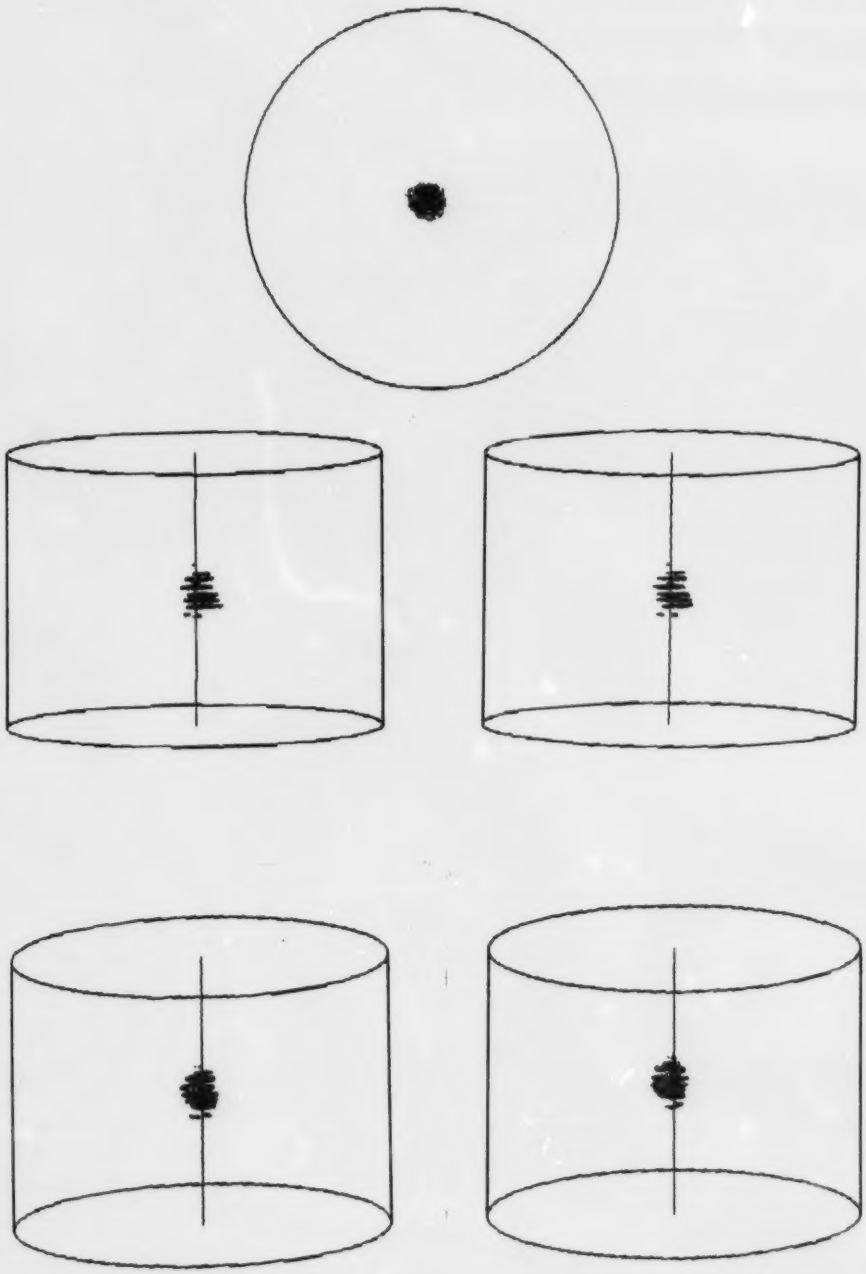

PROJECT No. 912-2055 DRAWN RR REVIEWED KnK DATE APR 92

PROJECT No. 912-2055 DRAWN RR REVIEWED KMK DATE APR 92

Fracture Test No. 3 - Sample Dimensions

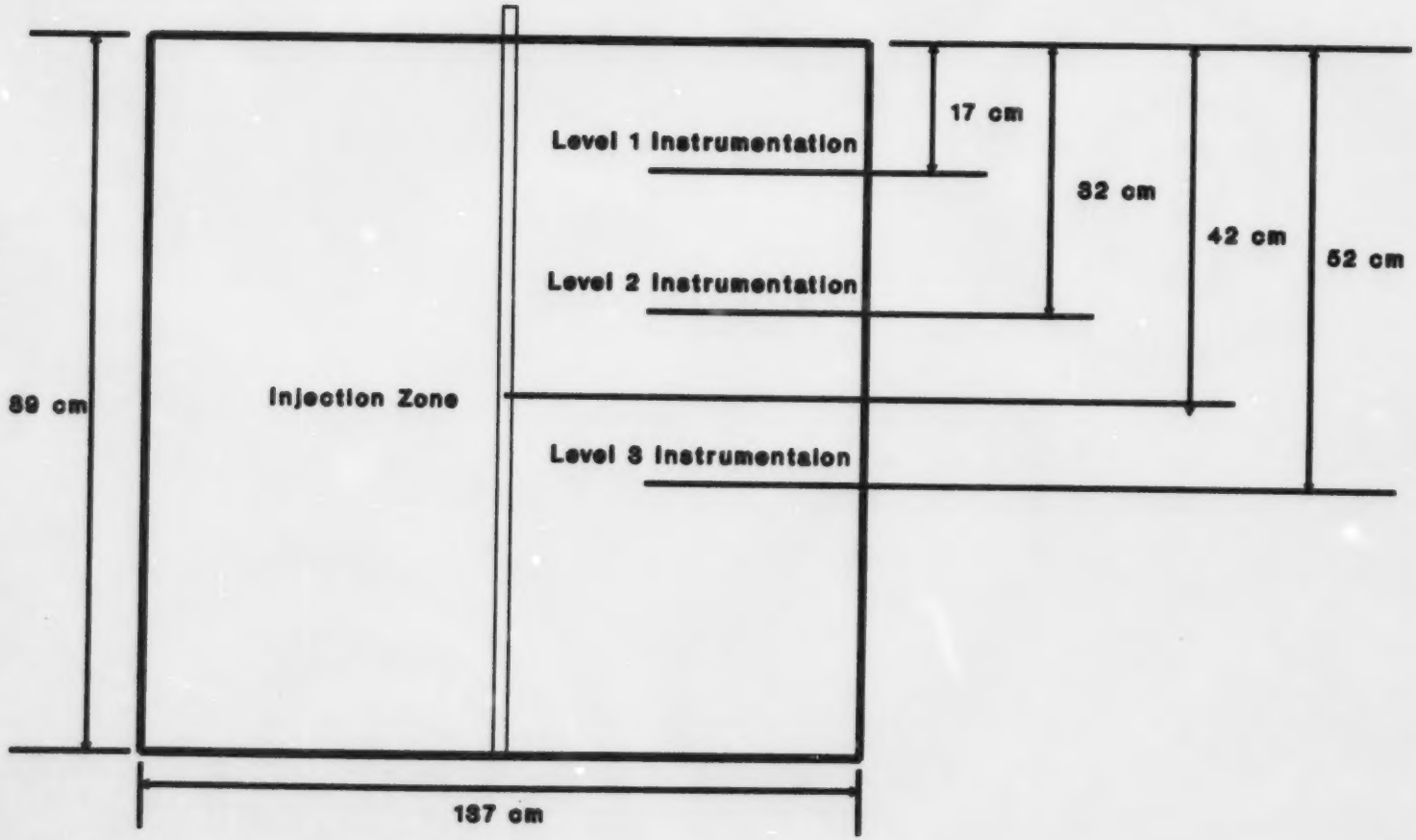

FRACTURE TEST No. 3
SAMPLE DIMENSIONS

Figure 3.4

Golder Associates

FRACTURE TEST No. 3
RESPONSE OF FLUID PRESSURE TRANSDUCERS

Figure 3.5

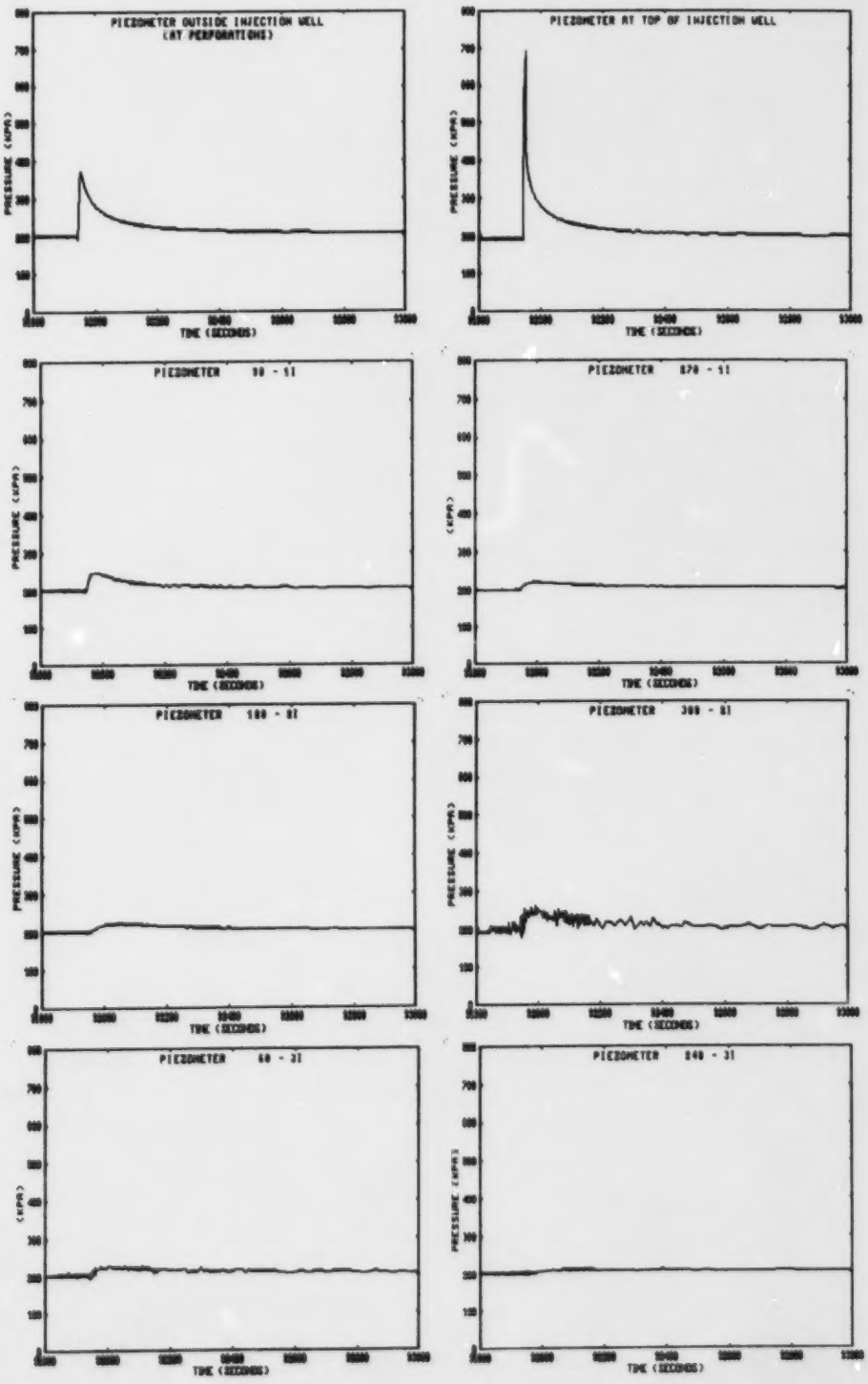

PROJECT No. 912-2055 DRAWN RR REVIEWED KMK DATE APR 92

FRACTURE TEST No. 3
PATTERN OF FLUORESCENT DYE IN SAMPLE

Figure 3.6

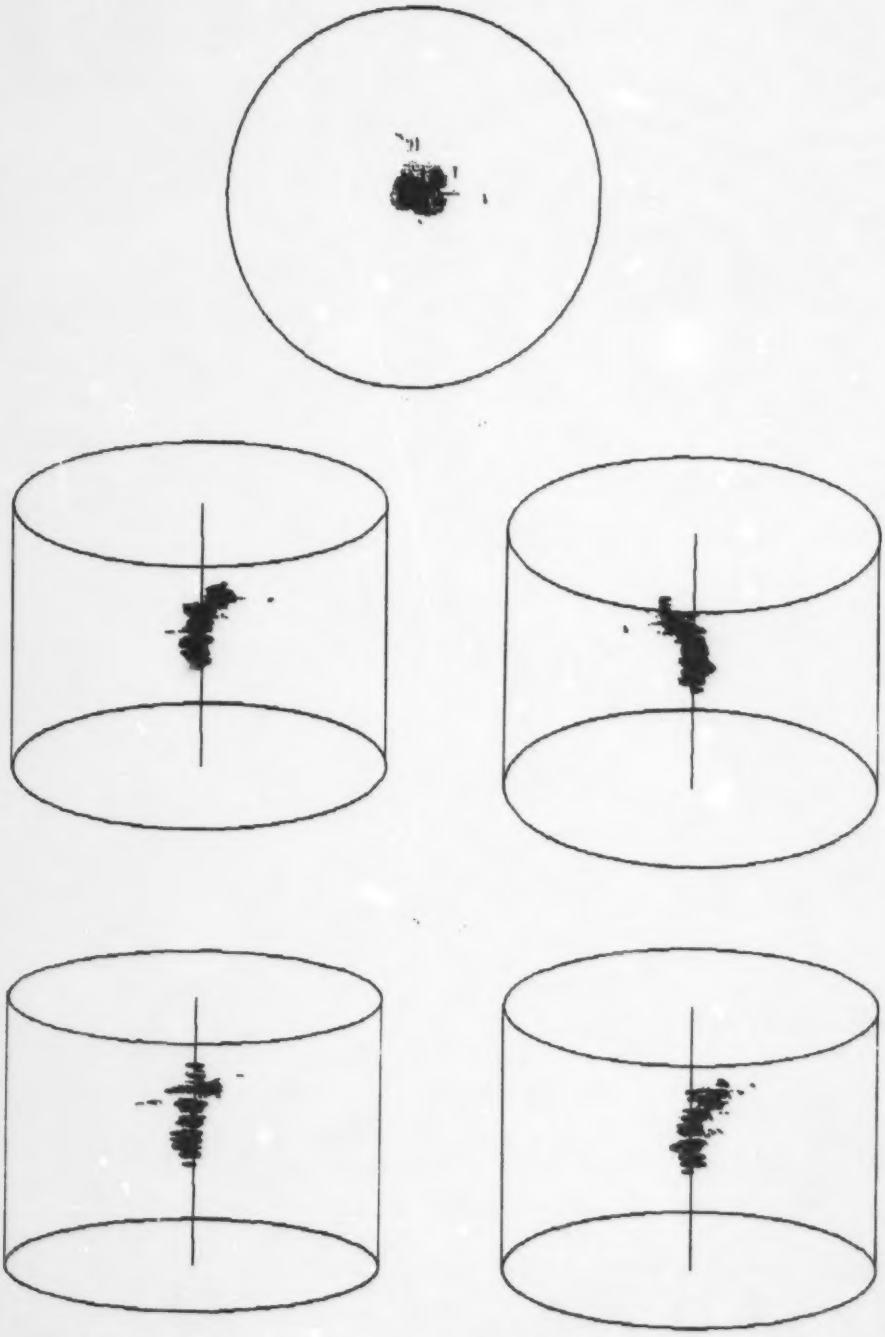

PROJECT No. 912-2055 DRAWN RR REVIEWED KHK DATE APR 92

PROJECT No. 912-2055 DRAWN RR REVIEWED KHK DATE APR 92

Fracture Test No. 4 - Sample Dimensions

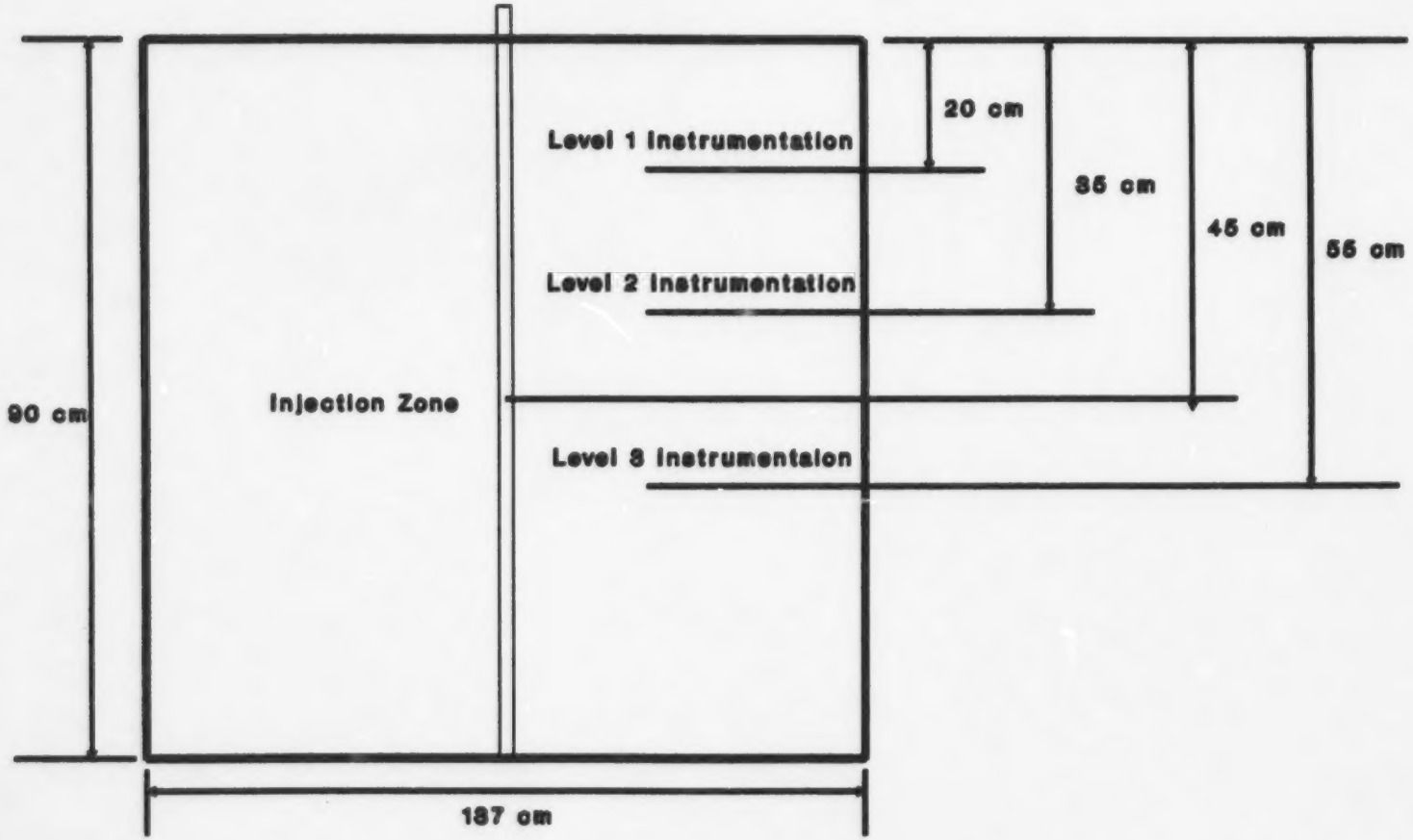

FRACTURE TEST No. 4
SAMPLE DIMENSIONS

Figure 3.7

Golder Associates

FRACTURE TEST No. 4
RESPONSE OF FLUID PRESSURE TRANSDUCERS

Figure 3.8

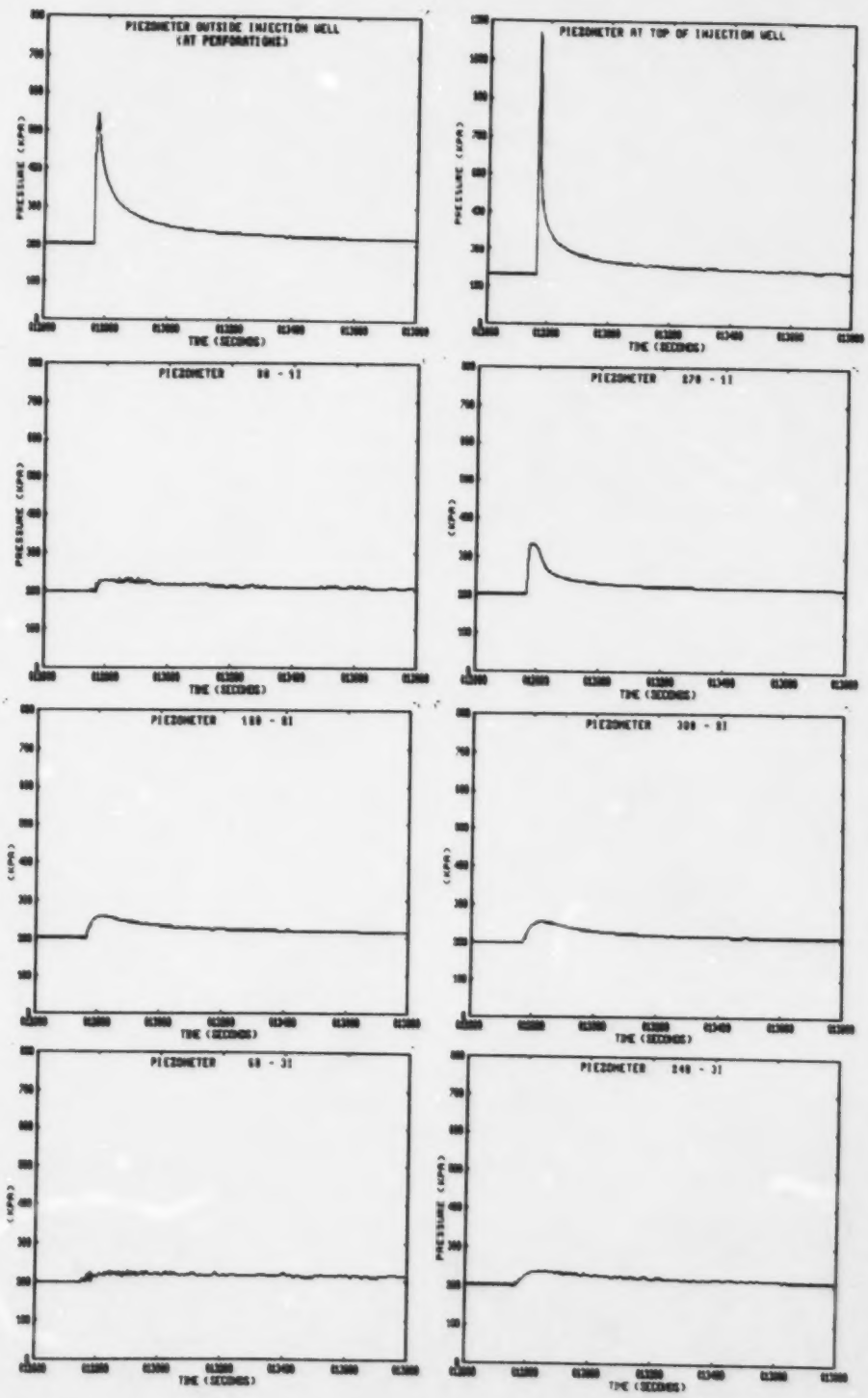

PROJECT No. 912-2055 DRAWN RR REVIEWED KHK DATE APR 92

FRACTURE TEST No. 4
PATTERN OF FLUORESCENT DYE IN SAMPLE

Figure 3.9

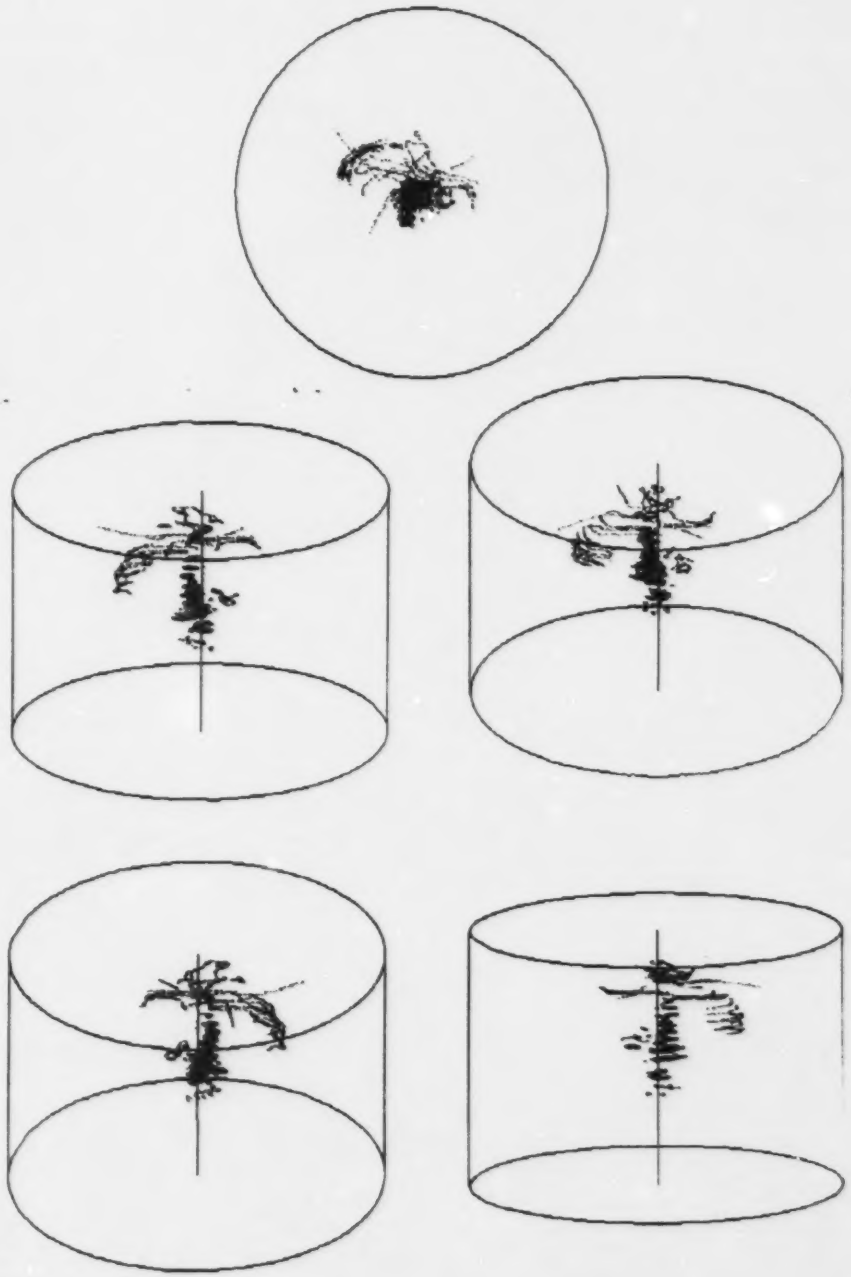

PROJECT No. 912-2055 DRAWN RR REVIEWED KHK DATE APR 92

PROJECT No. 912-2055 DRAWN RR REVIEWED KMK DATE APR 92

Fracture Test No. 5 - Sample Dimensions

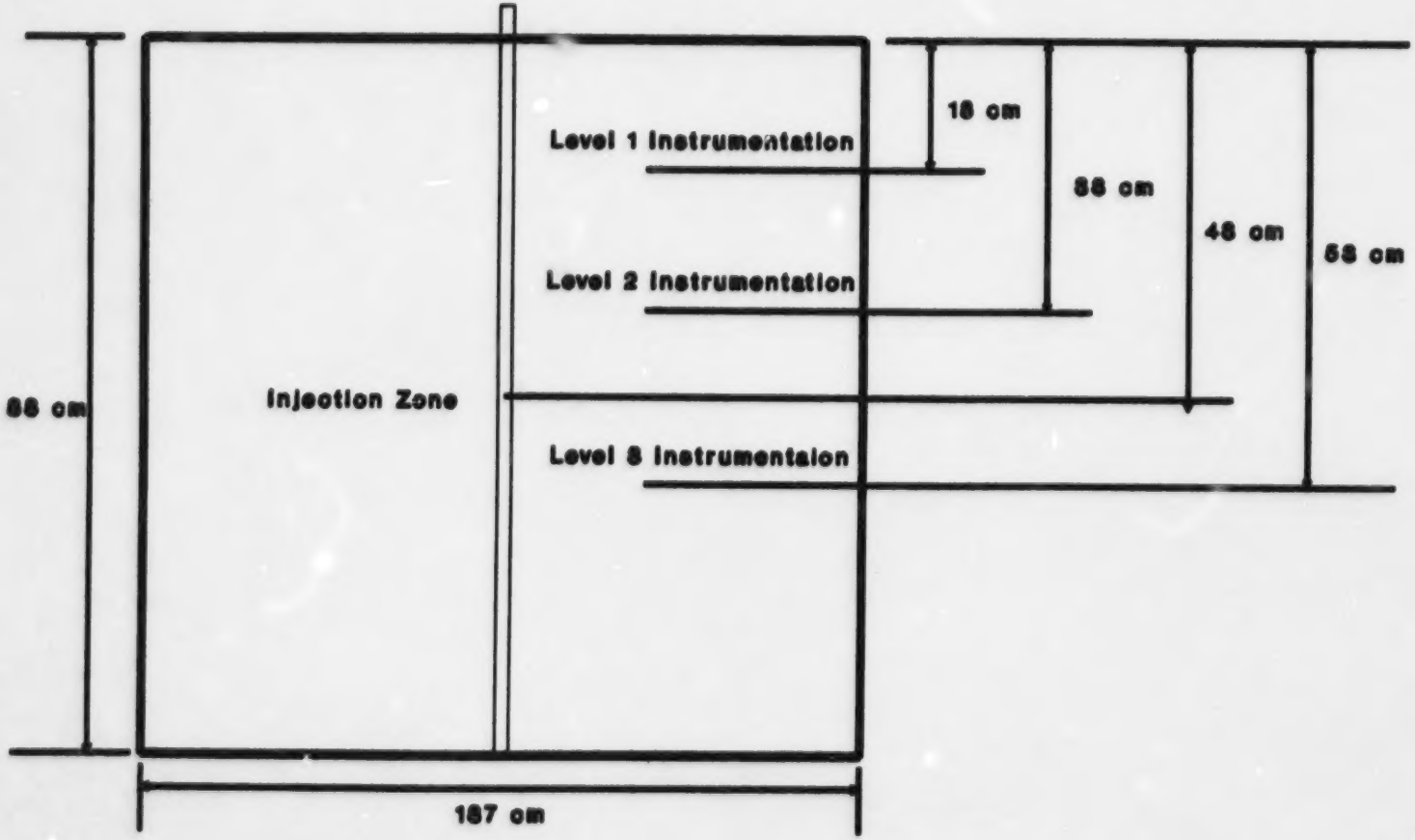

FRACTURE TEST No. 5
SAMPLE DIMENSIONS

Figure 3.10

Golder Associates

FRACTURE TEST No. 5
RESPONSE OF FLUID PRESSURE TRANSDUCERS

Figure 3.11

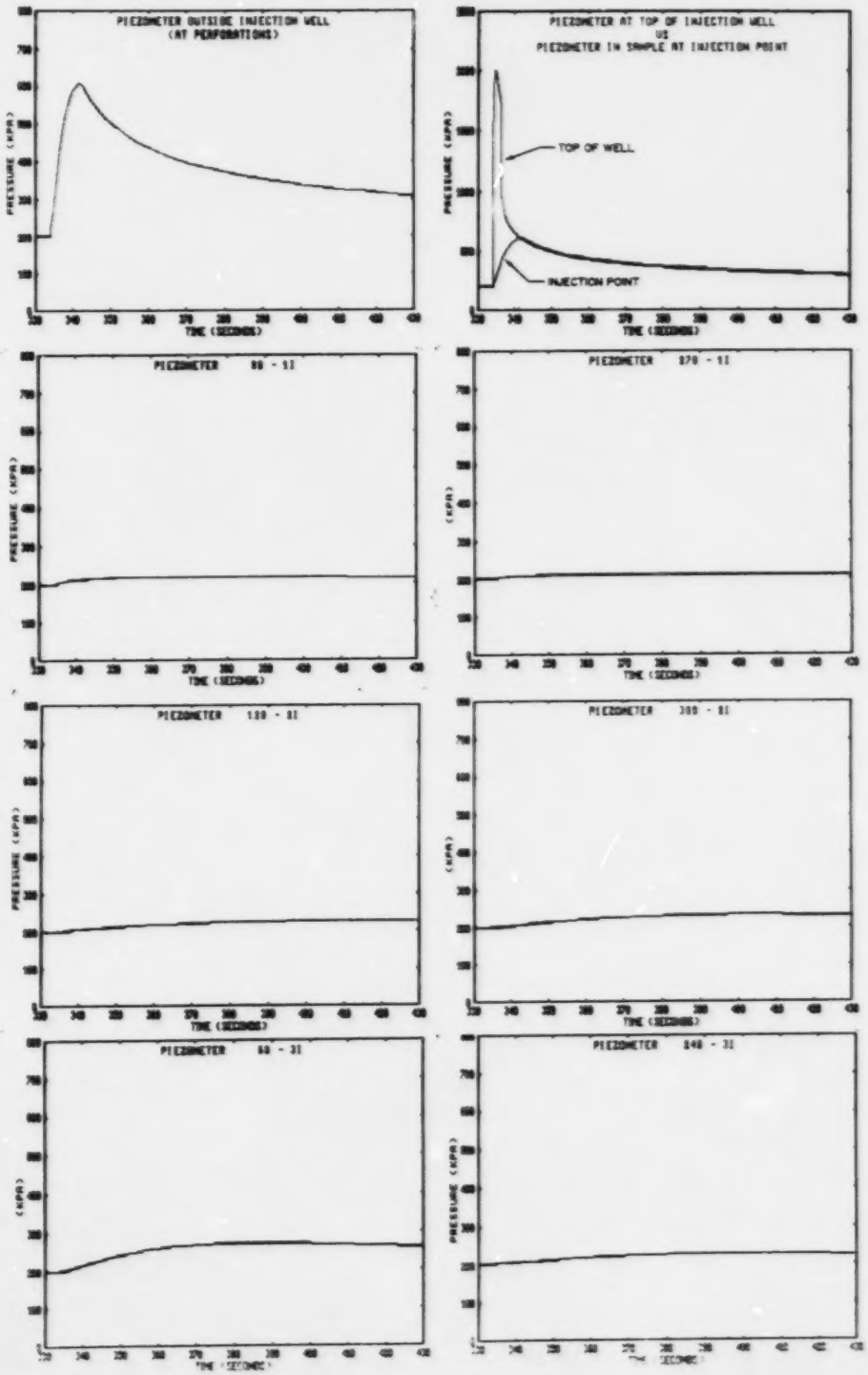

PROJECT No. 912-2055 DRAWN RR REVIEWED KMK DATE APR 92

FRACTURE TEST No. 5
PATTERN OF FLUORESCENT DYE IN SAMPLE

Figure 3.12

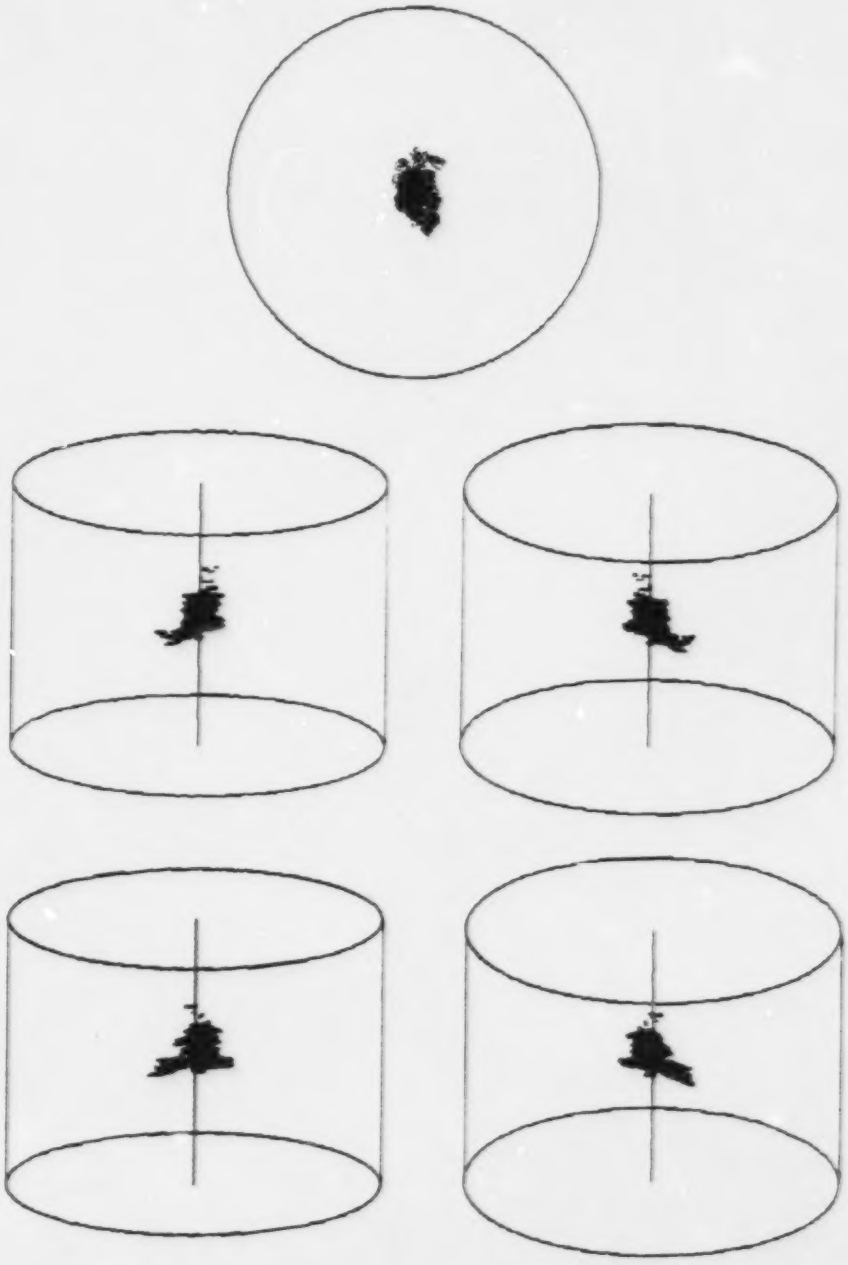

PROJECT No. 912-2055 DRAWN RR REVIEWED KHK DATE APR 92

PROJECT No. 912-2055 DRAWN RR REVIEWED KMK DATE APR 92

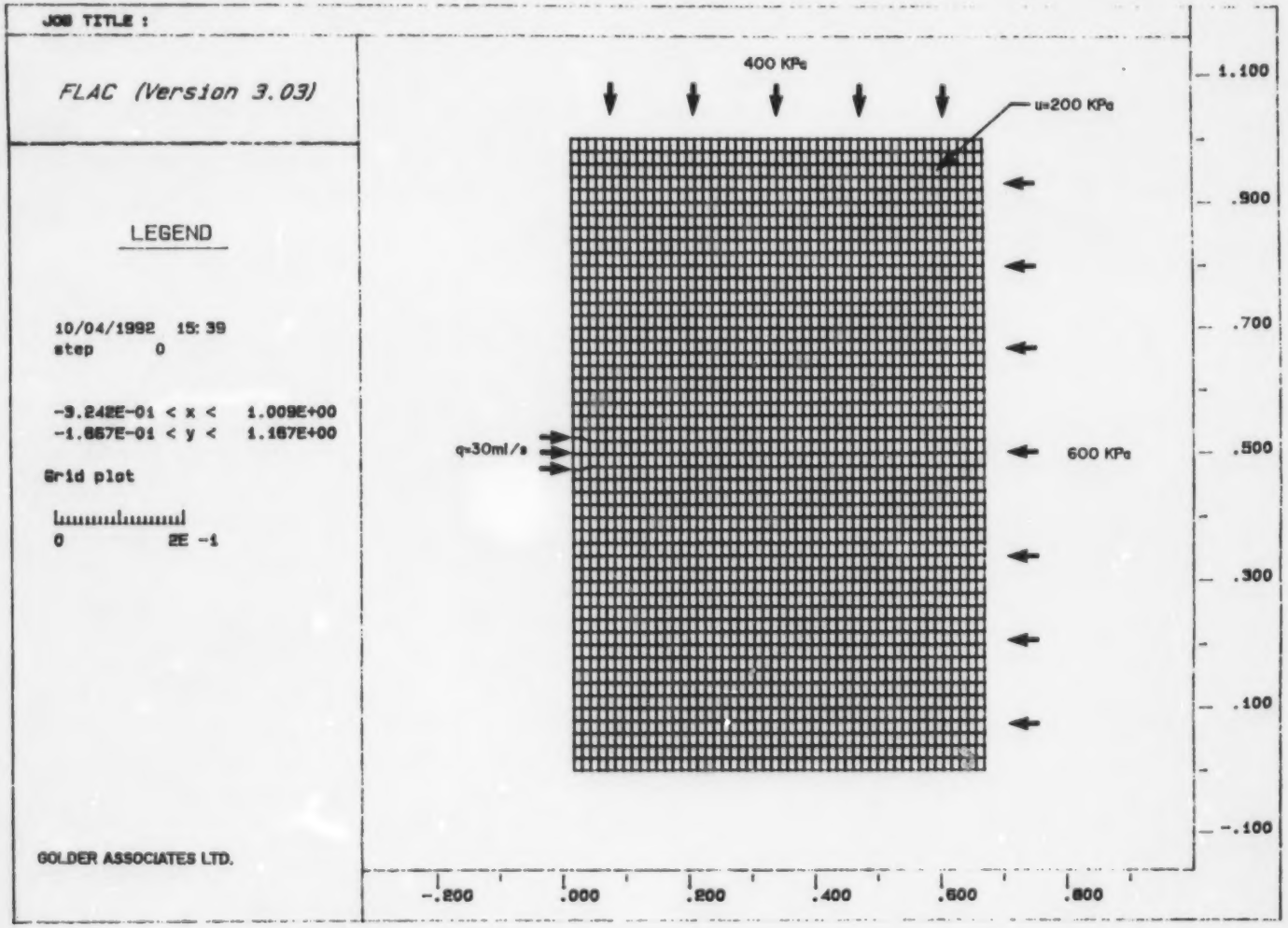

FINITE DIFFERENCE GRID

Figure 4.1

Golder Associates

PROJECT No. 912-2055 DRAWN RR REVIEWED KMK DATE APR 92

Fracture Test No. 4 - Sample Dimensions

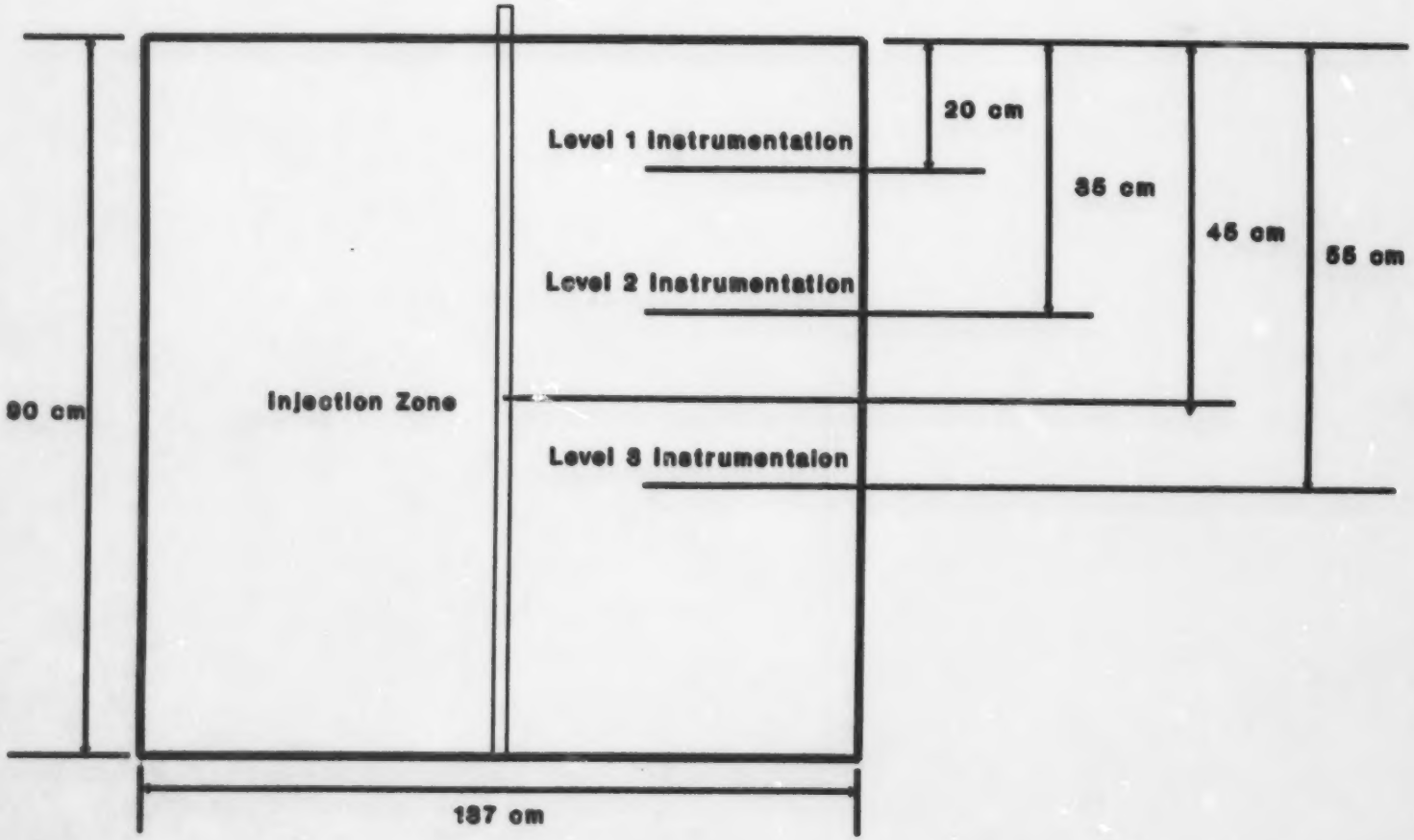

LOCATIONS FOR MONITORING PORE PRESSURE DEVELOPMENT

Figure 4.2

Golder Associates

PLOT OF MAXIMUM UNBALANCED NODAL FORCE AGAINST TIME STEP

Figure 4.3

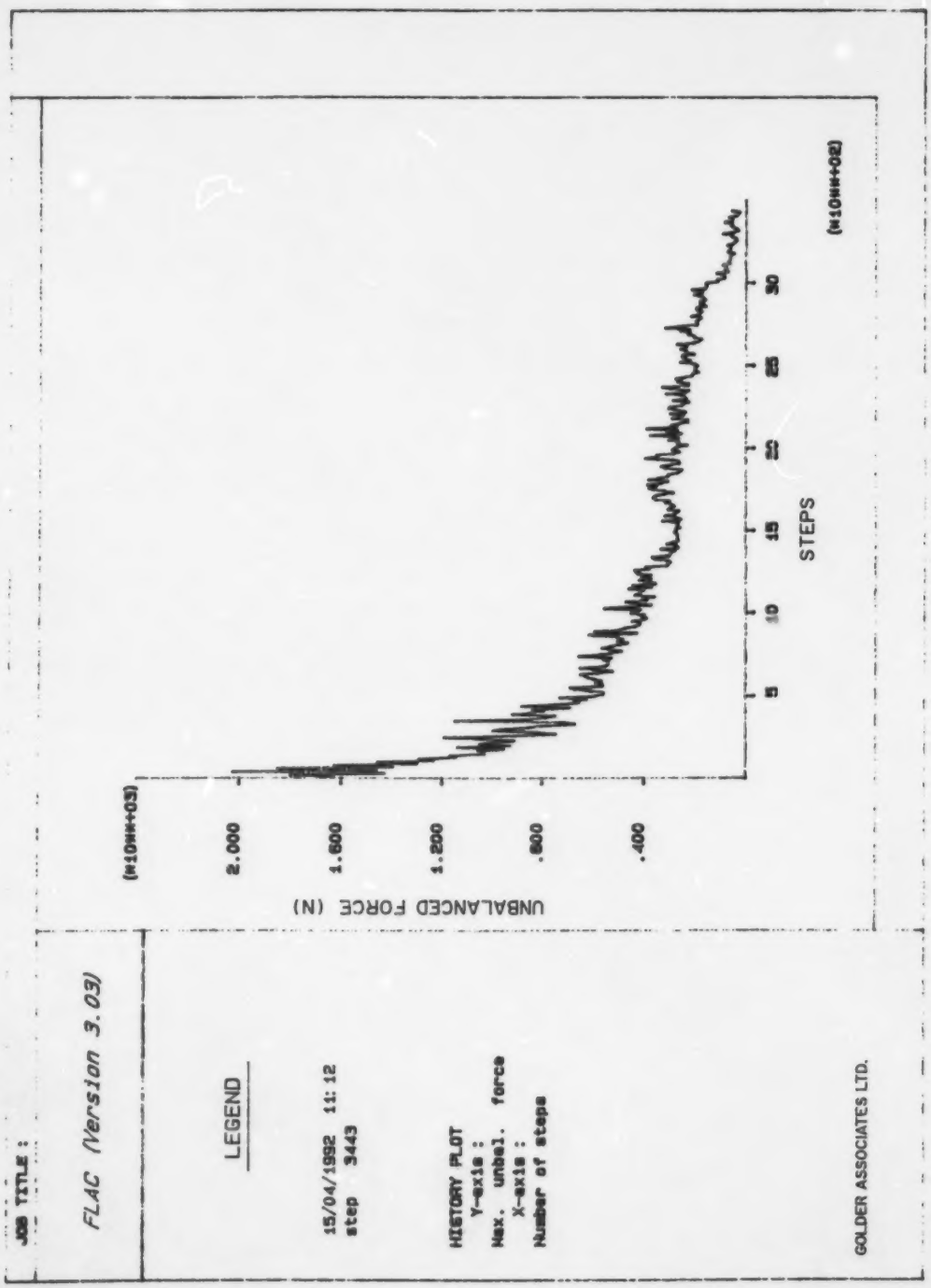

PROJECT No. 912-2055 DRAWN RR REVIEWED KMK DATE APR 92

PROJECT No. 912-2055 DRAWN RR REVIEWED KMK DATE APR 92

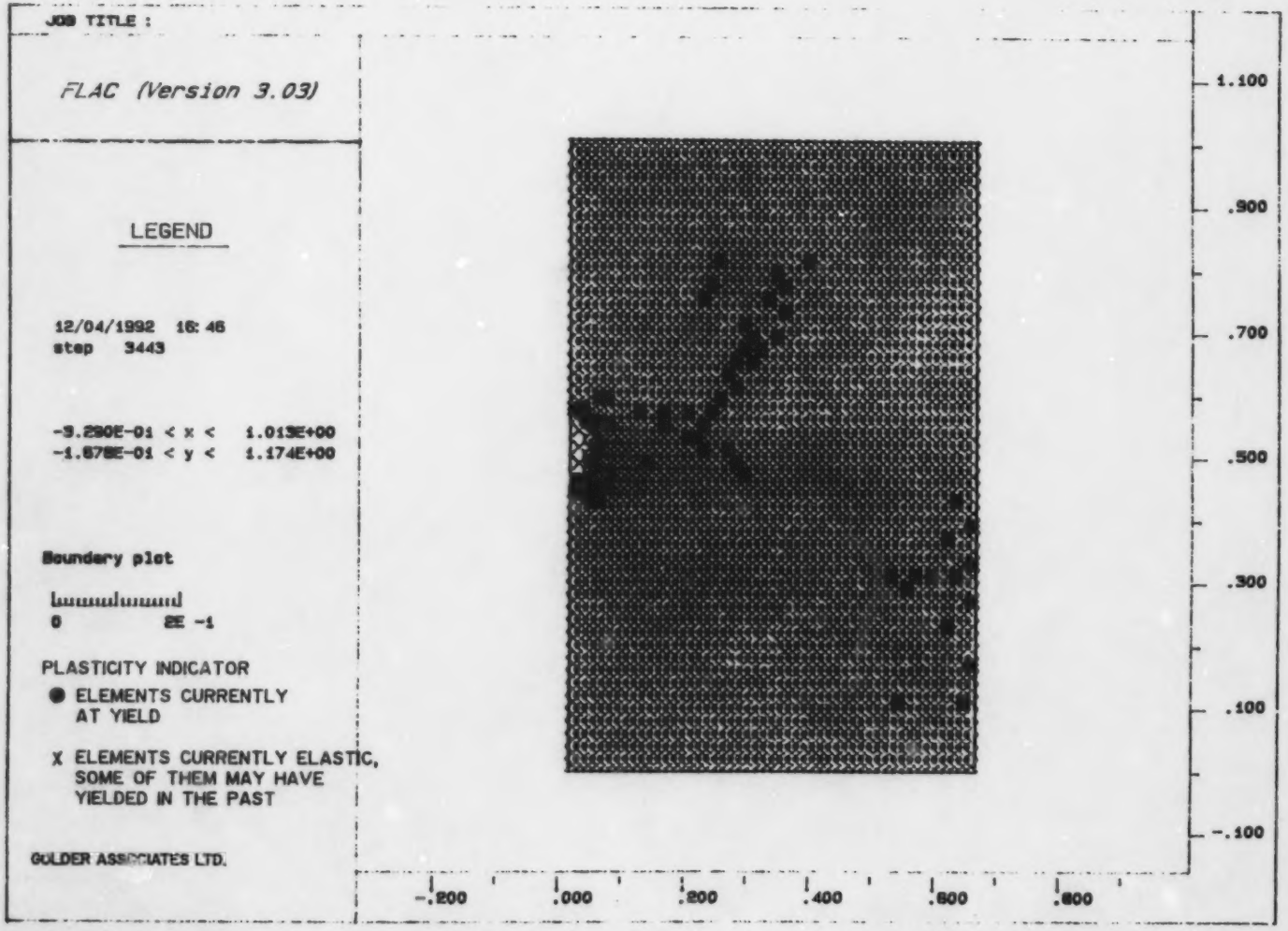

EXTENT OF YIELDING
AT END OF FLUID INJECTION

Figure 4.4

Golder Associates

DISTRIBUTION OF PORE PRESSURES AT END OF FLUID INJECTION

Figure 4.5

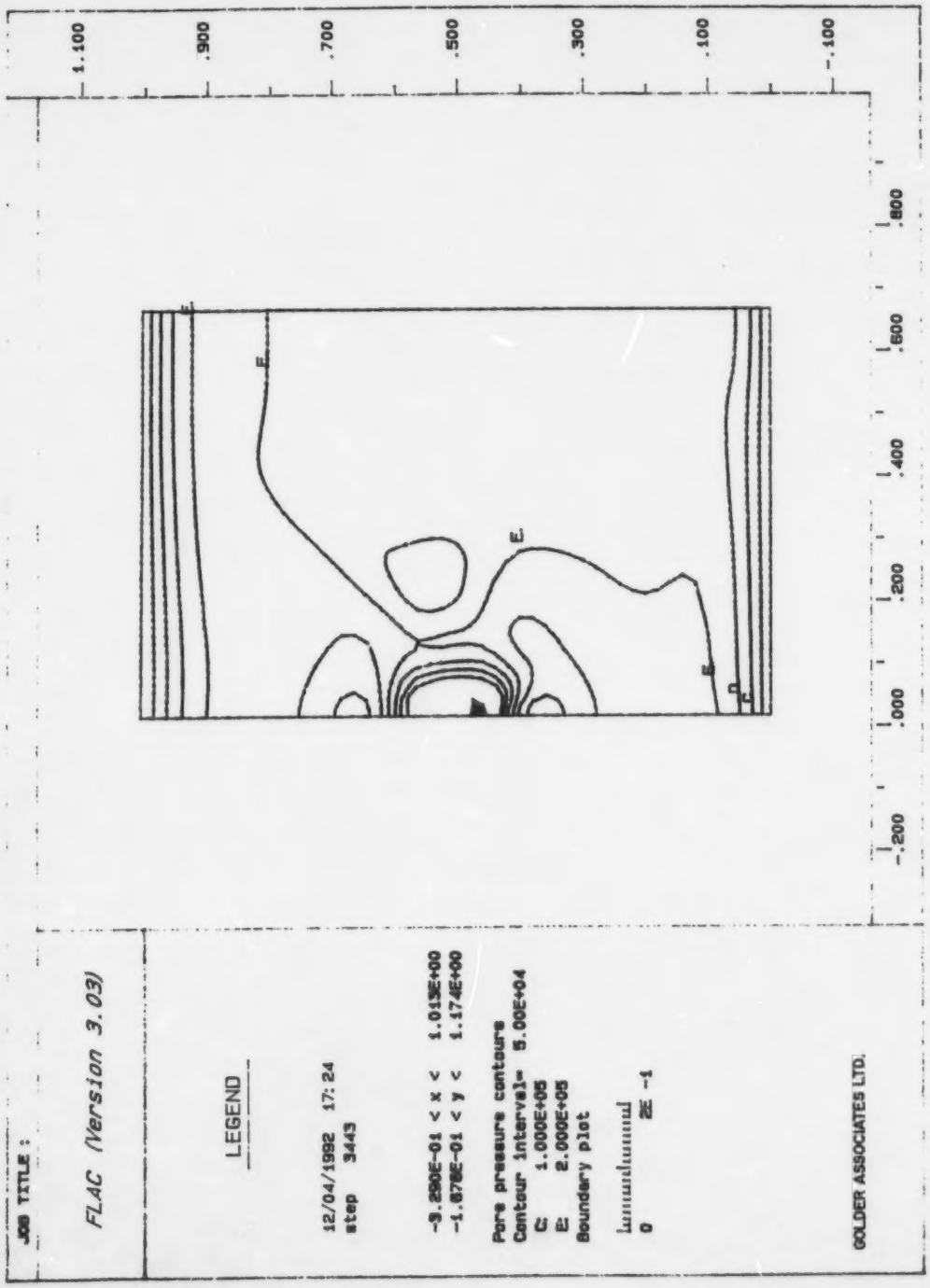

PROJECT No. 912-2055 DRAWN RR REVIEWED KAK DATE APR 92

PROJECT No. 912-2055 DRAWN RR REVIEWED KMK DATE APR 92

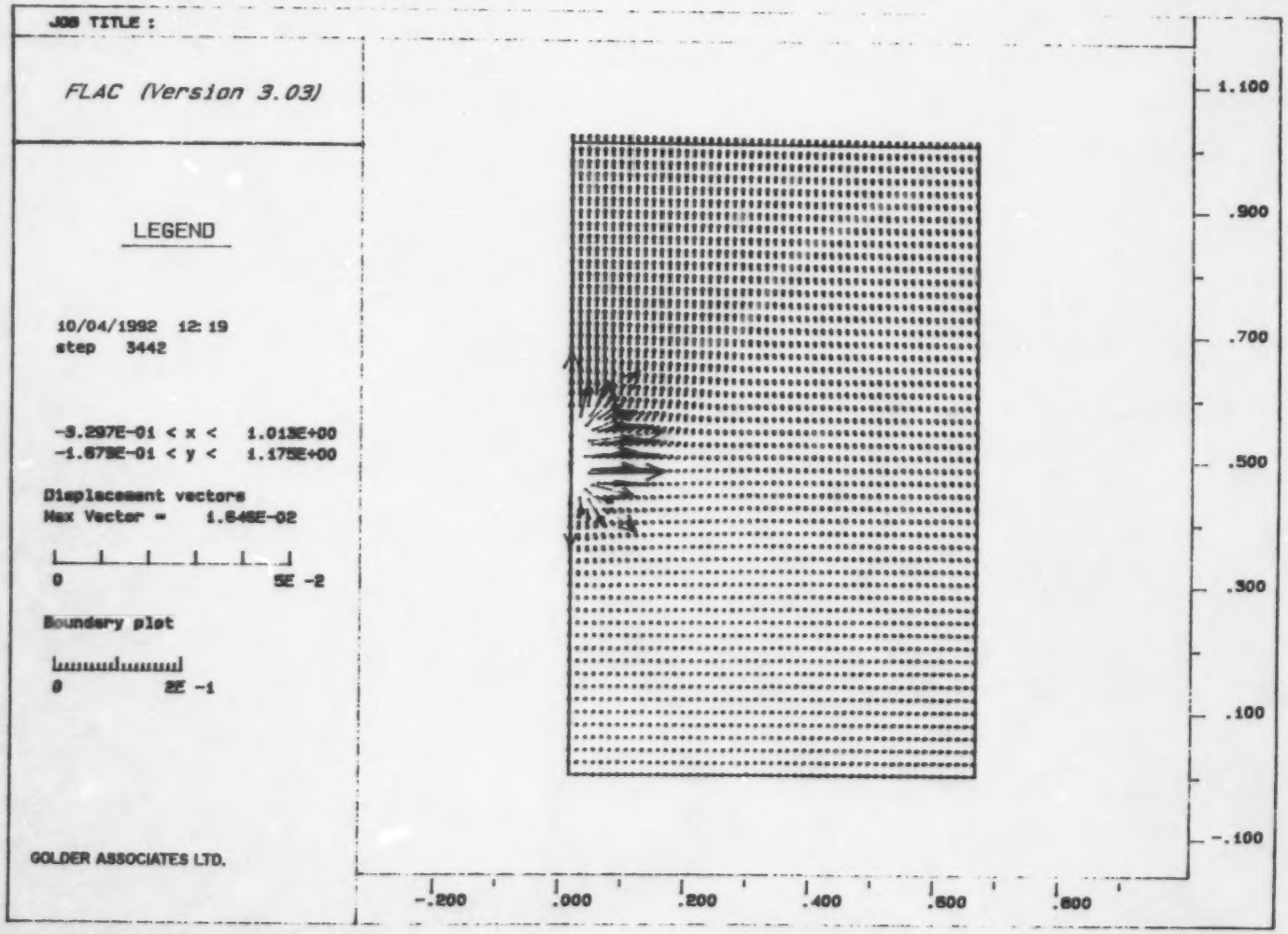

DISPLACEMENT VECTORS
AT END OF FLUID INJECTION

Figure 4.6

Golder Associates

PRINCIPAL STRESS VECTORS AT END OF FLUID INJECTION

Figure 4.7

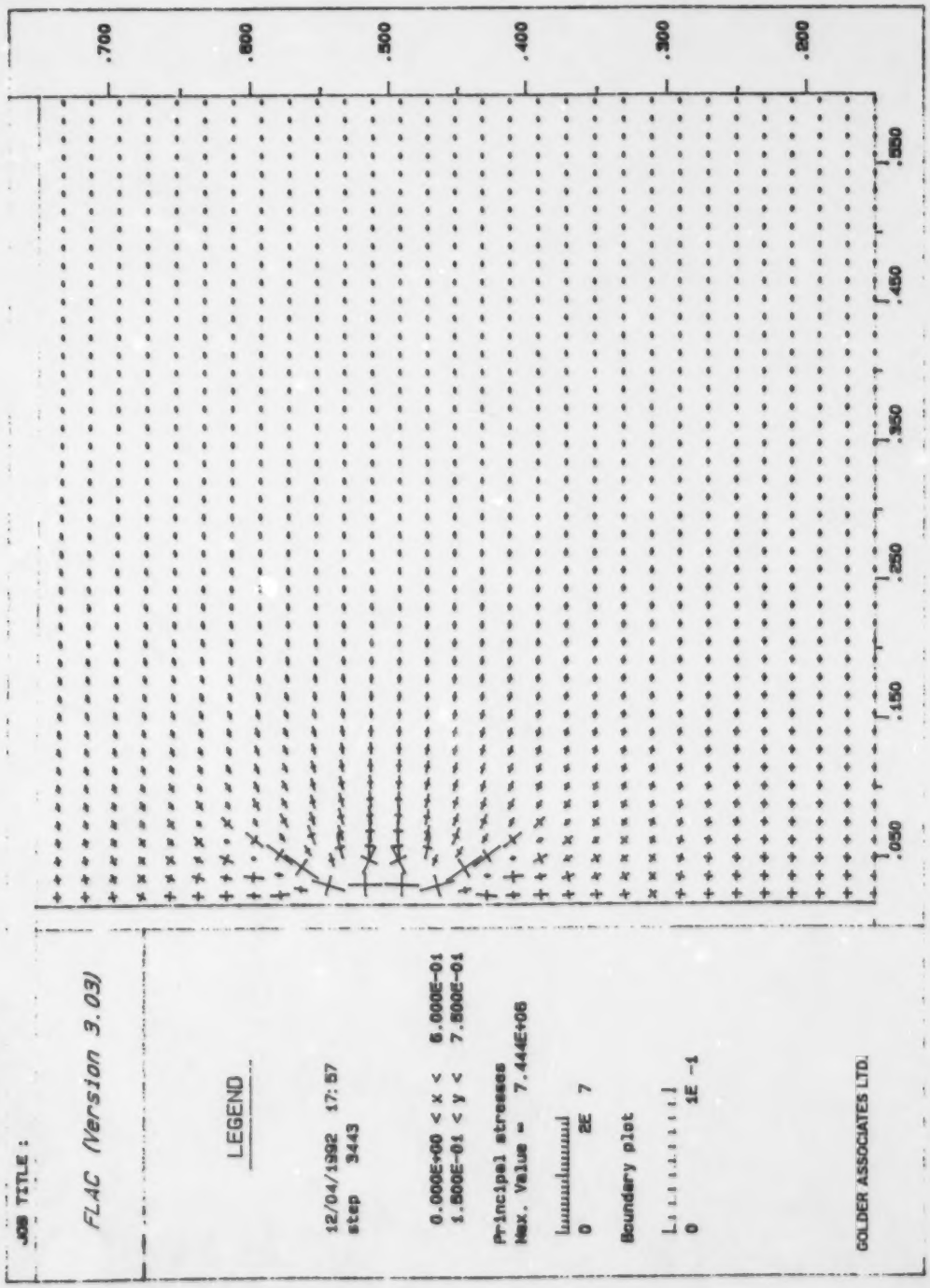

PROJECT No. 912-2035 DRAWN RR REVIEWED KMK DATE APR 92

PROJECT No. 912-2055 DRAWN RR REVIEWED KMK DATE APR 92

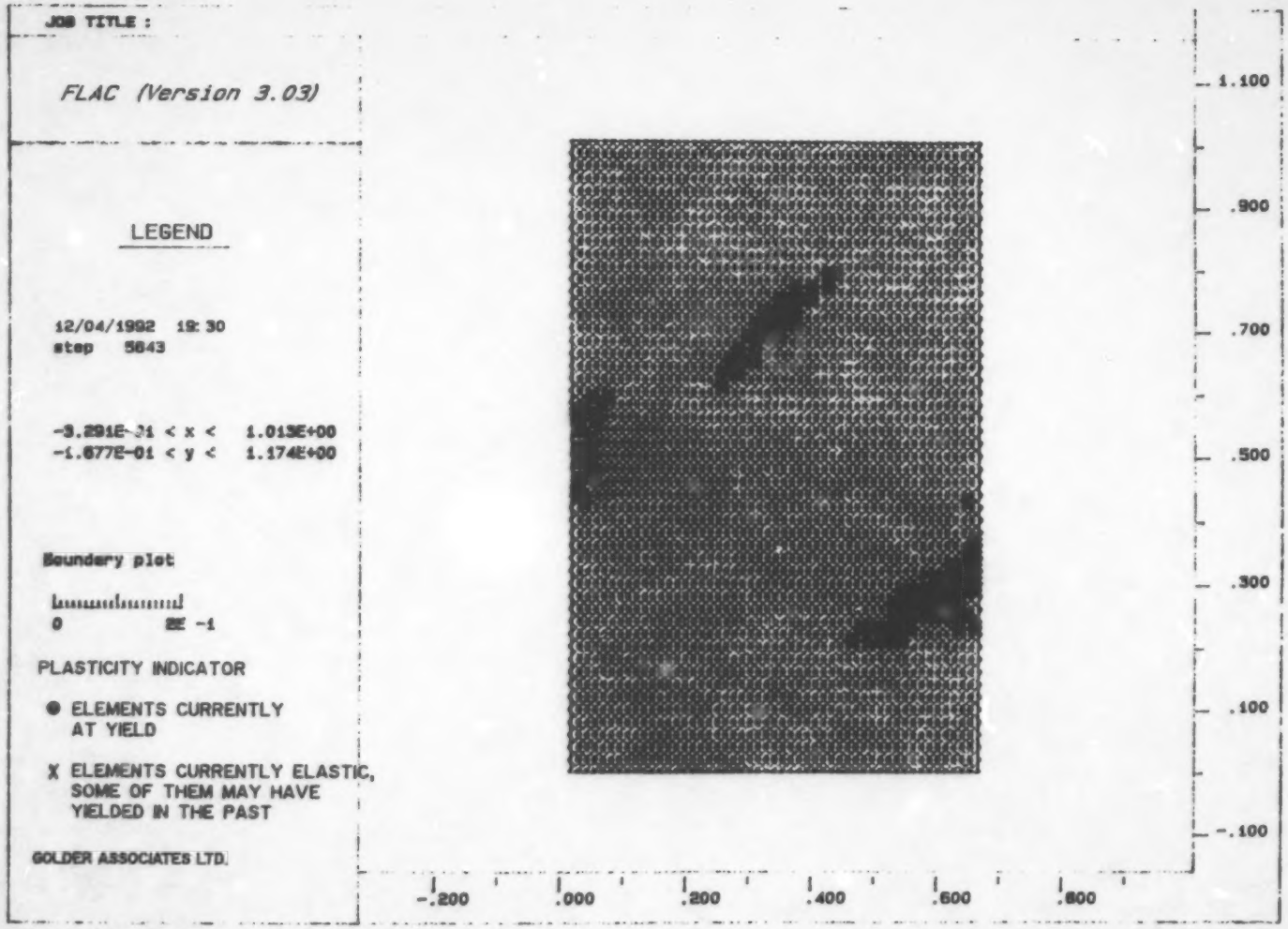

EXTENT OF YIELDING
AT END OF NUMERICAL SIMULATION

Figure 4.8

Golder Associates

DISTRIBUTION OF FLUORESCENT DYE IN LABORATORY SAMPLE

Figure 4.9

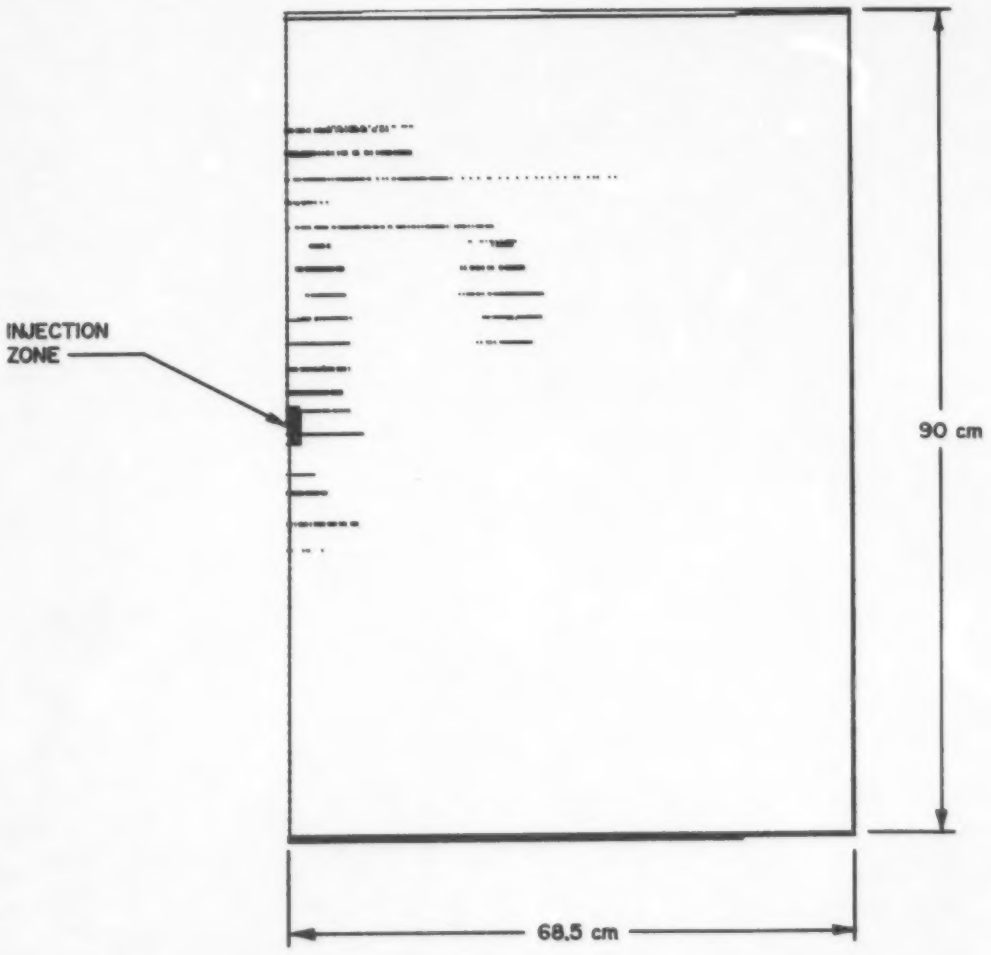

PROJECT No. 912-2055 DRAWN RR REVIEWED KMK DATE APR 92

PLOT OF PORE PRESSURE DEVELOPMENT (NUMERICAL VERSUS LABORATORY)

Figure 4.10

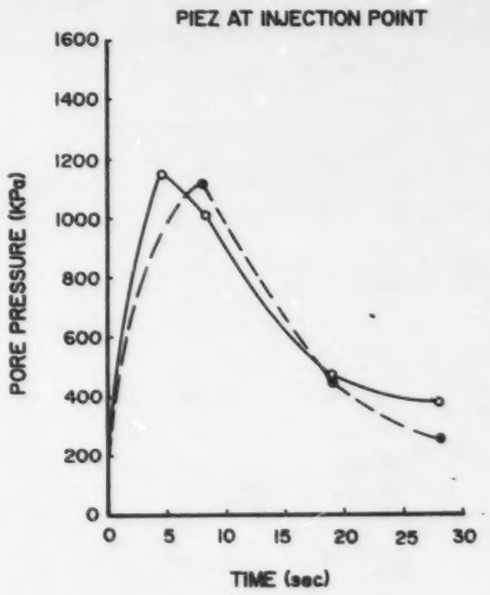

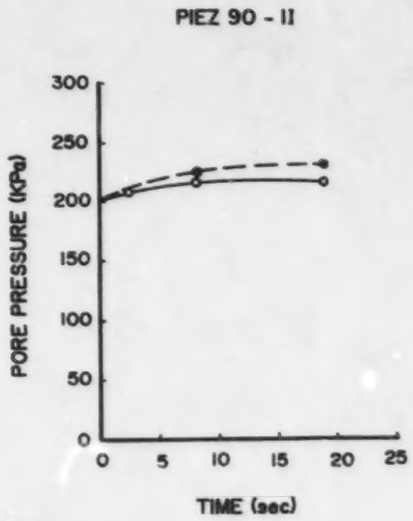

LEGEND

LABORATORY

NUMERICAL

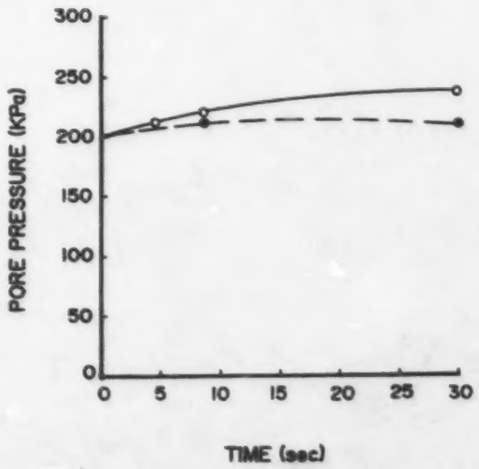

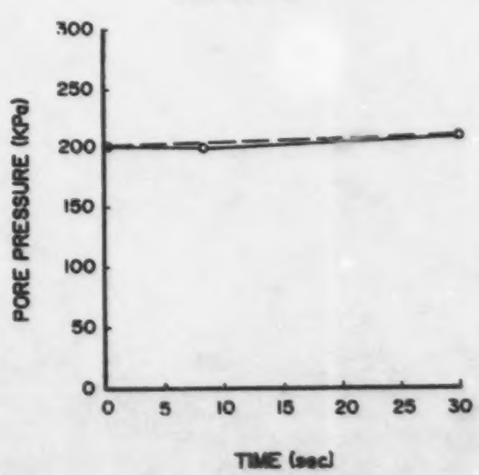

NOTE

FLOW INJECTED INTO SAMPLE AT TIME 0.

Golder Associates			
PROJECT: 912-2058	DRAWN BY: RR	DATE: APRIL 92	REVIEWED: KMK

LOCATION OF SAMPLES FOR MRI	Figure 5.1

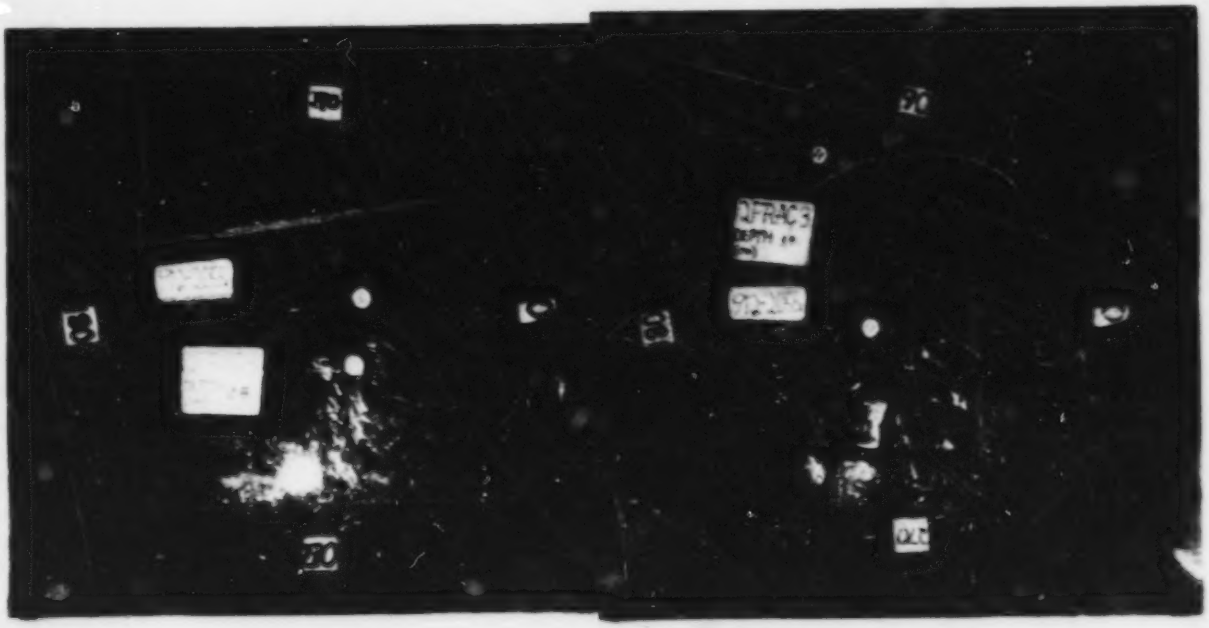

SAMPLE 2FRAC3-6

SAMPLE 2FRAC3-10

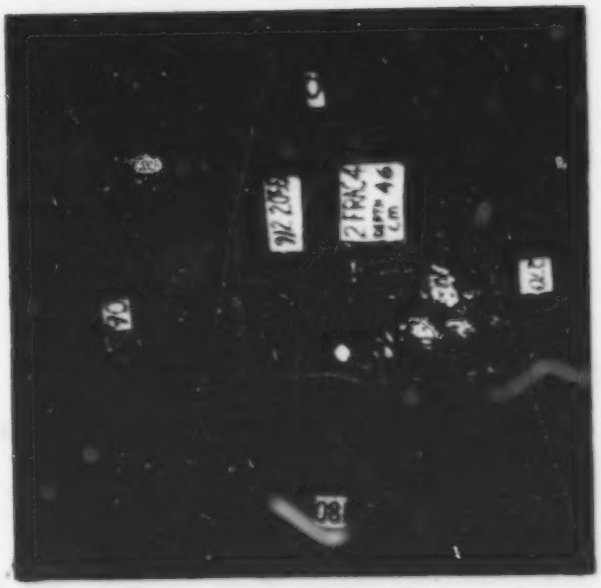

SAMPLE 2FRAC4-1

PROJECT No. 912-2055 DRAWN RR REVIEWED _____ DATE APR 92

MRI IMAGING SECTIONS

Figure 5.2

PROJECT No. 912-2055 DRAWN RR REVIEWED KMK DATE APR 92

Golder Associates

MRI OF SAMPLE 2FRAC3-6

Figure 5.3

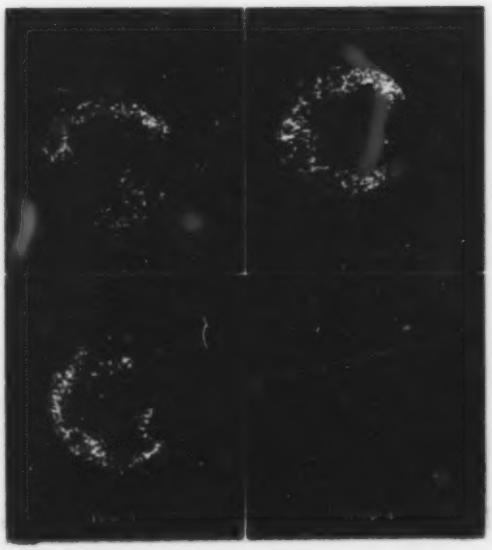

SLICE 1 IS FROM BOTTOM OF SAMPLE

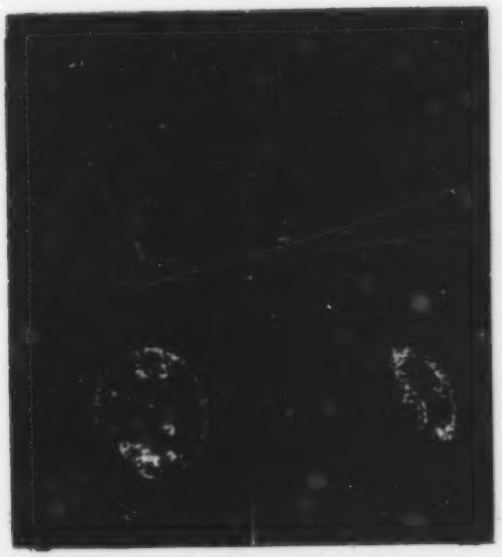

SLICE 8 IS FROM TOP OF SAMPLE

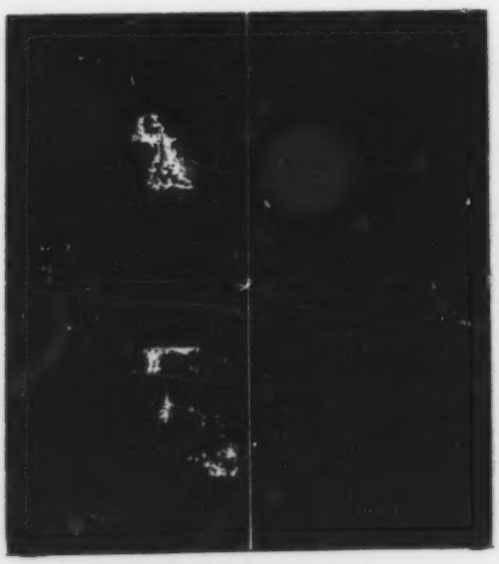

115° IS PERPENDICULAR TO AND OUT OF PAGE

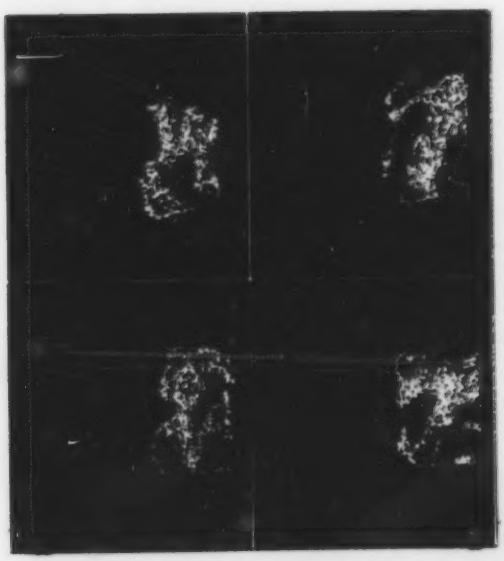

25° IS PERPENDICULAR TO AND OUT OF PAGE

PROJECT No. 912-2055 DRAWN RR REVIEWED SMK DATE APR 92

MRI OF SAMPLE 2FRAC3-10

Figure 5.4

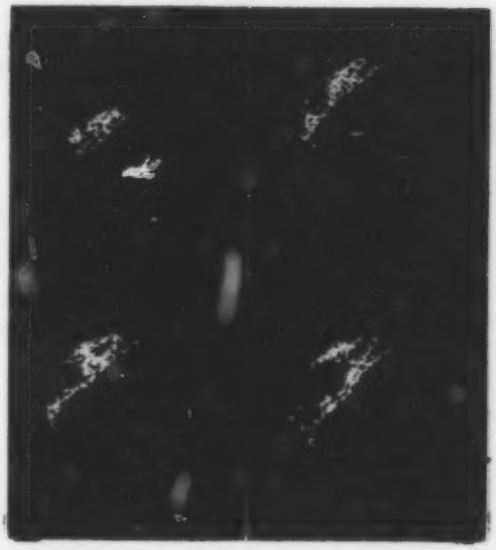

SLICE 1 IS FROM BOTTOM OF SAMPLE

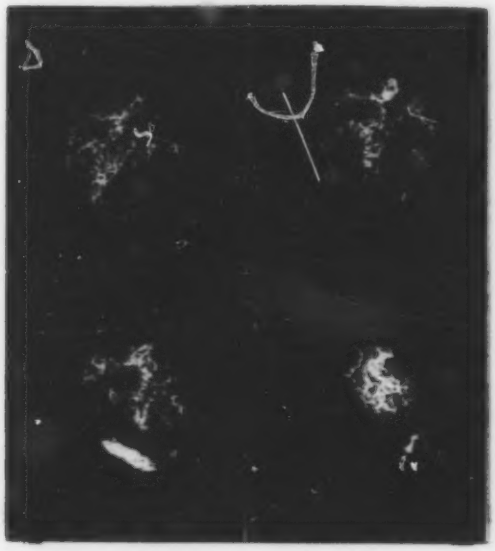

SLICE 8 IS FROM TOP OF SAMPLE

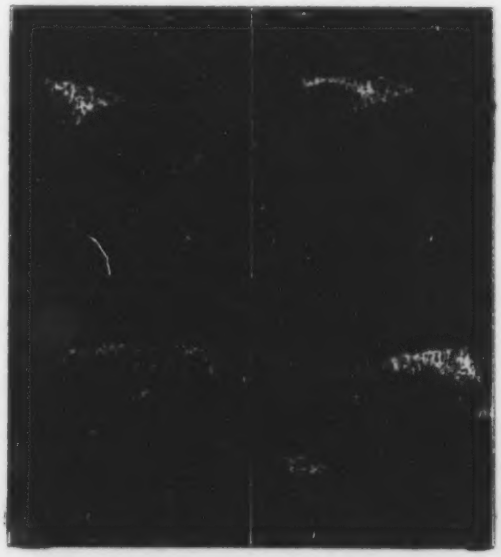

255° IS PERPENDICULAR TO AND OUT OF PAGE

165° IS PERPENDICULAR TO AND OUT OF PAGE

PROJECT No. 912-2055 DRAWN RR REVIEWED DHK DATE APR 92

MRI OF SAMPLE 2FRAC4-1

Figure 5.5

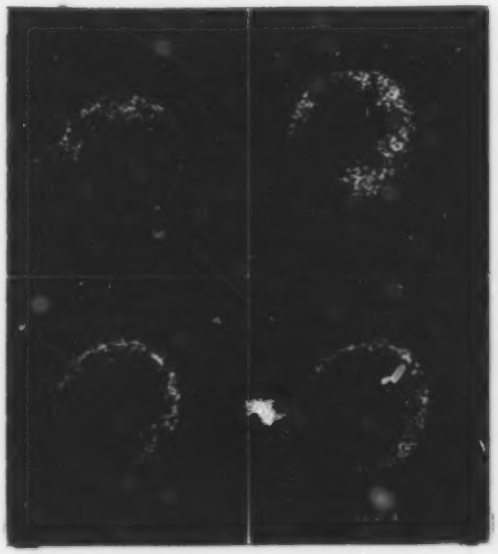

SLICE 1 IS FROM BOTTOM OF SAMPLE

SLICE 8 IS FROM TOP OF SAMPLE

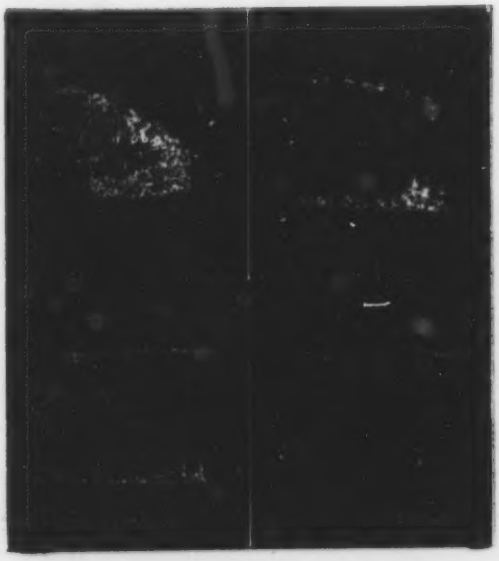

180° IS PERPENDICULAR AND
OUT OF PAGE

90° IS PERPENDICULAR AND
OUT OF PAGE

PROJECT No. 912-2055 DRAWN RR REVIEWED KAK DATE APR 92

APPENDIX I

PERMEABILITY TESTS

FRACTURE TEST 1 - PERMEABILITY TEST

q vs time (ΔP = 40 kPa)

Figure I-1

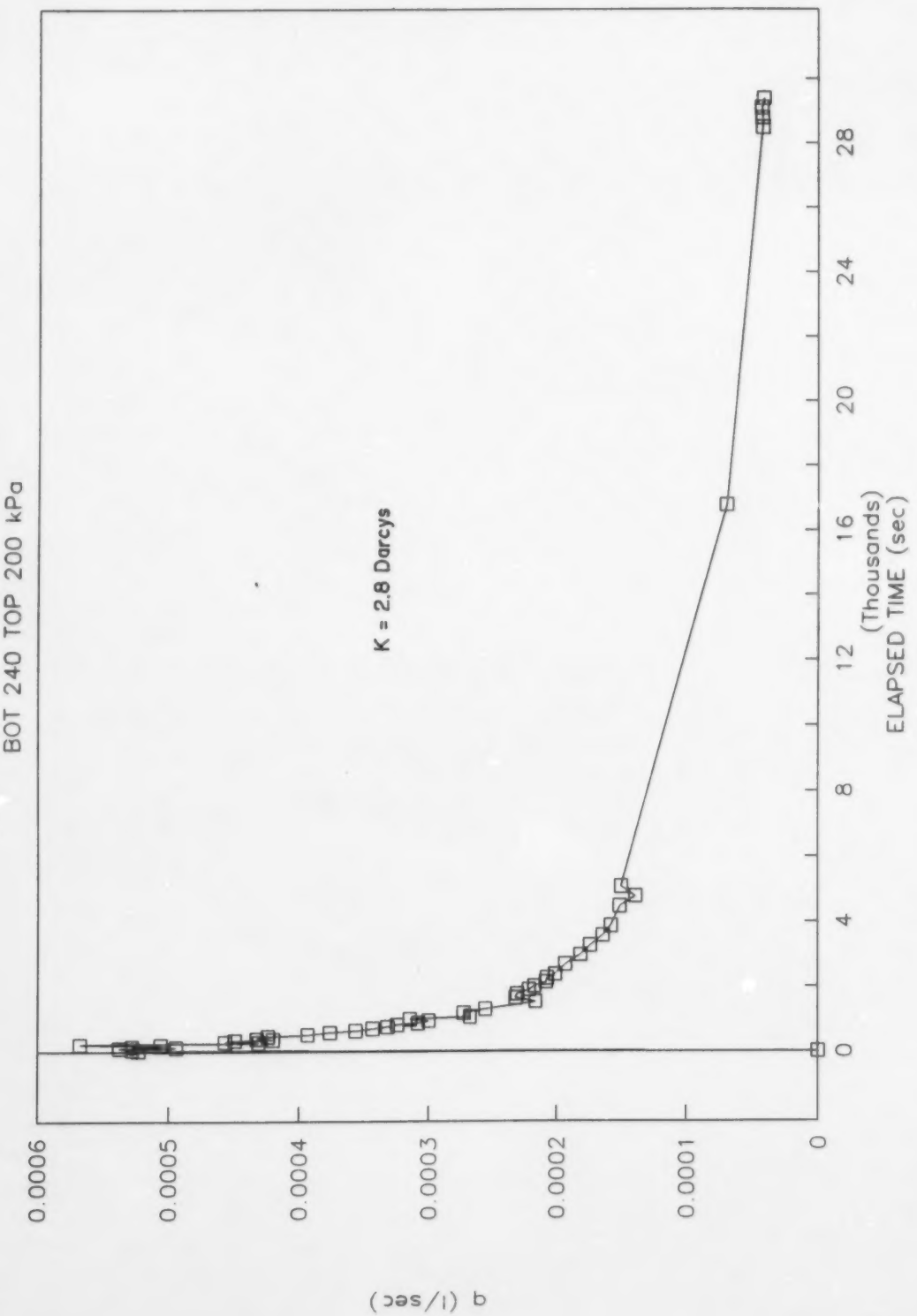

PROJECT No. 912-2055 DRAWN RR REVIEWED KMK DATE APR 92

Golder Associates

FRACTURE TEST 1 - PERMEABILITY TEST

v vs time (ΔP = 40 kPa)

Figure I-2

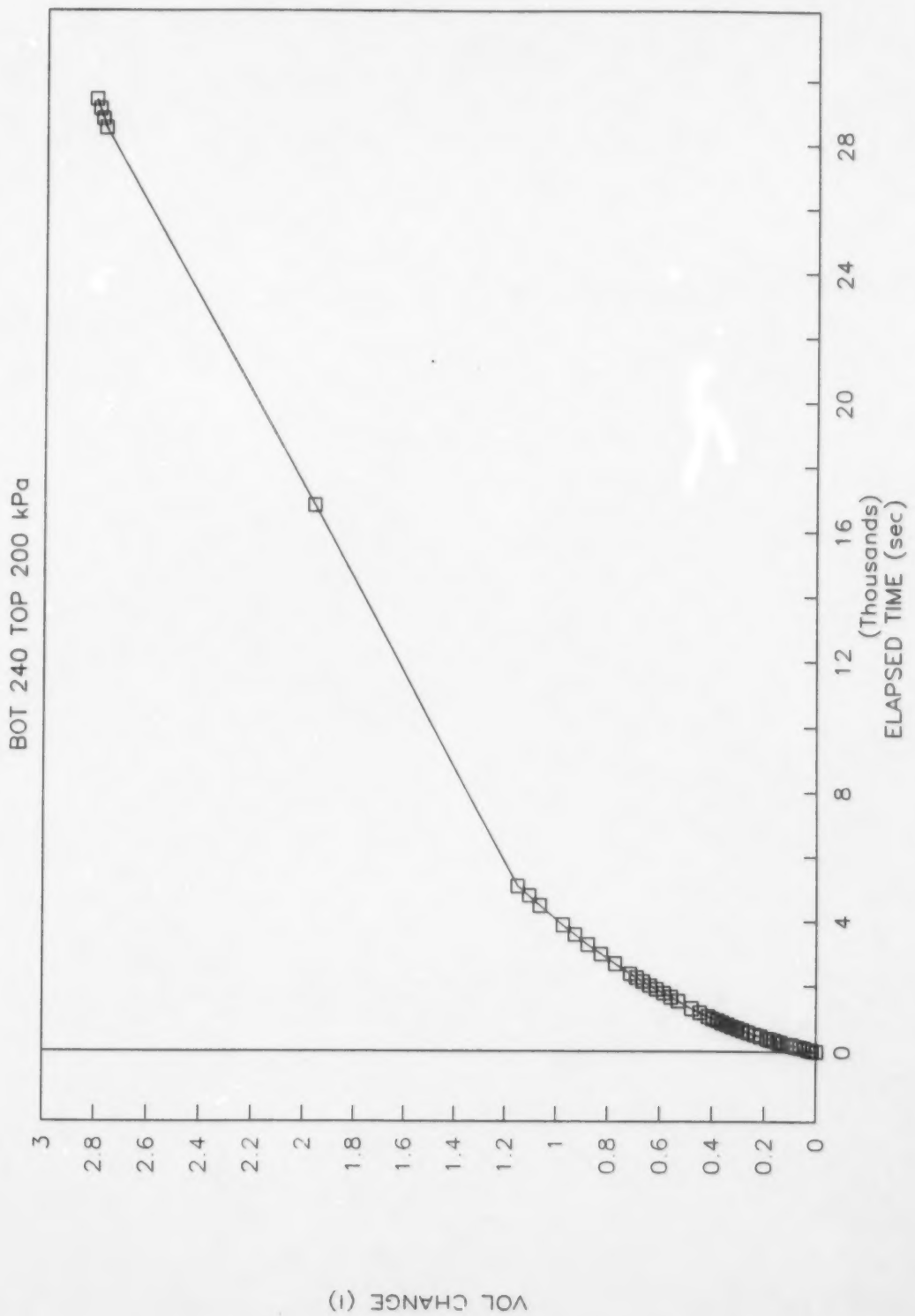

PROJECT No. 912-2055 DRAWN RR REVIEWED KMK DATE APR 92

Golder Associates

PROJECT No. 912-2055 DRAWN RR REVIEWED KMK DATE APR 92

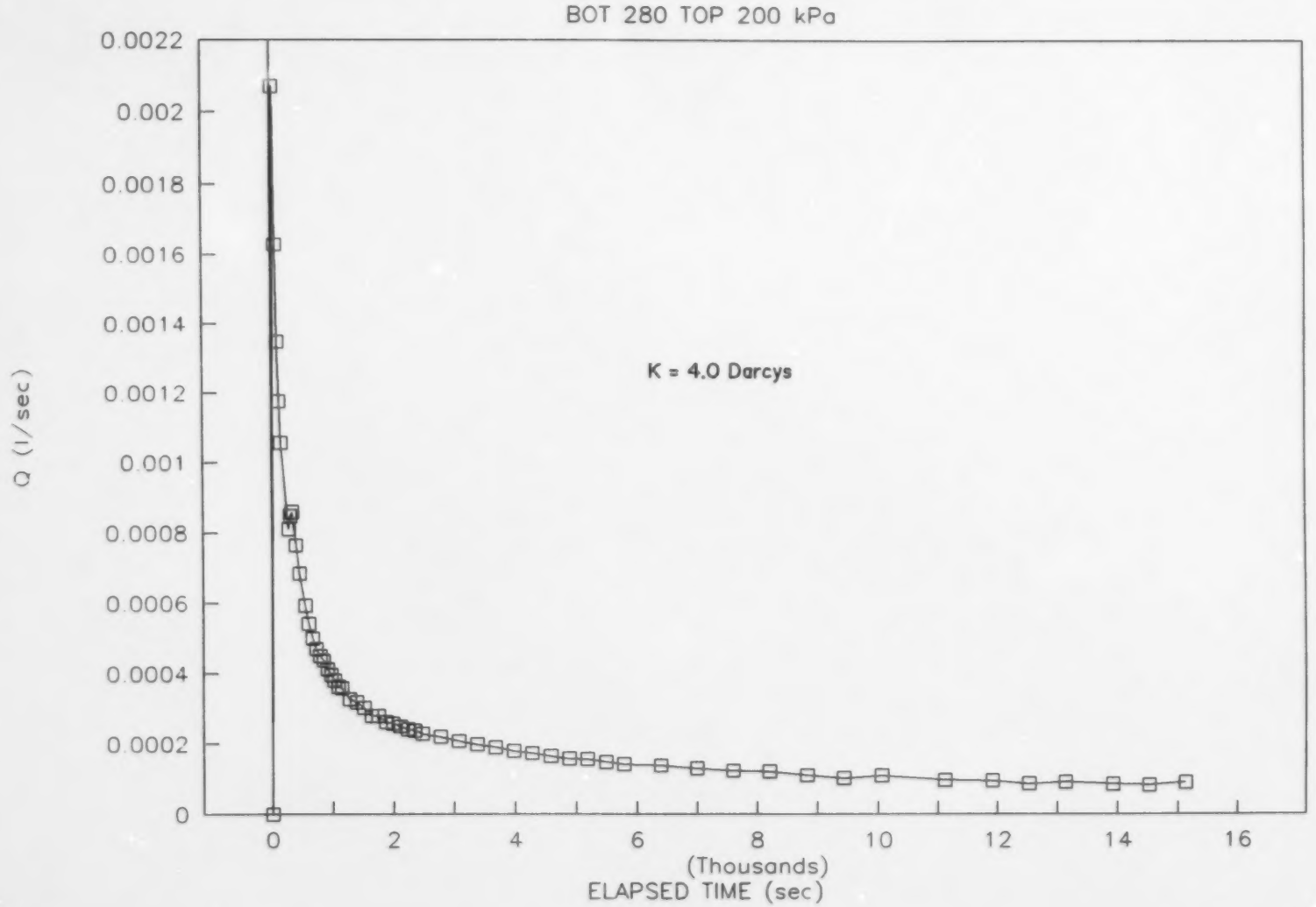

FRACTURE TEST 1 - PERMEABILITY TEST
q vs time (ΔP = 80 kPa)

Figure I-3

Golder Associates

FRACTURE TEST 1 - PERMEABILITY TEST

v vs time (ΔP = 80 kPa)

Figure I-4

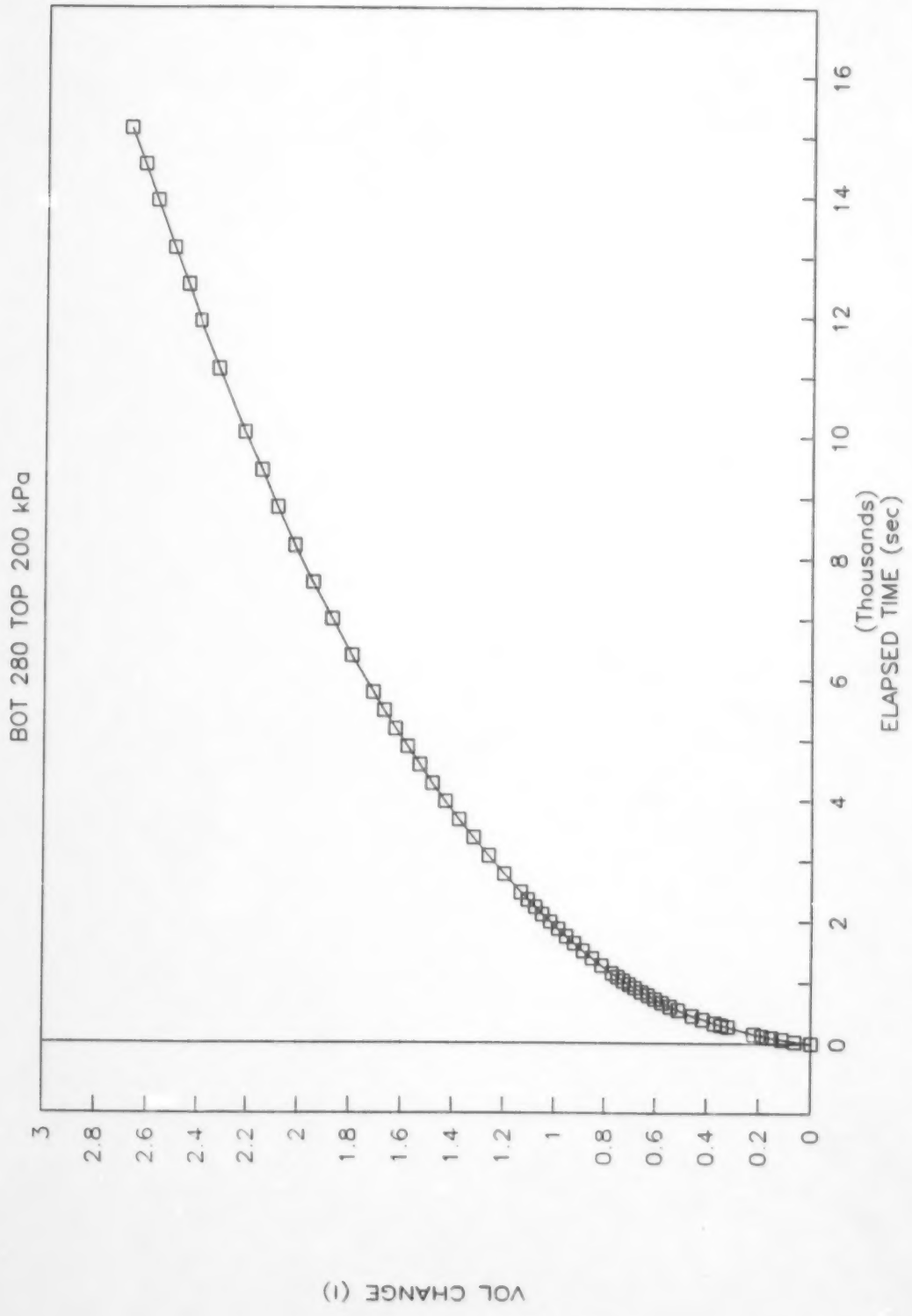

PROJECT No. 912-2055 DRAWN RR REVIEWED KHK DATE APR 92

Golder Associates

FRACTURE TEST 1 - PERMEABILITY TEST

q vs time (ΔP = 160 kPa)

Figure I-5

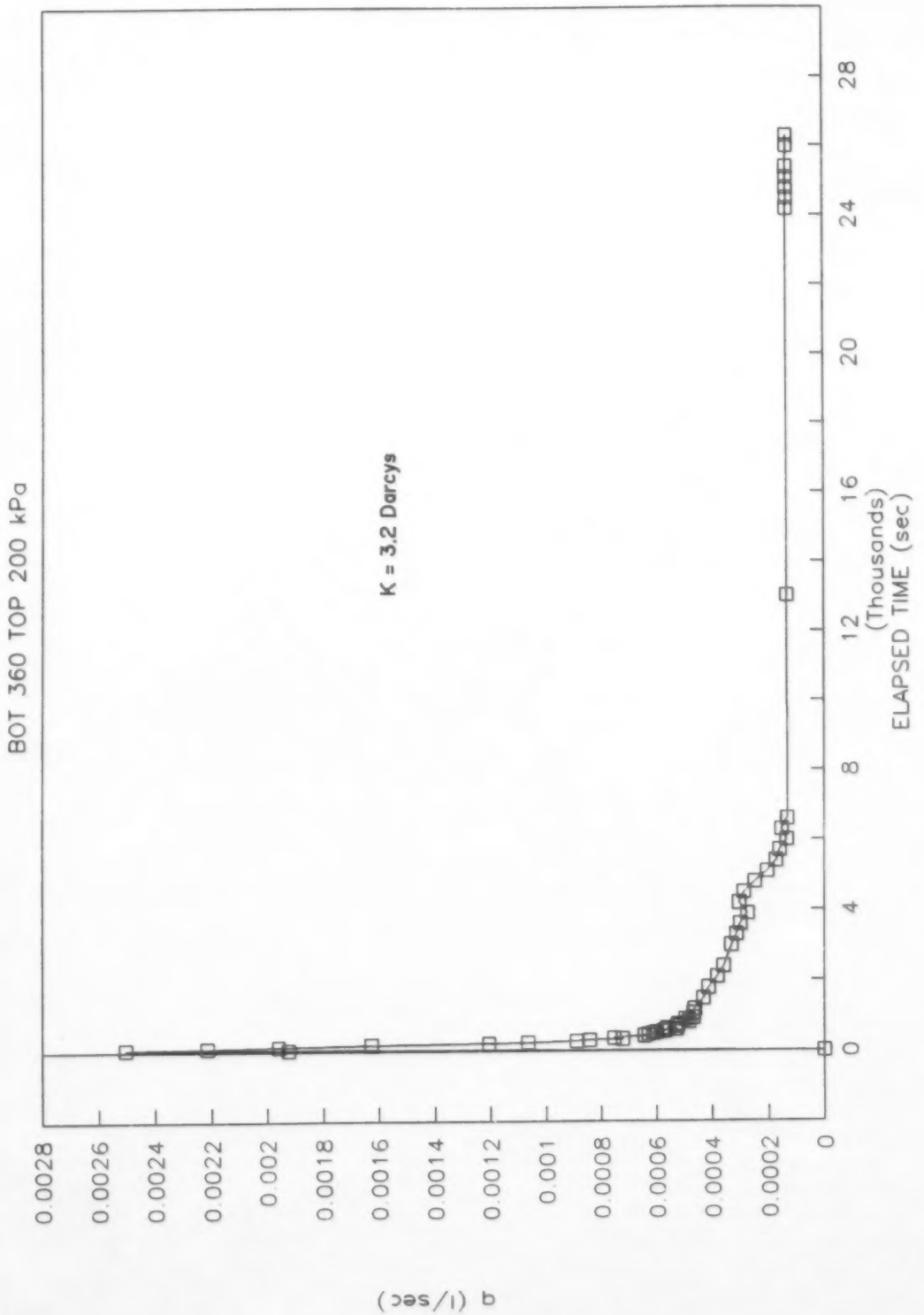

PROJECT No. 912-2055 DRAWN RR REVIEWED KNK DATE APR 92

Golder Associates

FRACTURE TEST 1 - PERMEABILITY TEST

v vs time (ΔP = 160 kPa)

Figure I-6

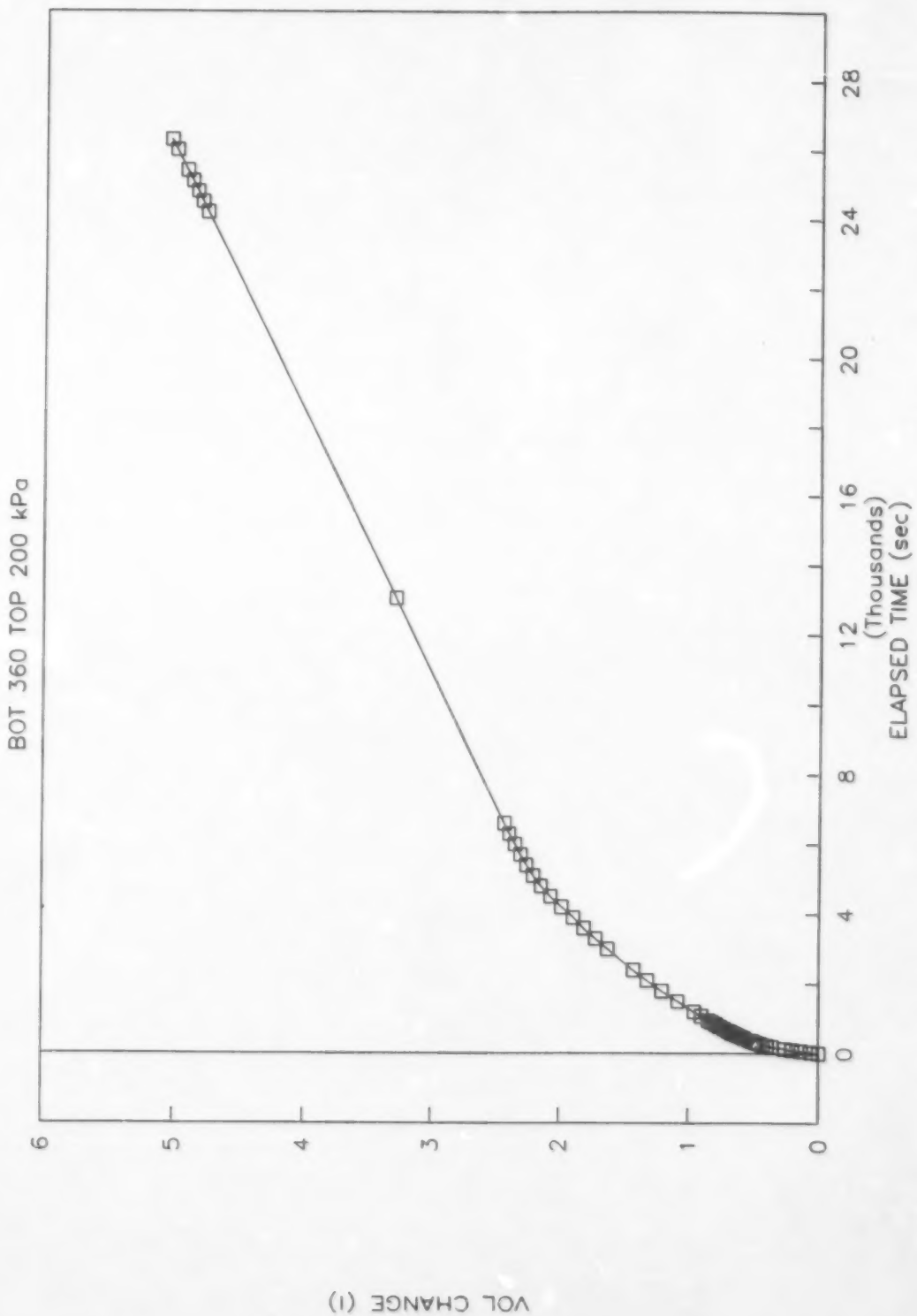

PROJECT No. 912-2055 DRAWN RR REVIEWED KMK DATE APR 92

FRACTURE TEST 2

RESULTS OF PERMEABILITY TESTS

Figure I-7

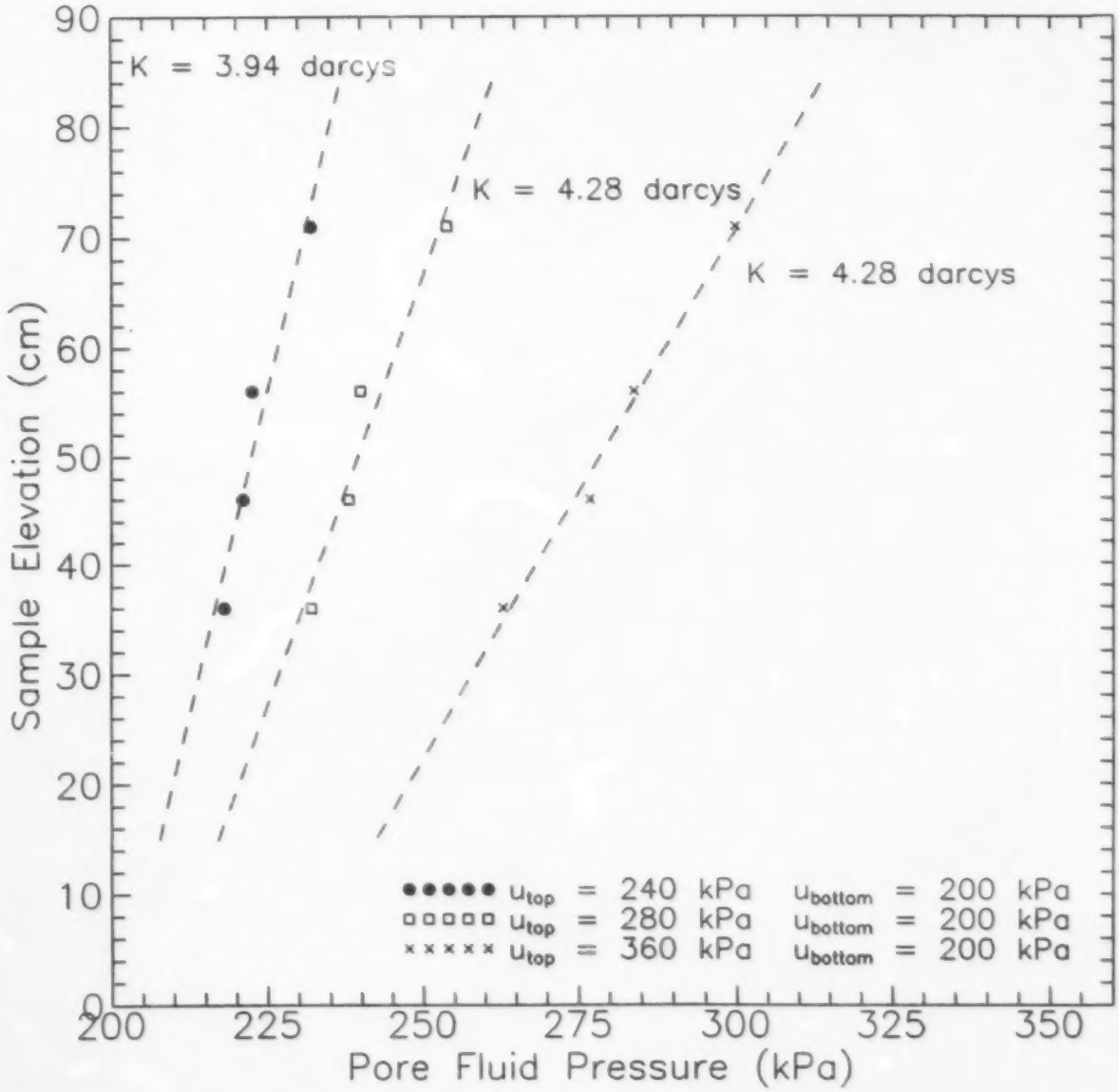

PROJECT No. 912-2055 DRAWN RR REVIEWED KMK DATE APR 92

PROJECT No. 912-2055 DRAWN RR REVIEWED KMK DATE APR 92

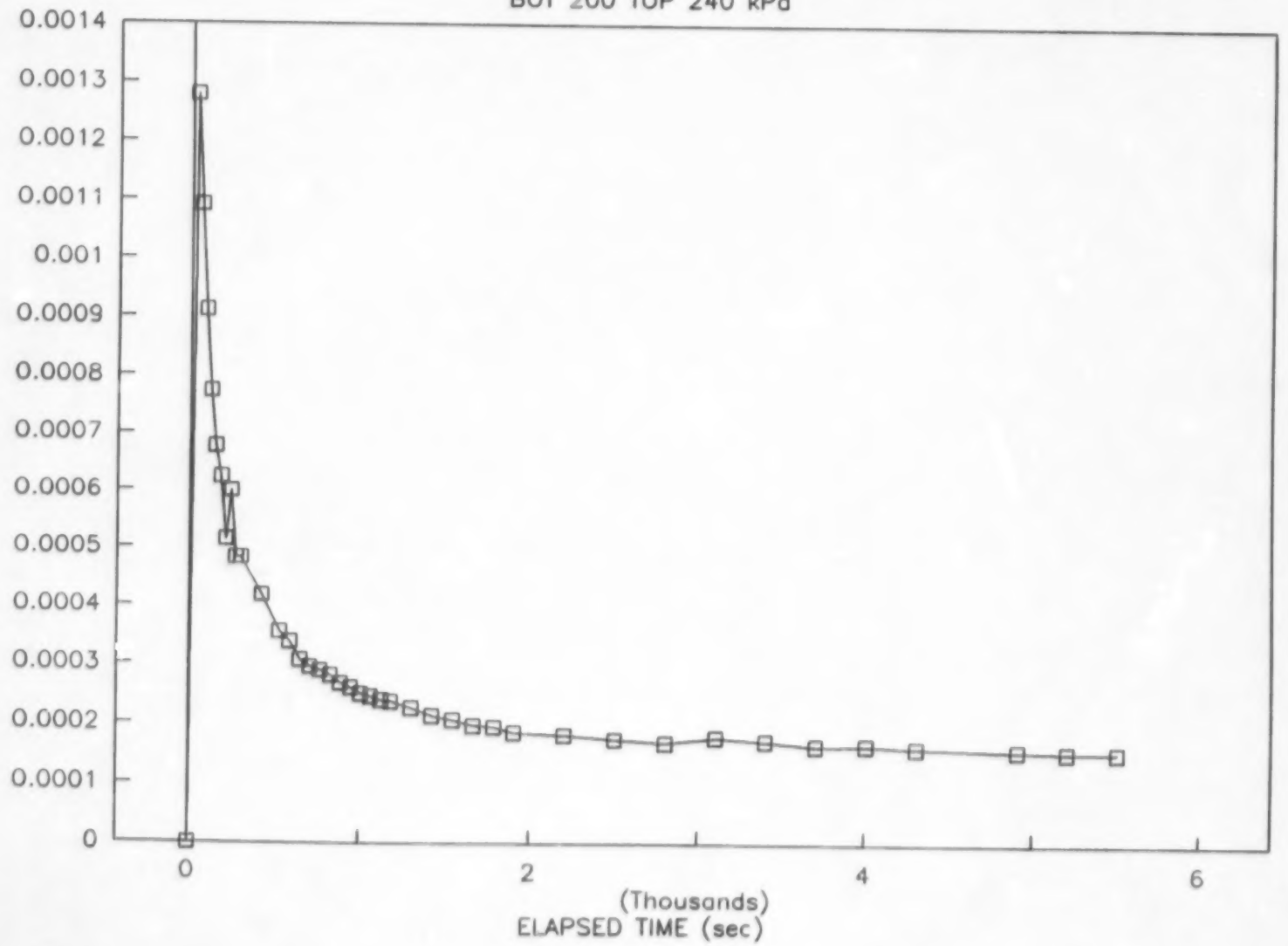

FRACTURE TEST 2 - PERMEABILITY TEST
q vs time (ΔP = 40 kPa)

Figure I-8

Golder Associates

FRACTURE TEST 2 - PERMEABILITY TEST

v vs time (ΔP = 40 kPa)

Figure I-9

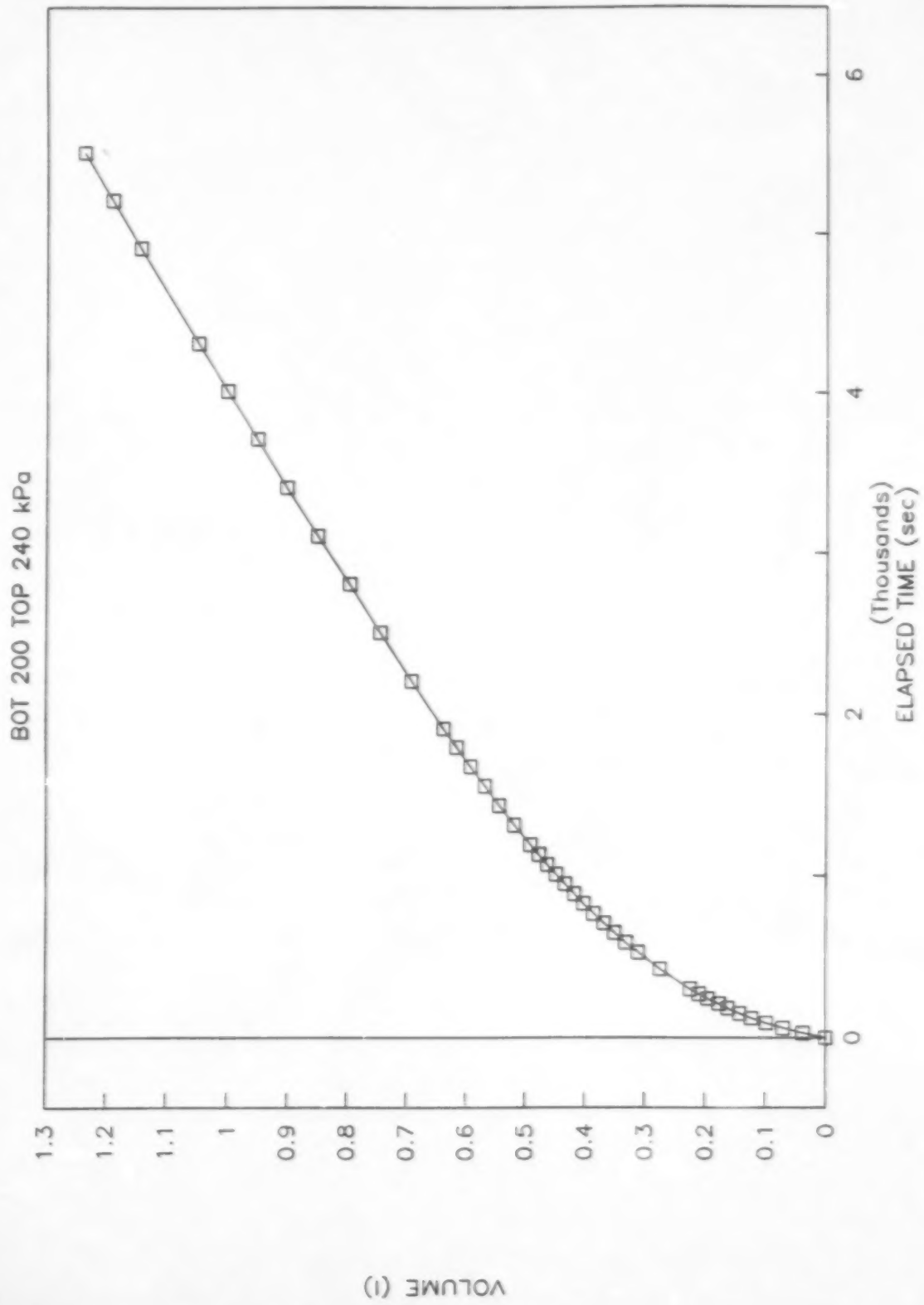

PROJECT No. 912-2055 DRAWN RR REVIEWED KAK DATE APR 92

Golder Associates

PROJECT No. 912-2055 DRAWN RR REVIEWED KMK DATE APR 92

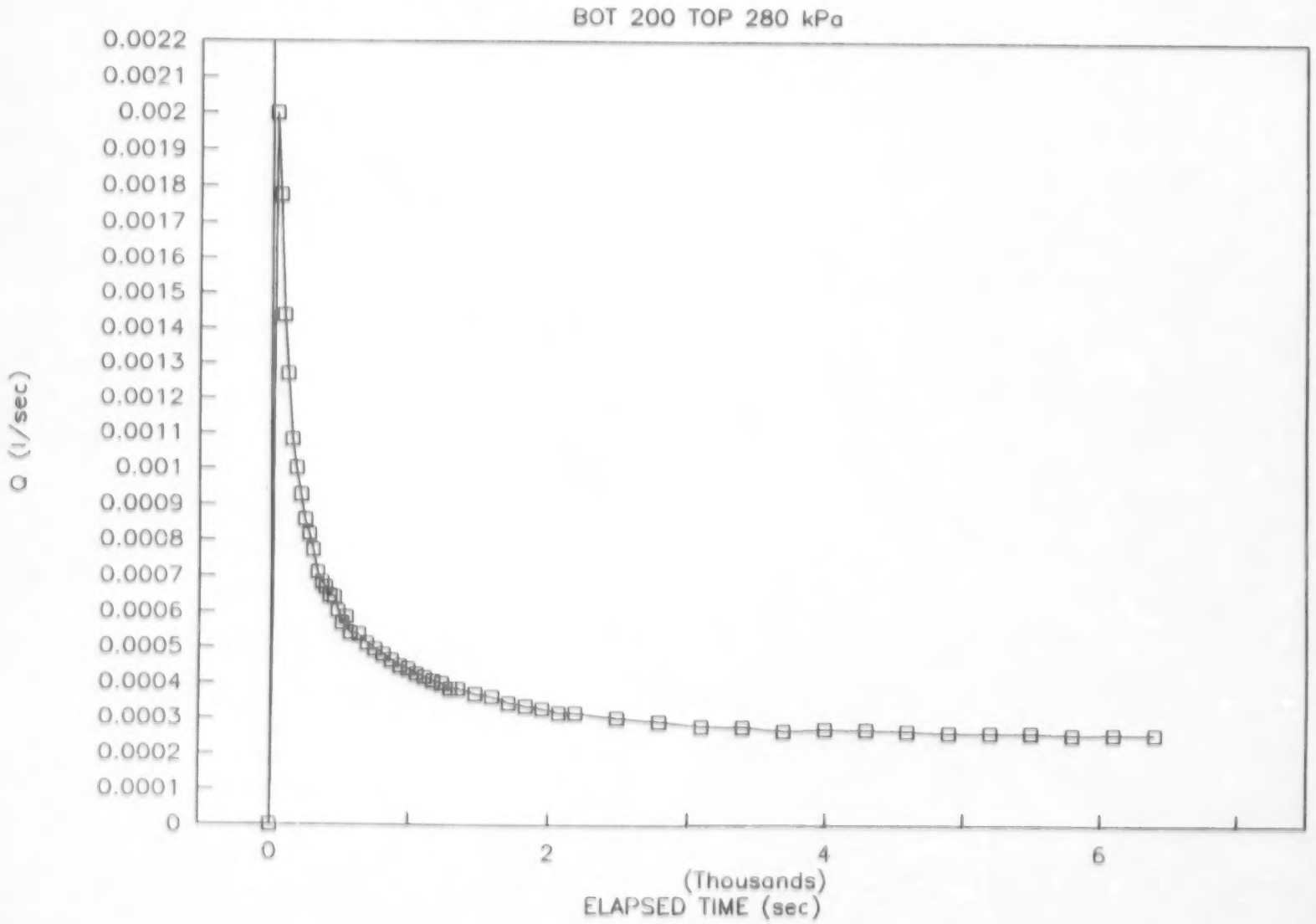

FRACTURE TEST 2 - PERMEABILITY TEST

q vs time (ΔP = 80 kPa)

Figure 1-10

Golder Associates

FRACTURE TEST 2 - PERMEABILITY TEST

v vs time (ΔP = 80 kPa)

Figure I-11

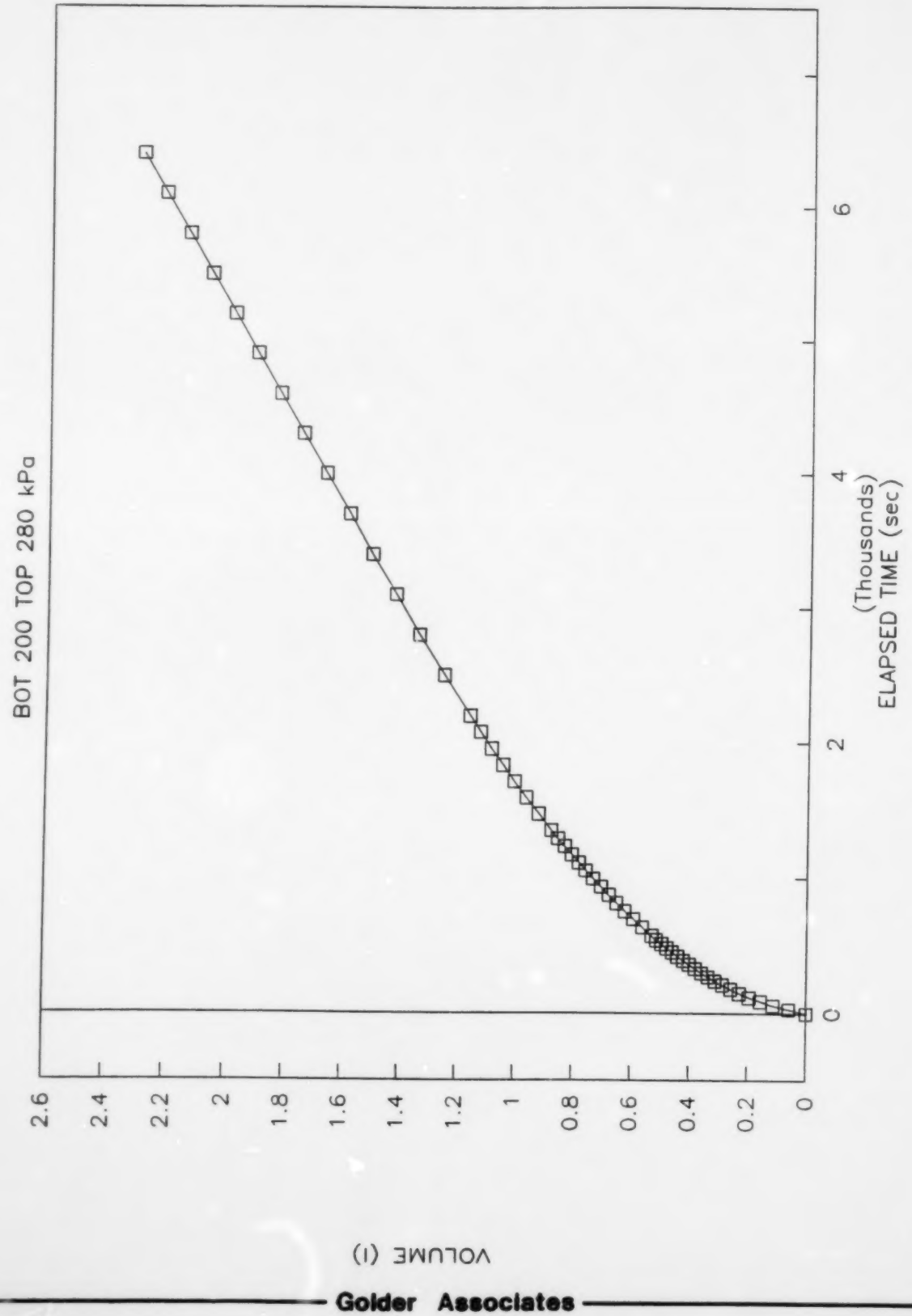

PROJECT No. 912-2055 DRAWN RR REVIEWED KMK DATE APR 92

Golder Associates

PROJECT No. 912-2055 DRAWN RR REVIEWED KHK DATE APR 92

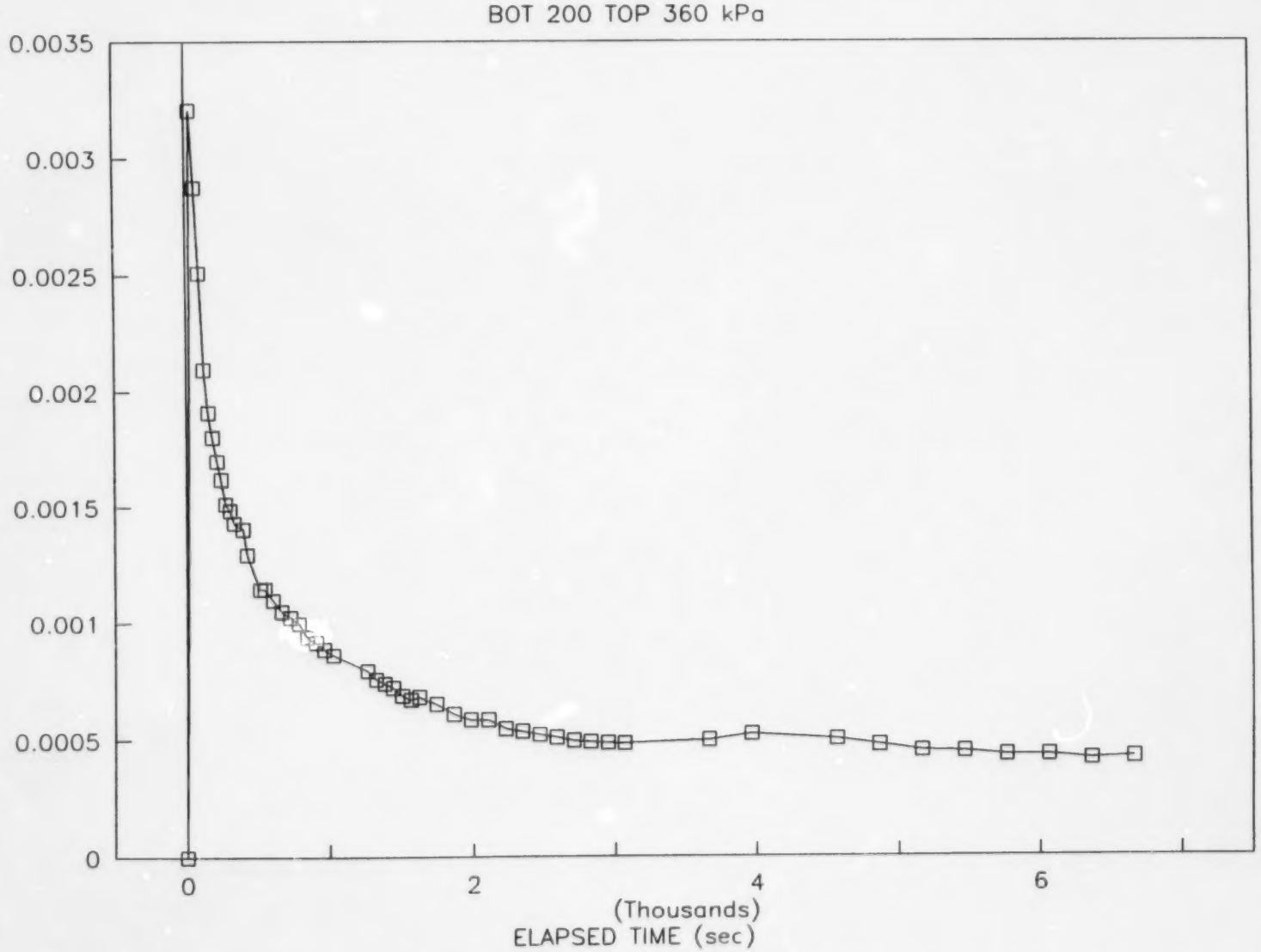

Golder Associates

FRACTURE TEST 2 - PERMEABILITY TEST
q vs time (ΔP = 160 kPa)

Figure 1-12

FRACTURE TEST 2 - PERMEABILITY TEST

v vs time (ΔP = 160 kPa)

Figure I-13

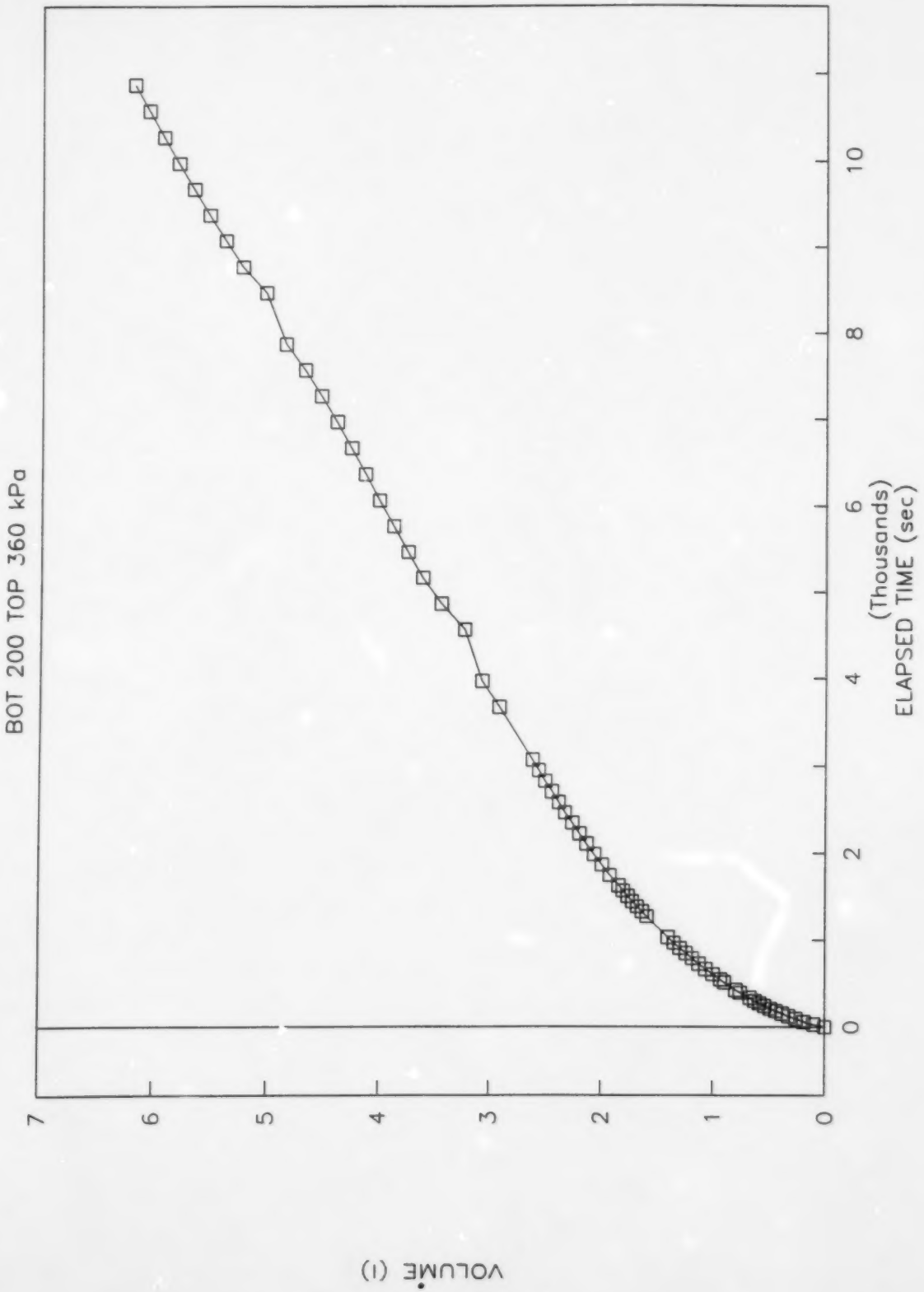

PROJECT No. 912-2055 DRAWN RR REVIEWED KMK DATE APR 92

Golder Associates

FRACTURE TEST 3

RESULTS OF PERMEABILITY TESTS

Figure I-14

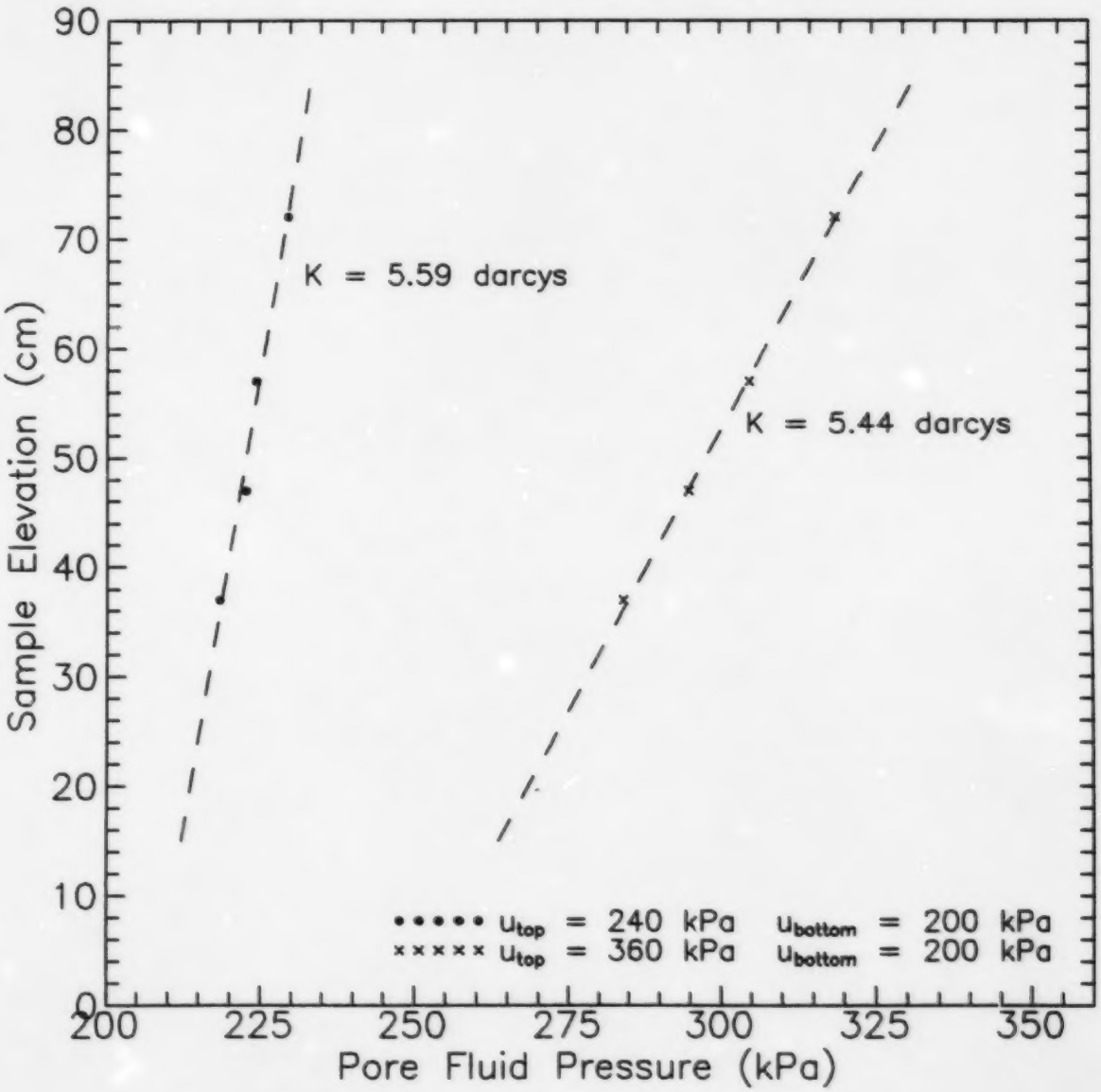

PROJECT No. 912-2055 DRAWN RR REVIEWED KMK DATE APR 92

PROJECT No. 912-2055 DRAWN RR REVIEWED KMK DATE APR 92

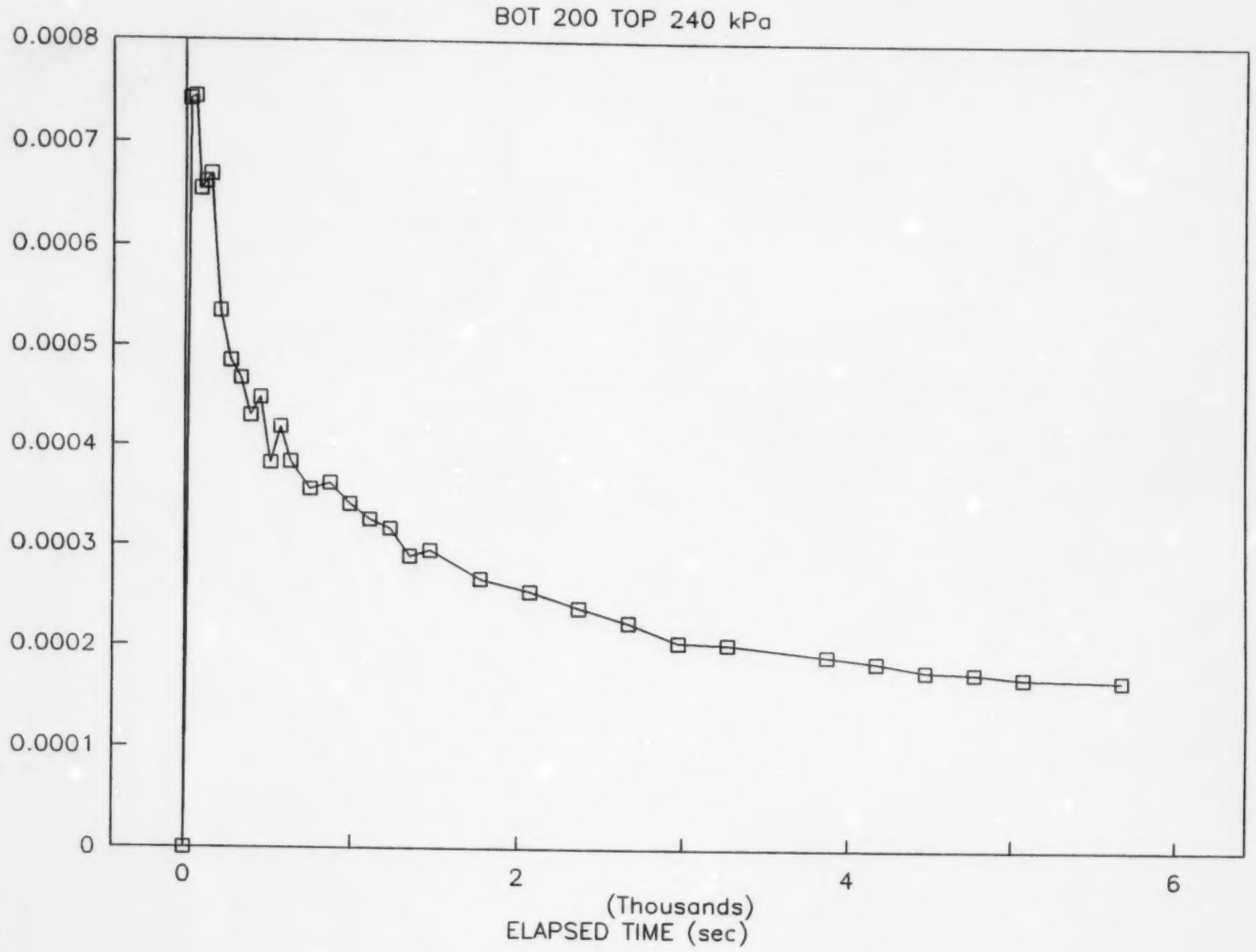

FRACTURE TEST 3 - PERMEABILITY TEST
q vs time (ΔP = 40 kPa)

Figure 1-15

Golder Associates

FRACTURE TEST 3 - PERMEABILITY TEST

v vs time (ΔP = 40 kPa)

Figure I-16

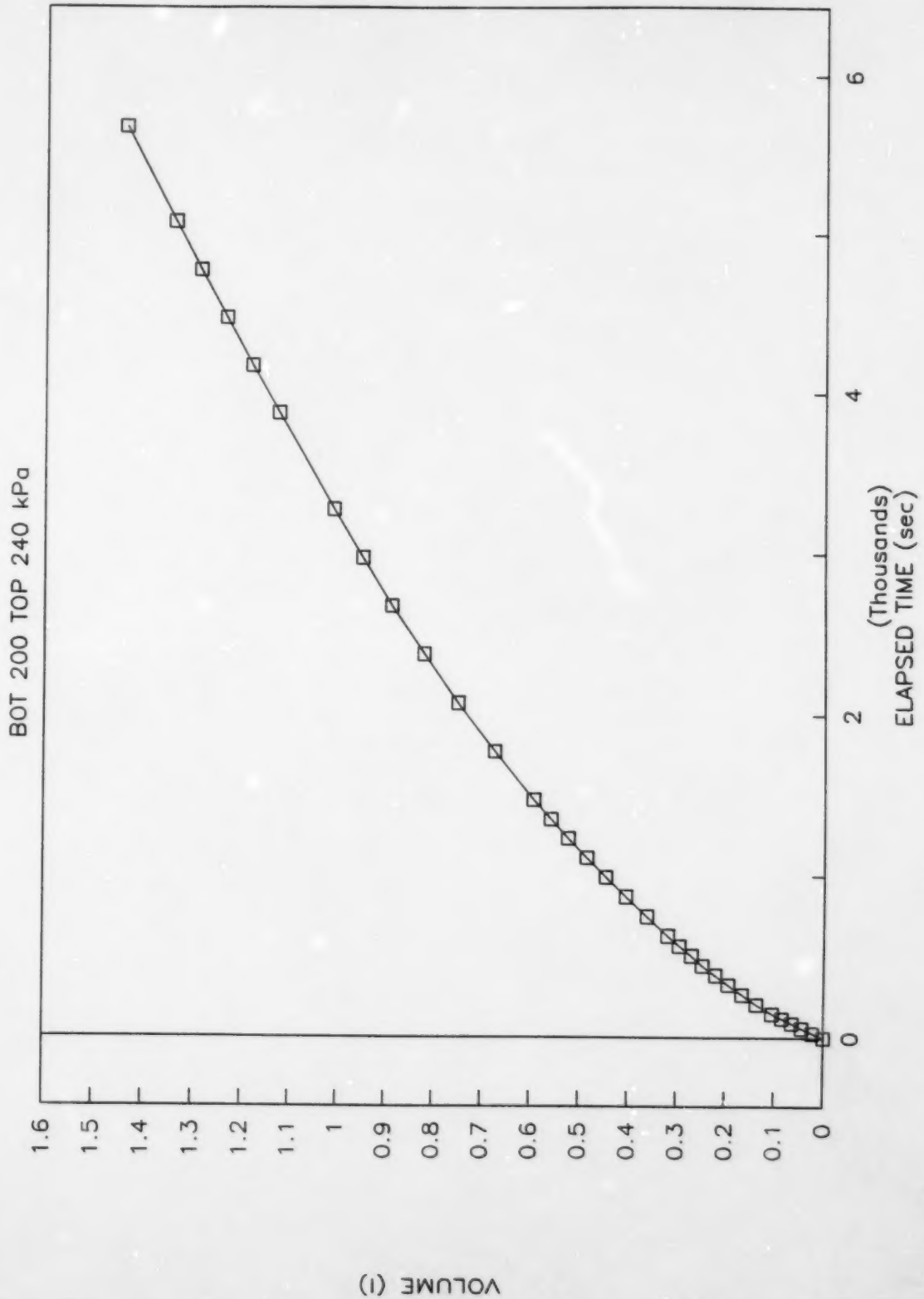

PROJECT No. 912-2055 DRAWN RR REVIEWED KMK DATE APR 92

Golder Associates

PROJECT No. 912-2055 DRAWN RR REVIEWED KMK DATE APR 92

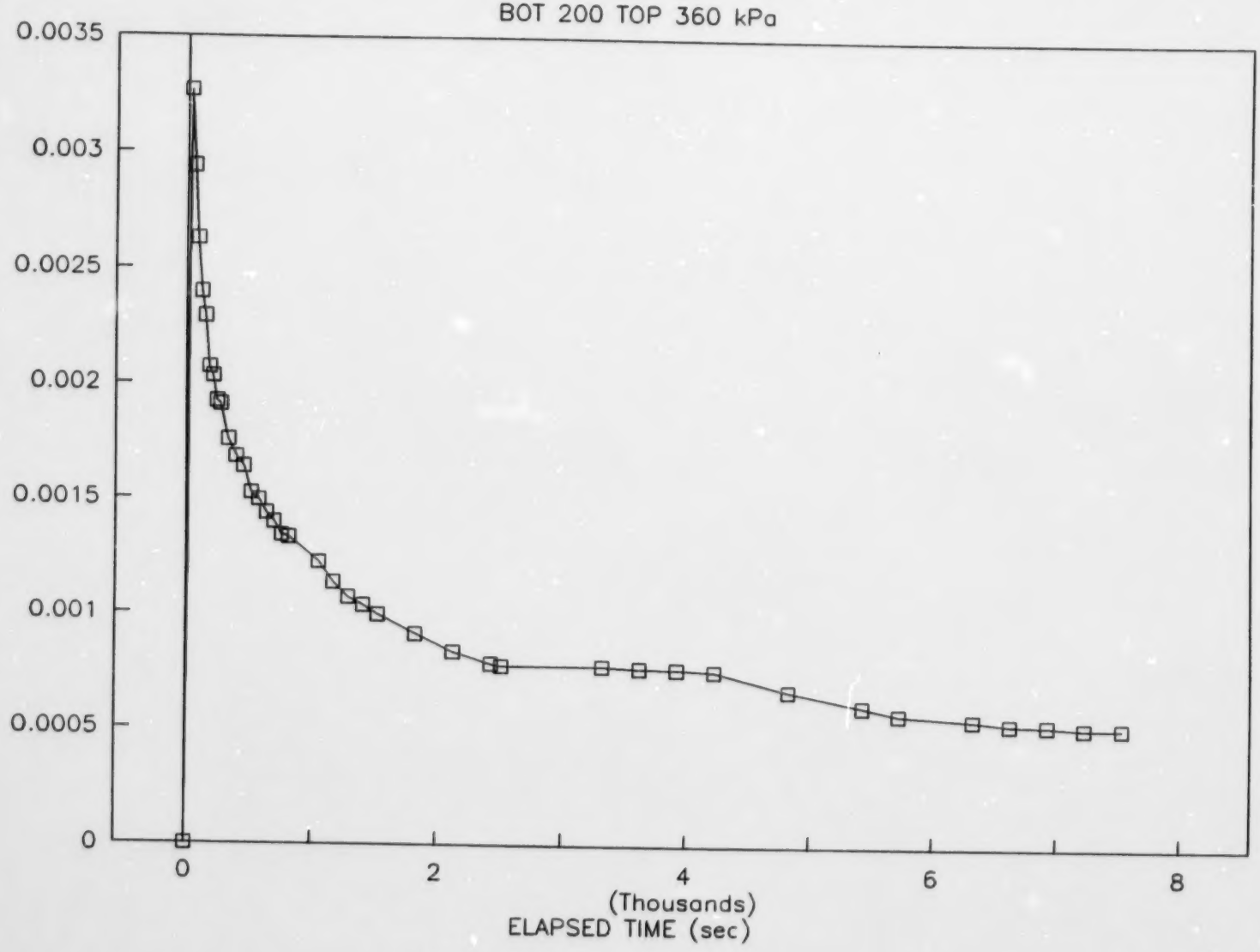

Golder Associates

FRACTURE TEST 3 - PERMEABILITY TEST
q vs time (ΔP = 160 kPa)

Figure I-17

FRACTURE TEST 3 - PERMEABILITY TEST

v vs time (ΔP = 160 kPa)

Figure I-18

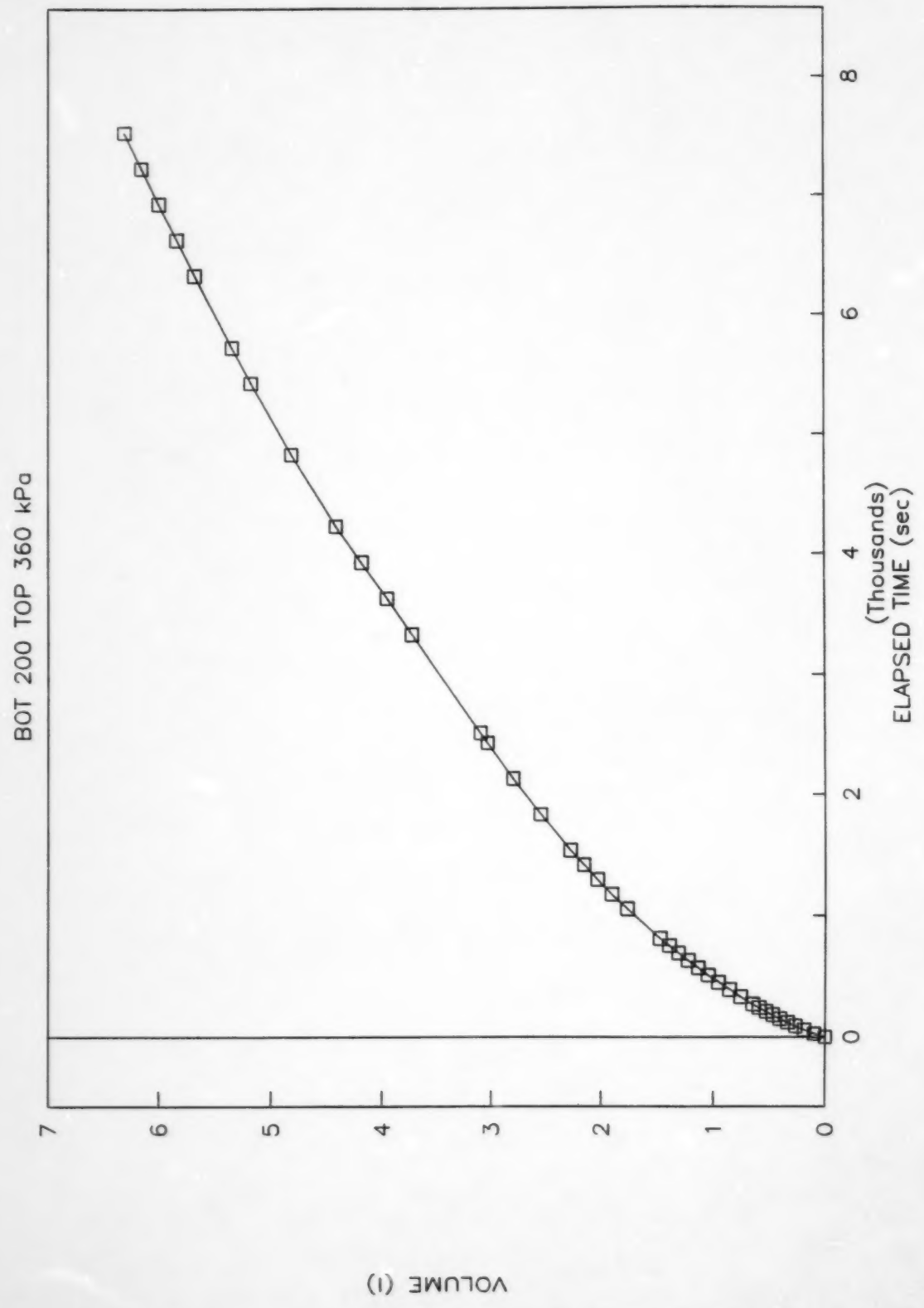

PROJECT No. 912-2055 DRAWN RR REVIEWED KMK DATE APR 92

Golder Associates

FRACTURE TEST 4

RESULTS OF PERMEABILITY TESTS

Figure I-19

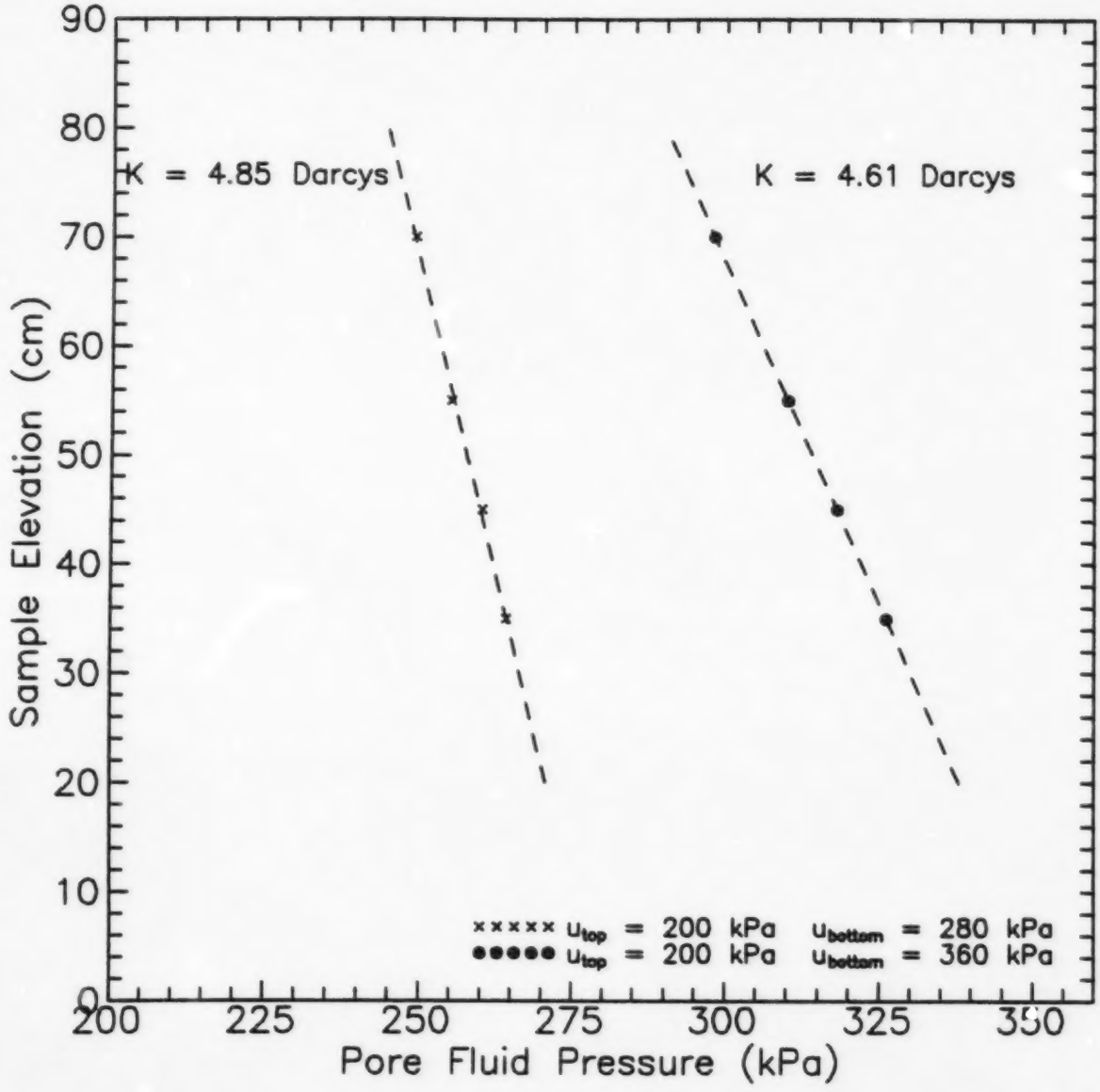

PROJECT No. 912-2055 DRAWN RR REVIEWED KMK DATE APR 92

Golder Associates

FRACTURE TEST 4 - PERMEABILITY TEST

q vs time (ΔP = 80 kPa)

Figure I-20

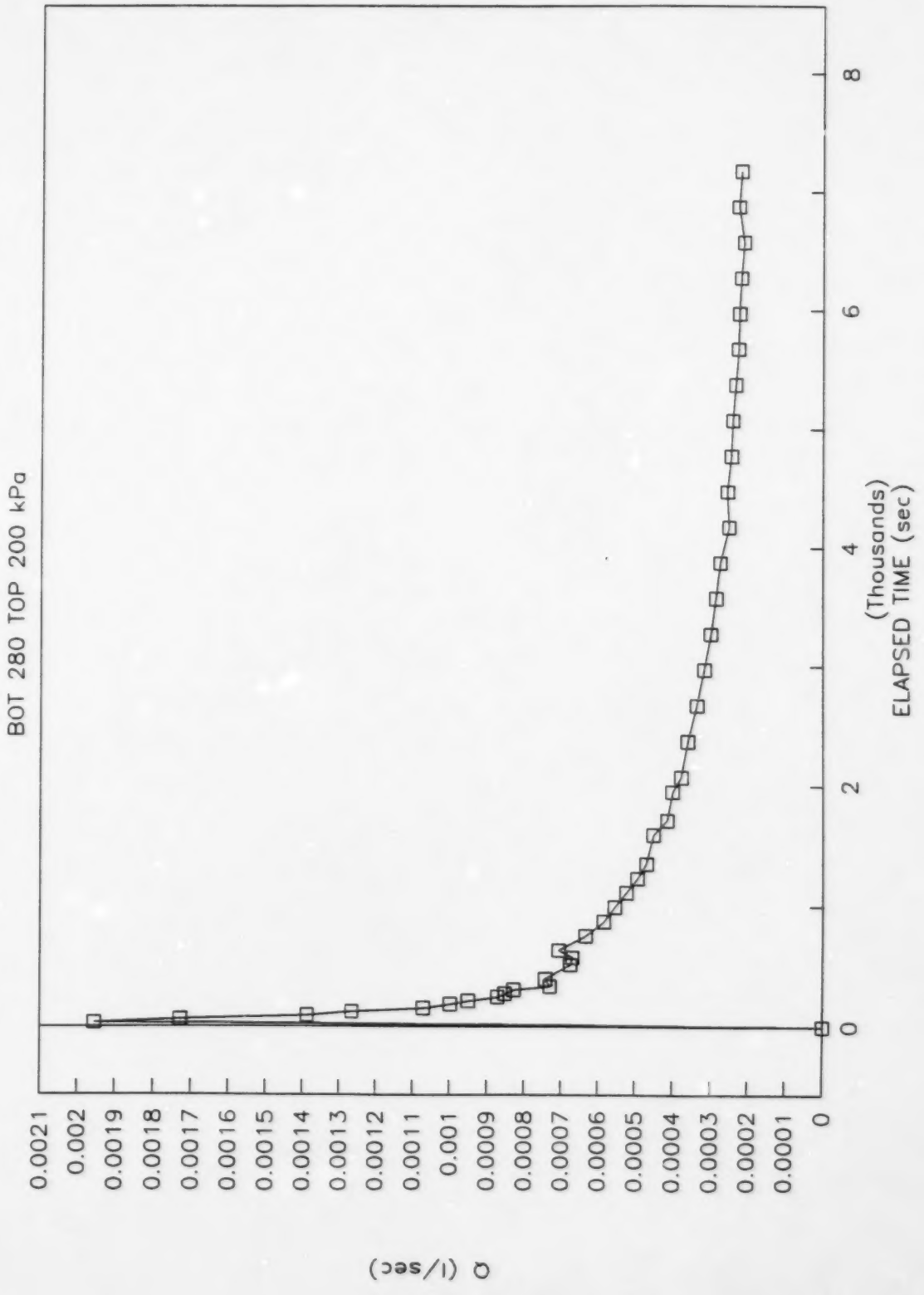

PROJECT No. 912-2055 DRAWN RR REVIEWED KMK DATE APR 92

Golder Associates

FRACTURE TEST 4 - PERMEABILITY TEST

v vs time (ΔP = 80 kPa)

Figure I-21

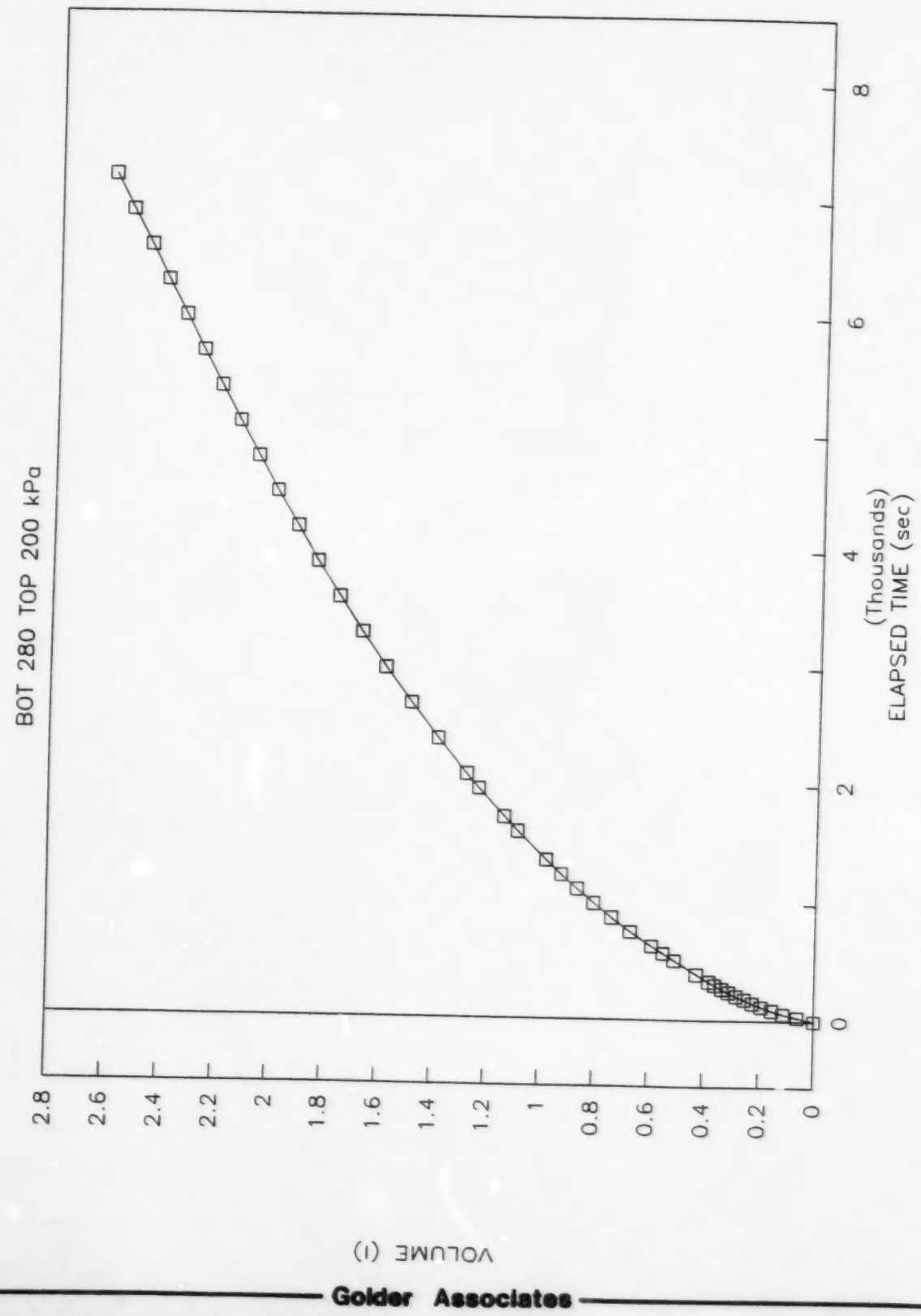

PROJECT No. 912-2055 DRAWN RR REVIEWED KMK DATE APR 92

Golder Associates

PROJECT No. 912-2055 DRAWN RR REVIEWED KMK DATE APR 92

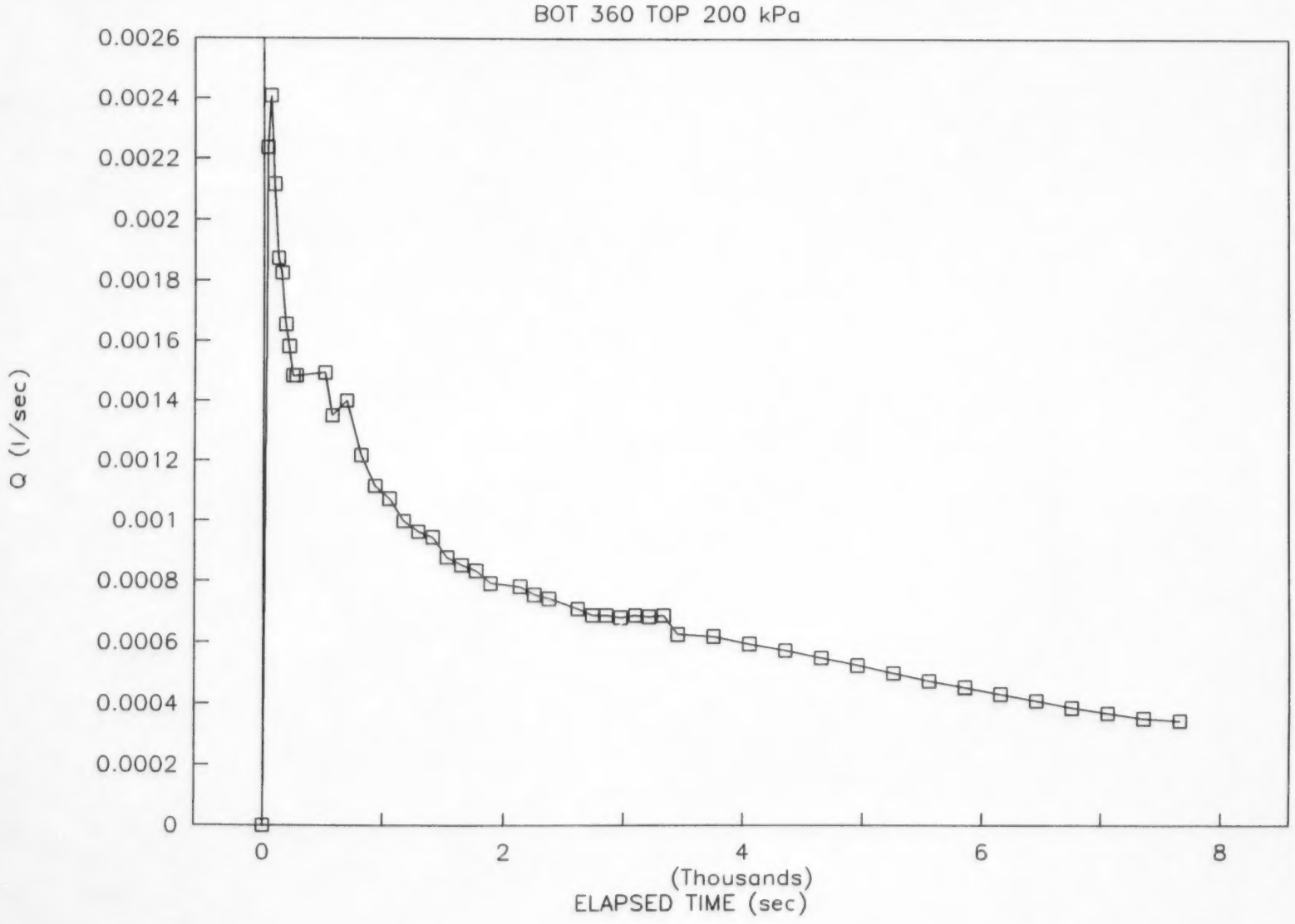

FRACTURE TEST 4 - PERMEABILITY TEST
q vs time (ΔP = 160 kPa)

Figure I-22

Golder Associates

FRACTURE TEST 4 - PERMEABILITY TEST

v vs time (ΔP = 160 kPa)

Figure I-23

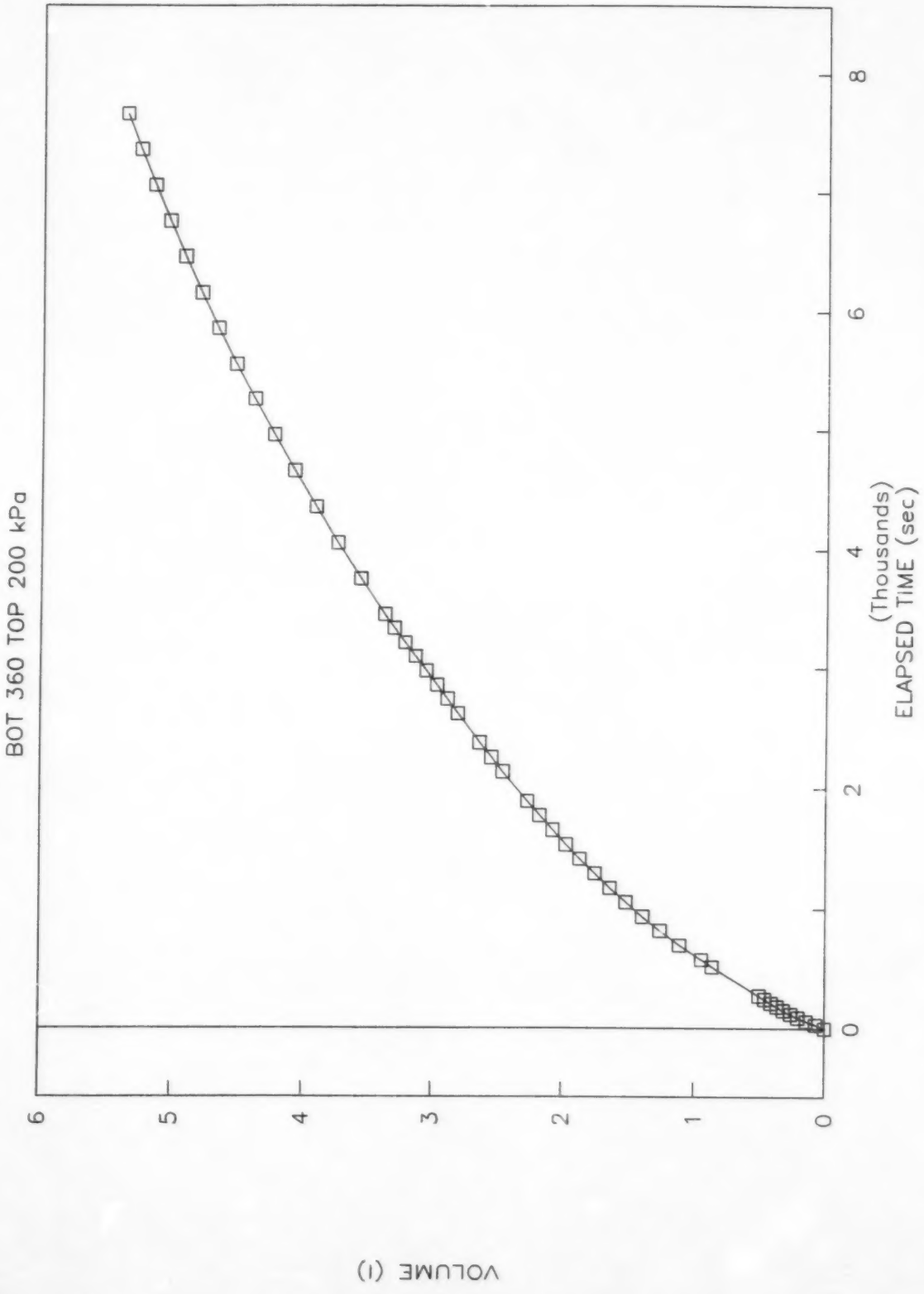

PROJECT No. 912-2055 DRAWN RR REVIEWED KMK DATE APR 92

Golder Associates

FRACTURE TEST 5
RESULTS OF PERMEABILITY TESTS

Figure I-24

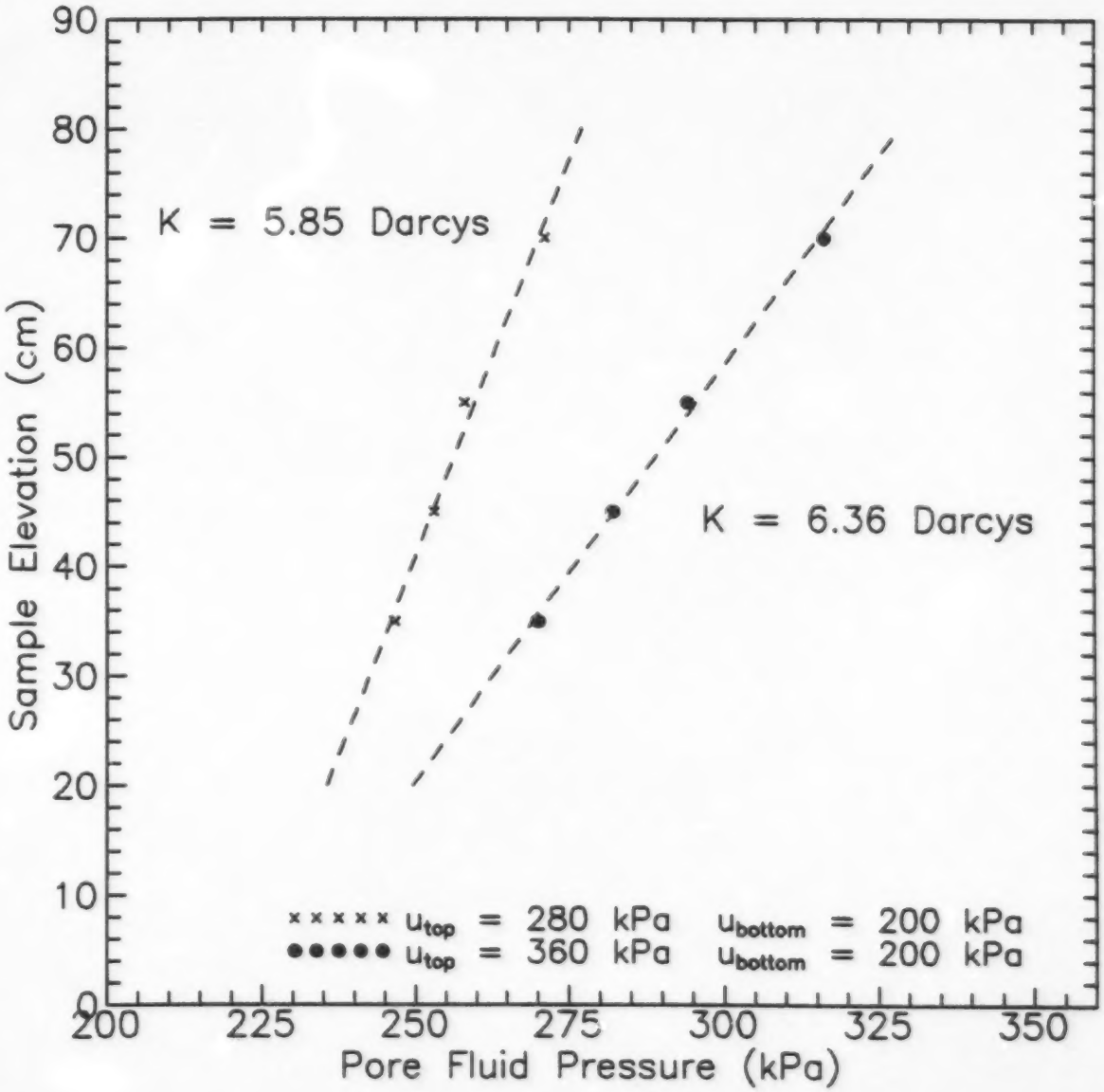

PROJECT No. 912-2055 DRAWN RR REVIEWED KMS DATE APR 92

Golder Associates

FRACTURE TEST 5 - PERMEABILITY TEST

q vs time (ΔP = 80 kPa)

Figure I-25

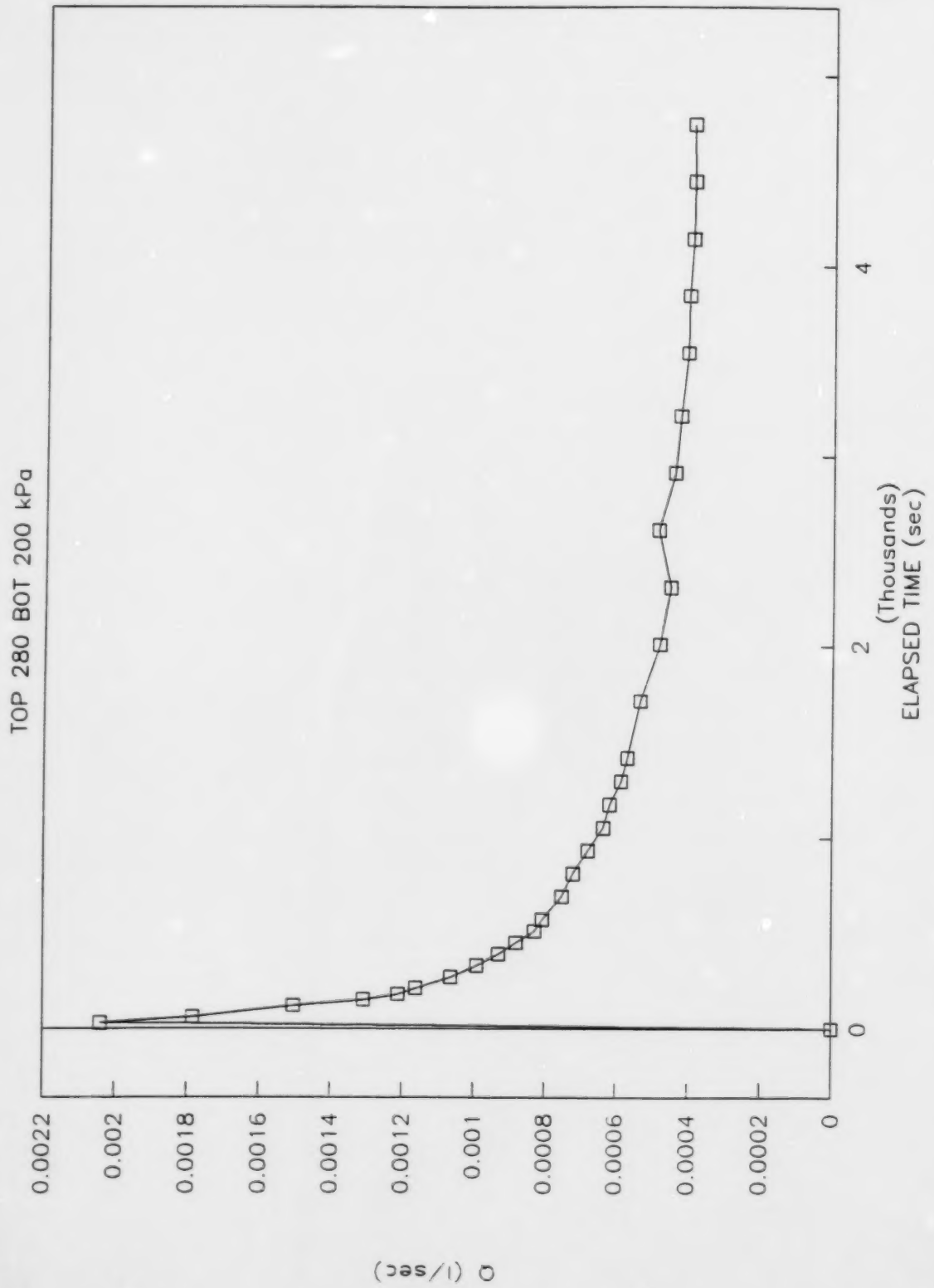

PROJECT No. 912-2055 DRAWN RR REVIEWED KMK DATE APR 92

Golder Associates

PROJECT No. 912-2055 DRAWN RR REVIEWED KMK DATE APR 92

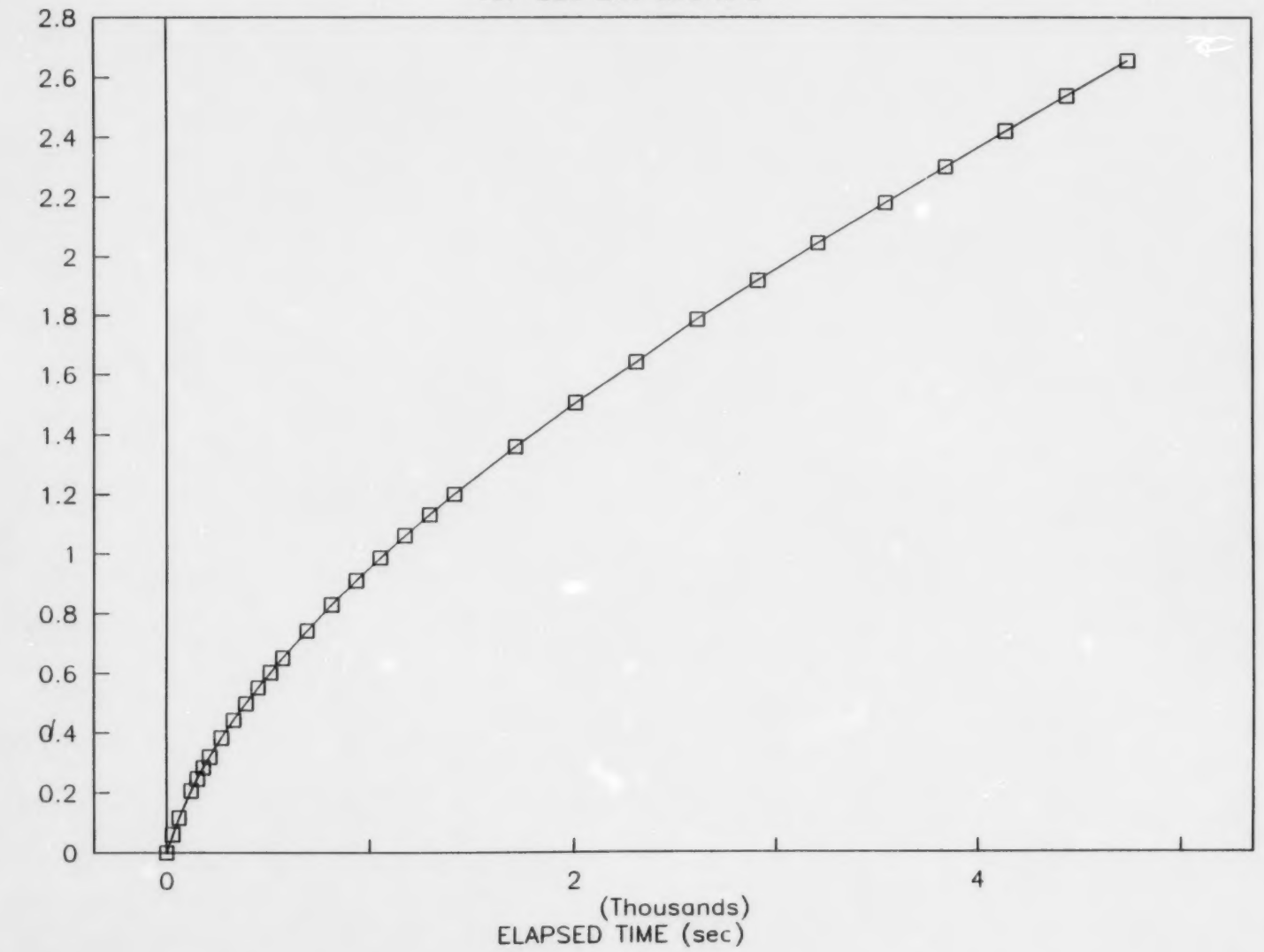

Golder Associates

FRACTURE TEST 5 - PERMEABILITY TEST
V vs time (ΔP = 80 kPa)

Figure 1-26

PROJECT No. 912-2055 DRAWN RR REVIEWED KMK DATE APR 92

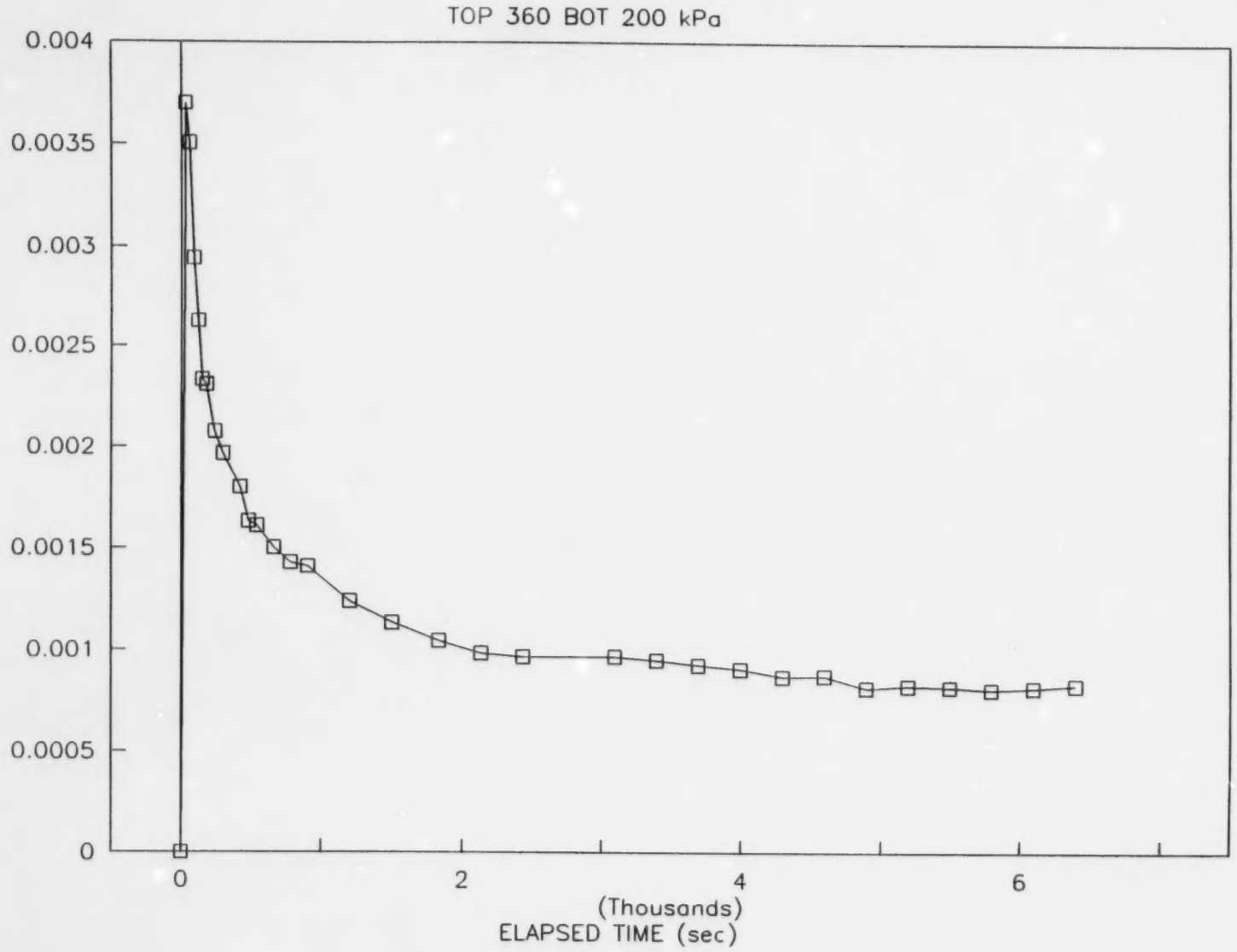

FRACTURE TEST 5 - PERMEABILITY TEST
q vs time (ΔP = 180 kPa)

Figure 1-27

Golder Associates

FRACTURE TEST 5 - PERMEABILITY TEST

v vs time (ΔP = 160 kPa)

Figure I-28

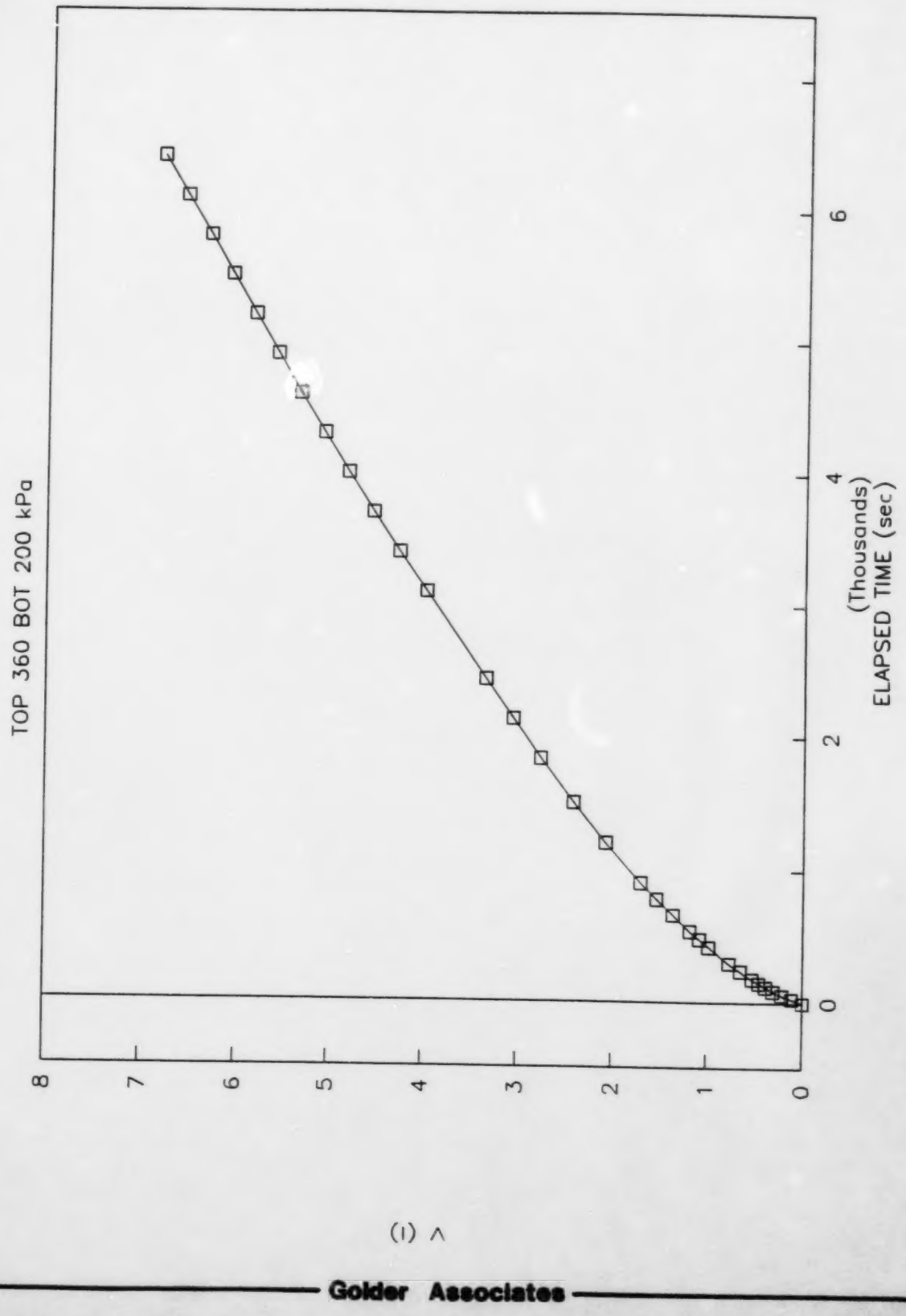

PROJECT No. 912-2055 DRAWN RR REVIEWED KMK DATE APR 92

APPENDIX II

SUB-FRACTURE PRESSURE INJECTION TESTS

FRACTURE TEST 1 - SUB-FRACTURE INJECTION
PIEZOMETRIC READINGS

Figure II-1

Piezometer	Angle	Radius	Vertical Distance from Injection Point	Pressure (kPa)		
Applied Pressure				240	280	360
Top of Injection Well				238	280	359
Injection Point				236	275	352
Q	60	17	-4	235	276	349
R	240	17	-4	233	272	349
O	120	17	+16	225	237	297
P	300	17	+16	238	278	359
T	270	17	+31	230	272	359
S	90	17	+31	237	277	356

PROJECT No. 912-2055 DRAWN RR REVIEWED _____ DATE APR 92

FRACTURE TEST 2-SUB-FRACTURE INJECTION PIEZOMETER READINGS

Figure II-2

Piezometer	Angle	Radius	Vertical Distance from Injection Point	Pressure (kPa)		
Applied Pressure				240	280	360
Top of Injection Well				240	280	360
Injection Point				240	280	360
Q	60	17	-10	200	200	200
R	240	17	-10	200	200	200
O	120	17	+10	200	200	200
P	300	17	+10	200	200	200
T	270	17	+25	200	200	200
S	90	17	+25	200	200	200

PROJECT No. 912-2055 DRAWN CG REVIEWED DATE JUNE 92

PROJECT No. 912-2055 DRAWN RR REVIEWED KMK DATE APR 92

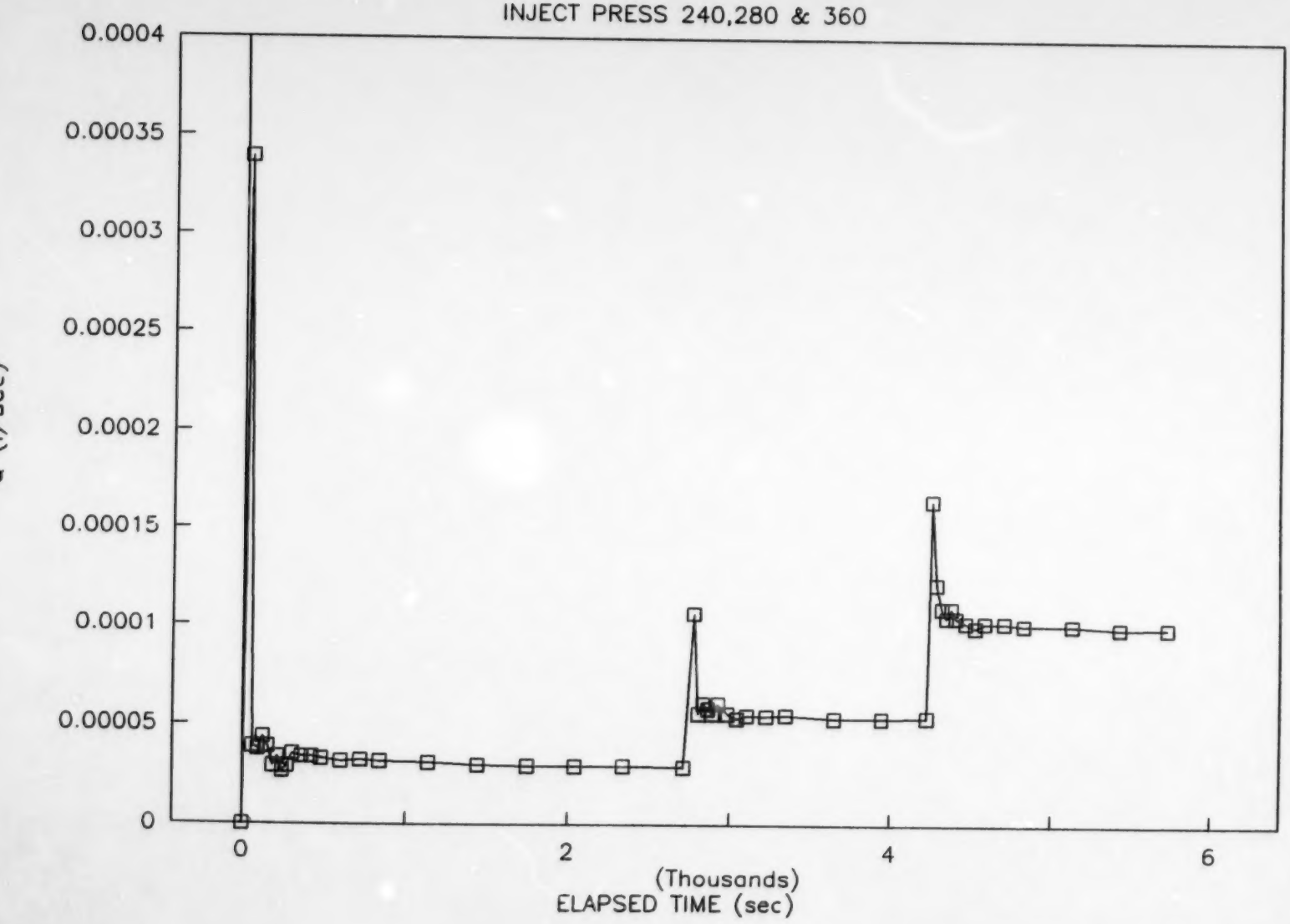

Golder Associates

FRACTURE TEST 2 - SUB-FRACTURE INJECTION
q vs time

Figure II-3

PROJECT No. 912-2055 DRAWN RR REVIEWED KMK DATE APR 92

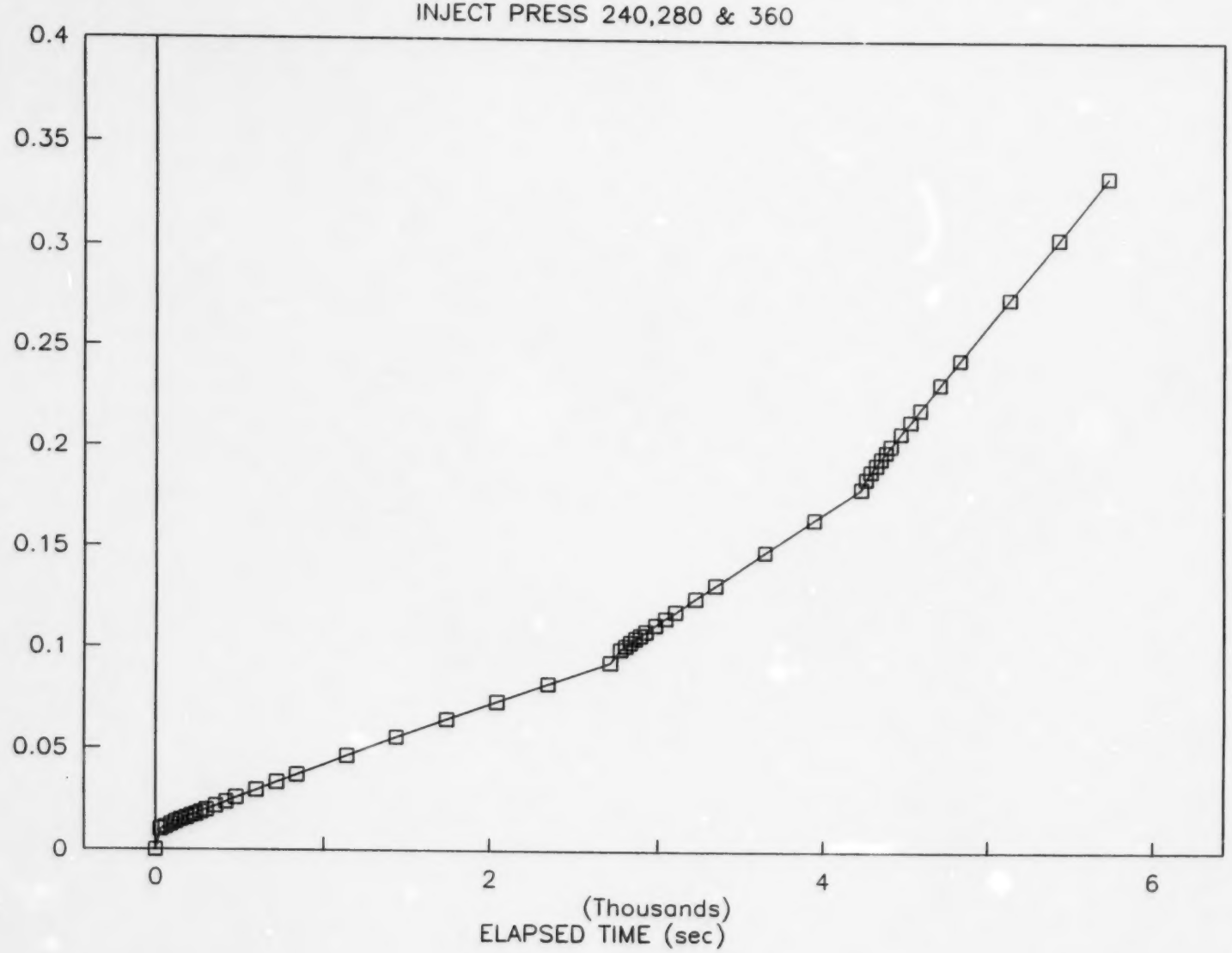

Golder Associates

FRACTURE TEST 2 - SUB-FRACTURE INJECTION
V vs time

Figure II-4

FRACTURE TEST 2 - SUB-FRACTURE INJECTION
PIEZOMETRIC READINGS

Figure II-5

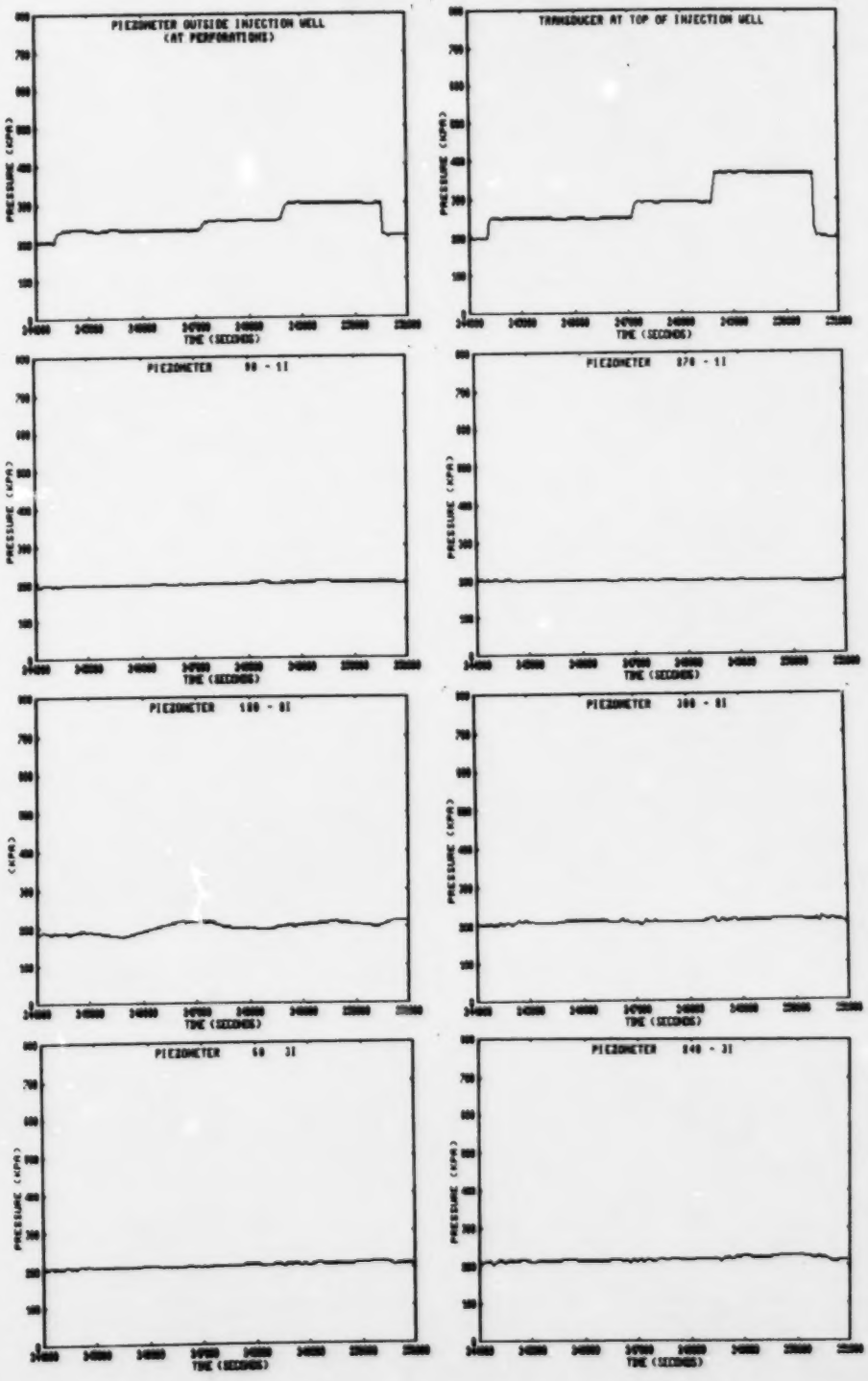

PROJECT No. 912-2055 DRAWN RR REVIEWED KMK DATE APR 92

FRACTURE TEST 3 - SUB-FRACTURE INJECTION PIEZOMETER READINGS

Figure II-6

Piezometer	Angle	Radius	Vertical Distance from Injection Point	Pressure (kPa)		
Applied Pressure				240	280	360
Top of Injection Well				240	280	360
Injection Point				240	280	360
Q	60	17	-10	200	200	200
R	240	17	-10	200	200	200
O	120	17	+10	200	200	200
P	300	17	+10	200	200	200
T	270	17	+25	200	200	200
S	90	17	+25	200	200	200

PROJECT No. 912-2055 DRAWN CG REVIEWED KMK DATE JUNE 92

PROJECT No. 912-2055 DRAWN RR REVIEWED KMK DATE APR 92

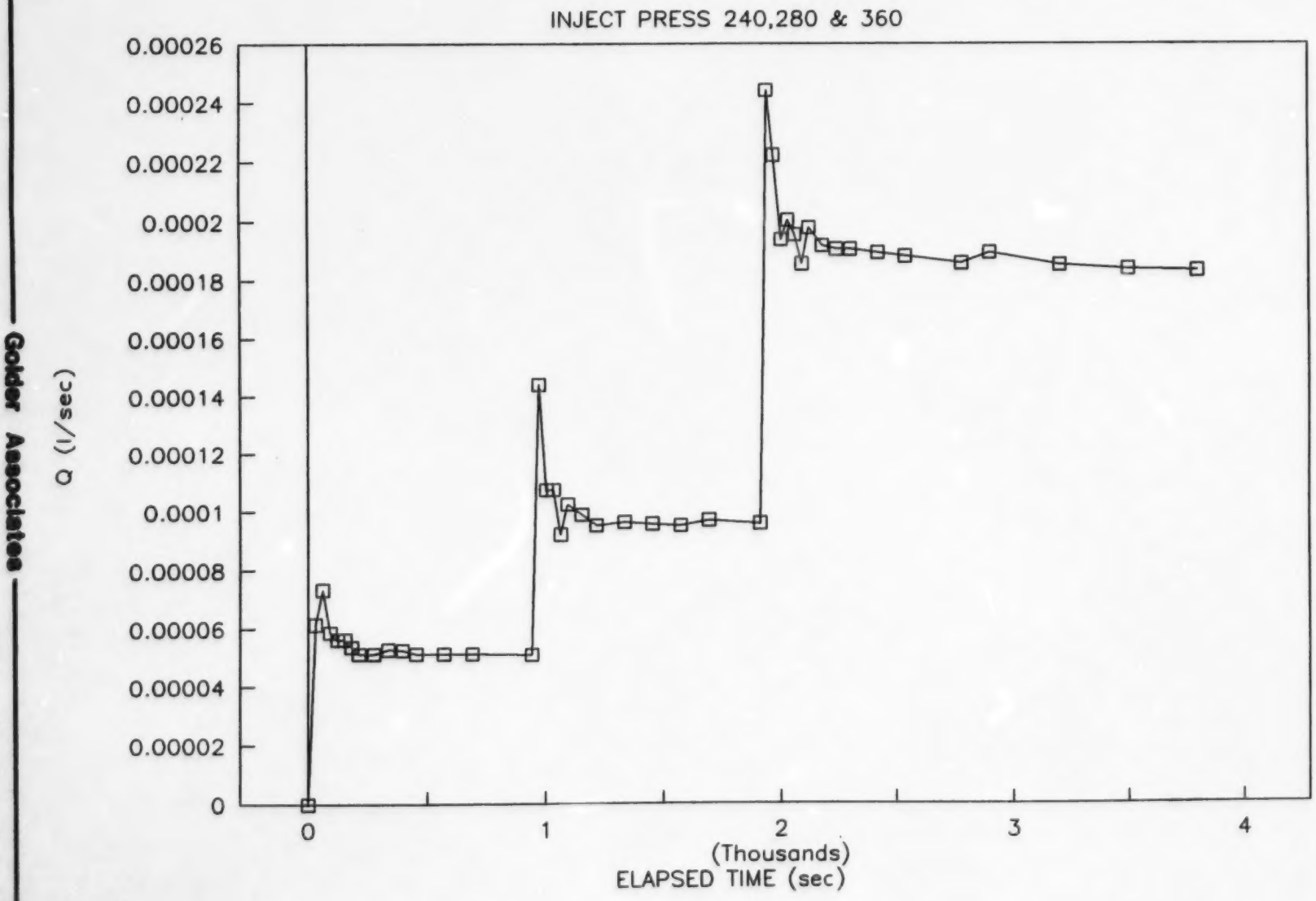

Golder Associates

FRACTURE TEST 3 - SUB-FRACTURE INJECTION - 1
q vs time

Figure II-7

PROJECT No. 912-2055 DRAWN RR REVIEWED KMK DATE APR 92

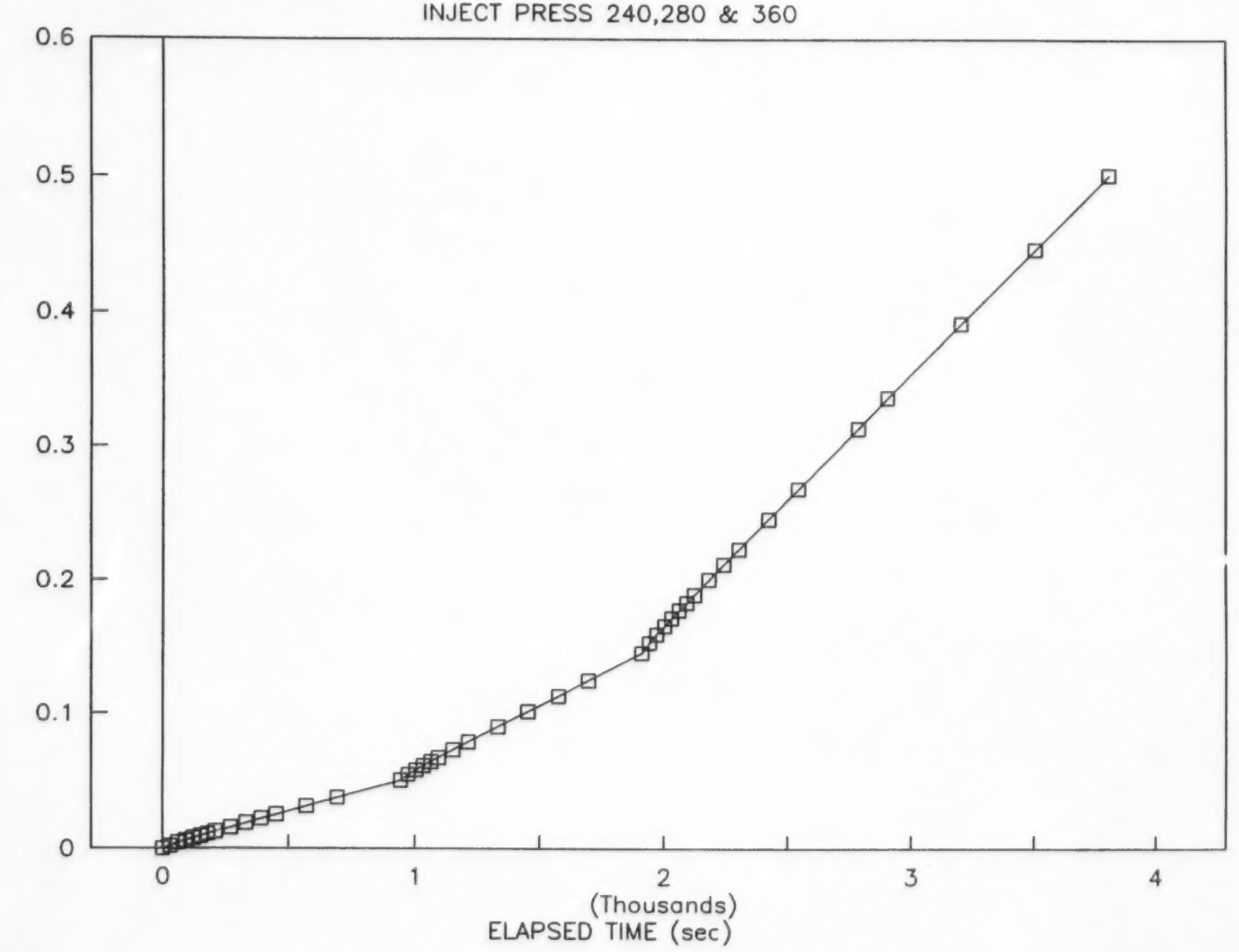

FRACTURE TEST 3 - SUB-FRACTURE INJECTION - 1
V vs time

Figure II-8

Golder Associates

PROJECT No. 912-2055 DRAWN RR REVIEWED KMK DATE APR 92

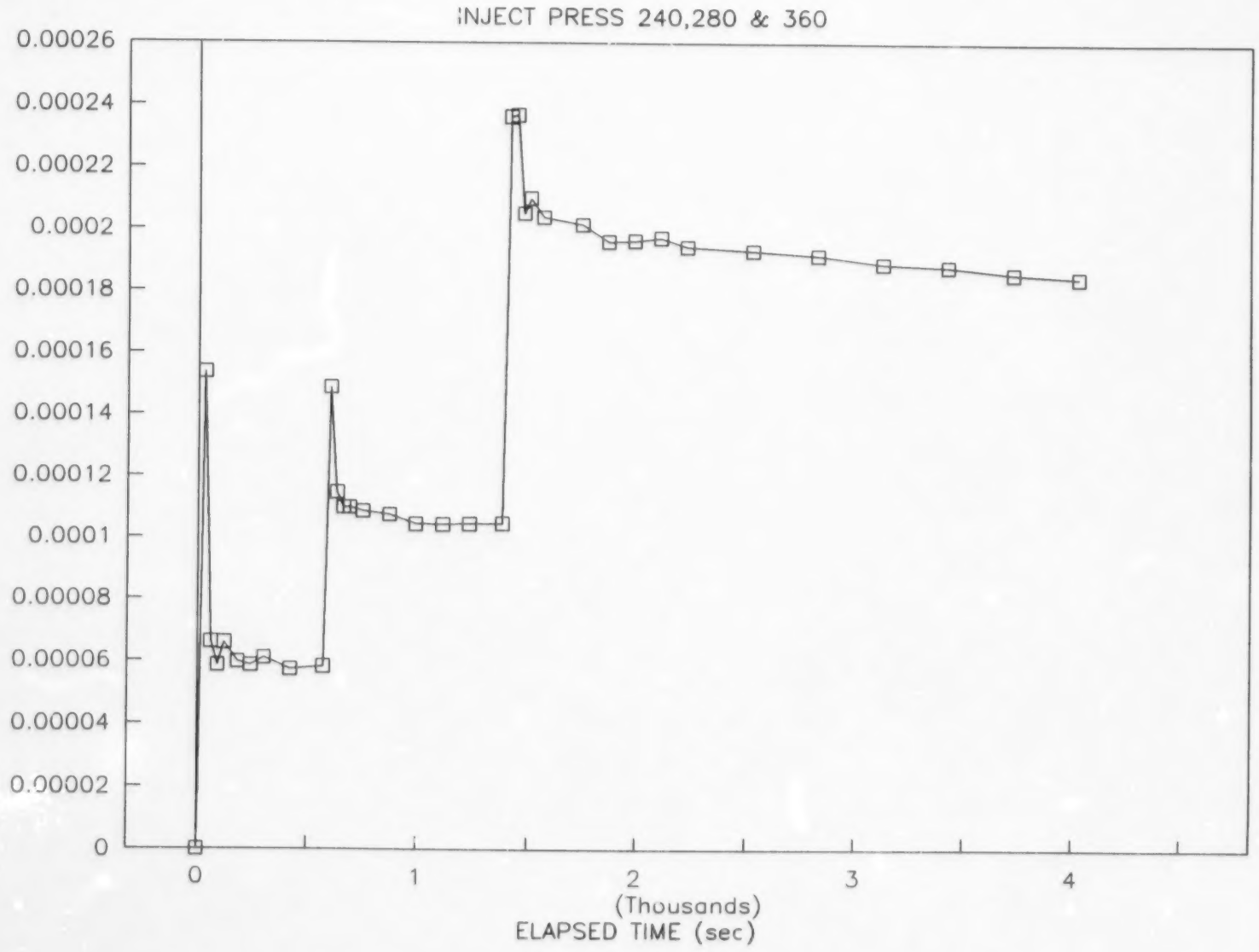

FRACTURE TEST 3 - SUB-FRACTURE INJECTION - 2
q vs time

Figure II-9

Golder Associates

PROJECT No. 912-2055 DRAWN RR REVIEWED KMK DATE APR 92

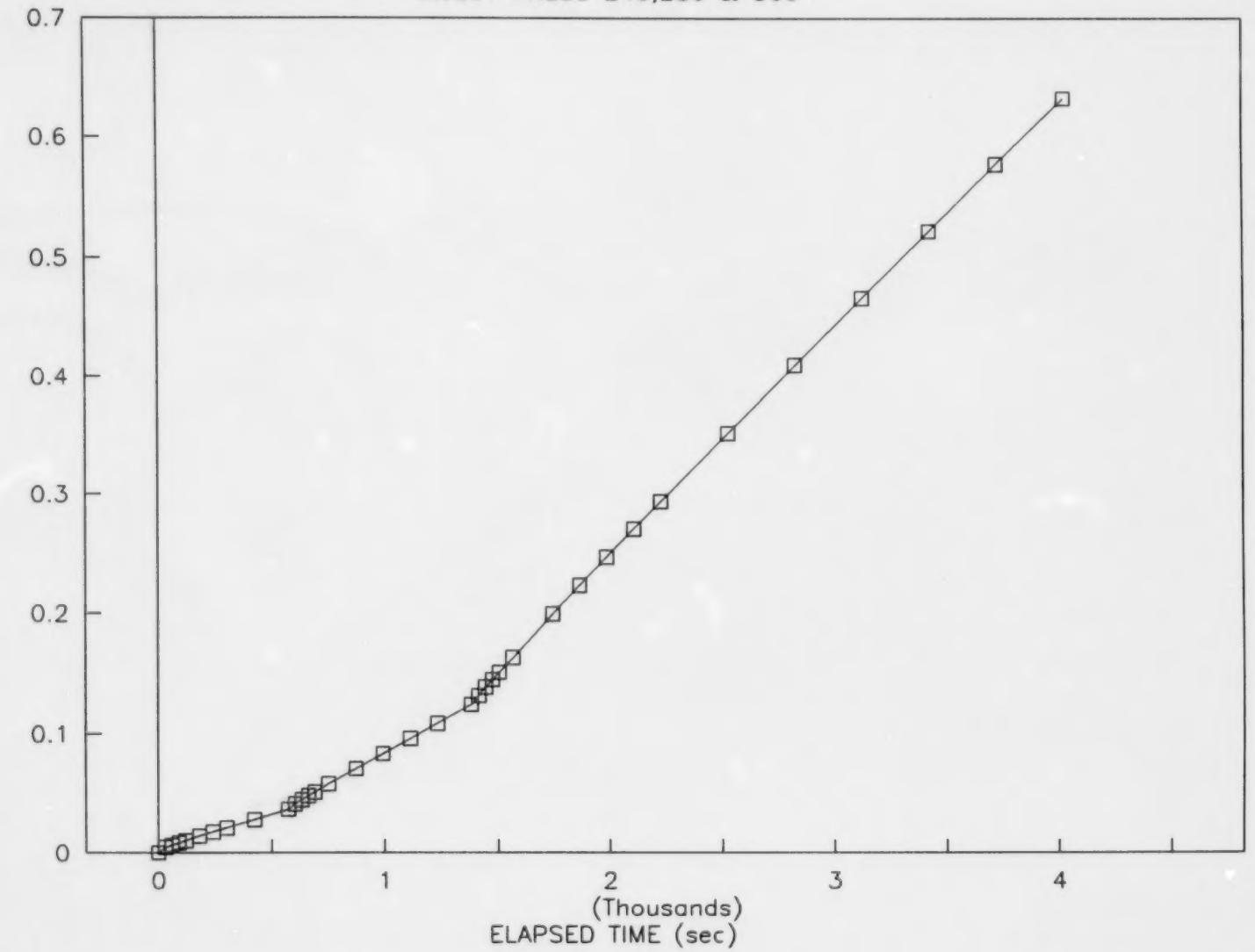

Golder Associates

FRACTURE TEST 3 - SUB-FRACTURE INJECTION - 2
V vs time

Figure II-10

FRACTURE TEST 4 - SUB-FRACTURE INJECTION PIEZOMETER READINGS

Figure II-11

Piezometer	Angle	Radius	Vertical Distance from Injection Point	Pressure (kPa)		
Applied Pressure				240	280	360
Top of Injection Well				240	280	360
Injection Point				240	280	360
Q	60	17	-10	200	200	200
R	240	17	-10	200	200	200
O	120	17	+10	200	200	200
P	300	17	+10	200	200	200
T	270	17	+25	200	200	200
S	90	17	+25	200	200	200

PROJECT No. 912-2055 DRAWN CG REVIEWED KMS DATE JUNE 92

PROJECT No. 912-2055 DRAWN RR REVIEWED KMK DATE APR 92

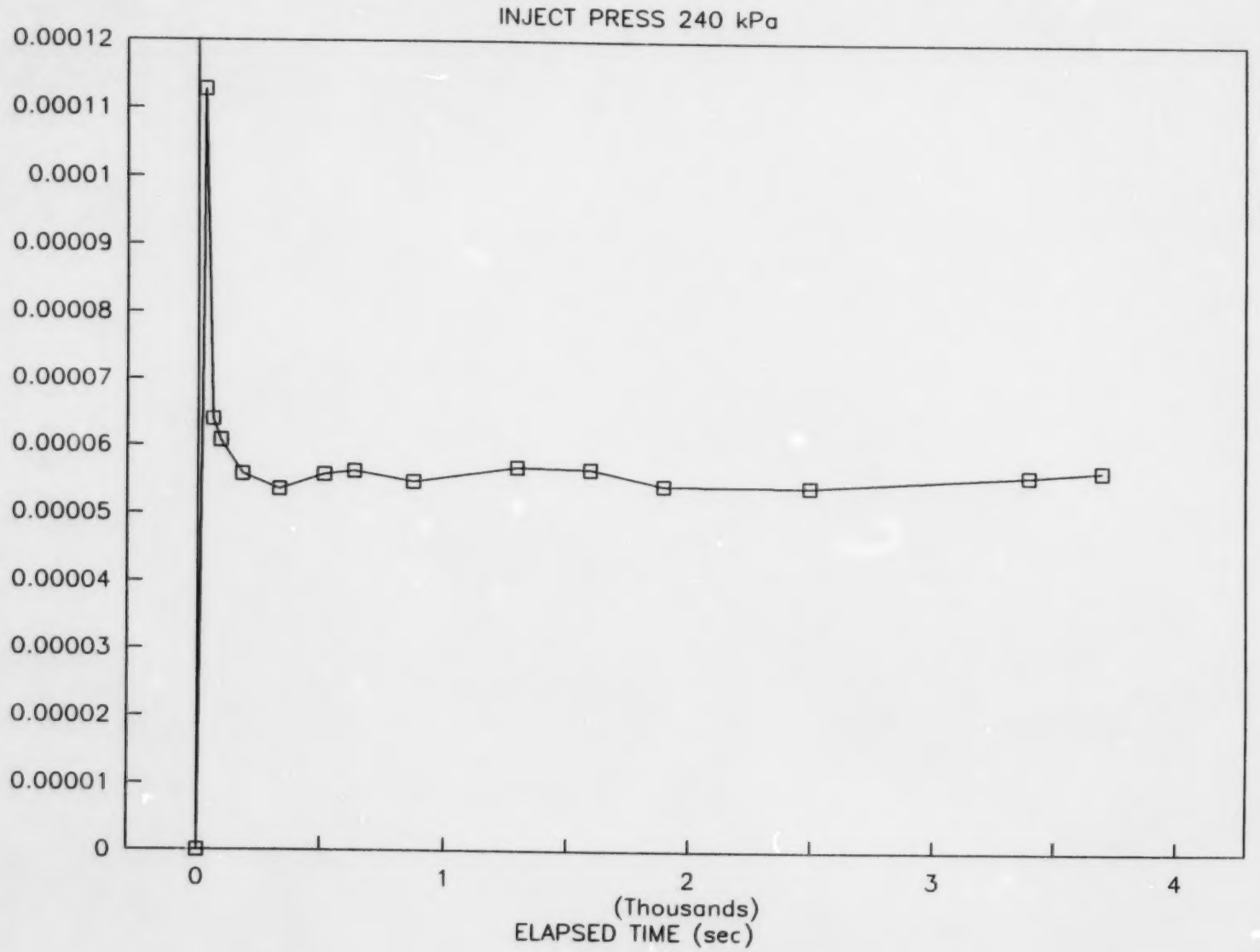

FRACTURE TEST 4 - SUB-FRACTURE INJECTION
q vs time

Figure II-12

Golder Associates

PROJECT No. 912-2055 DRAWN RR REVIEWED KMK DATE APR 92

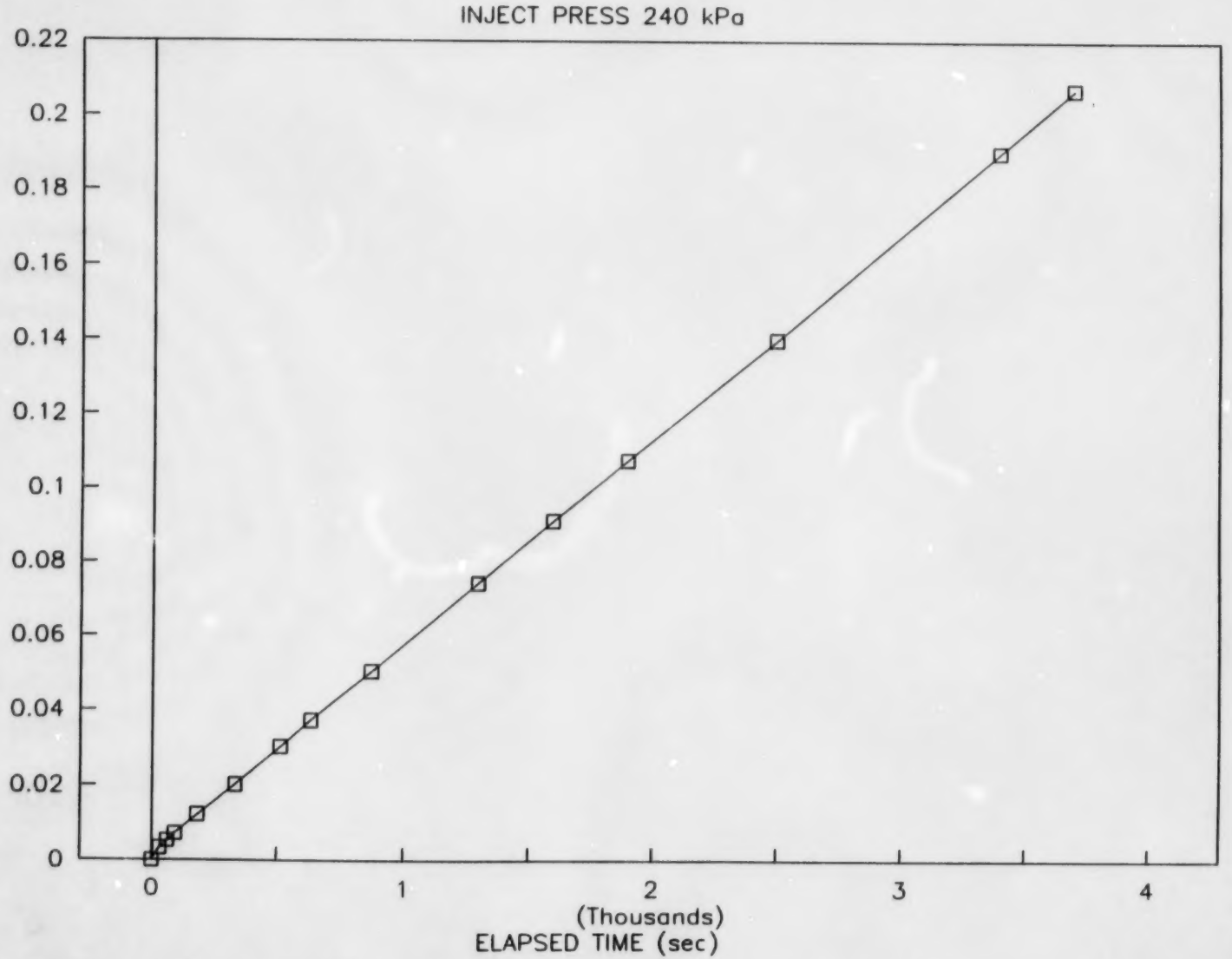

FRACTURE TEST 4 - SUB-FRACTURE INJECTION
V vs time

Figure II-13

Golder Associates

FRACTURE TEST 5 - SUB-FRACTURE INJECTION PIEZOMETER READINGS

Figure II-14

Piezometer	Angle	Radius	Vertical Distance from Injection Point	Pressure (kPa)		
Applied Pressure				240	280	360
Top of Injection Well				240	280	360
Injection Point				240	280	360
Q	60	17	-10	200	200	200
R	240	17	-10	200	200	200
O	120	17	+10	200	200	200
P	300	17	+10	200	200	200
T	270	17	+25	200	200	200
S	90	17	+25	200	200	200

PROJECT No. 912-2055 DRAWN CG REVIEWED _____ DATE JUNE 92

FRACTURE TEST 5 - SUB-FRACTURE INJECTION

q vs time

Figure II-15

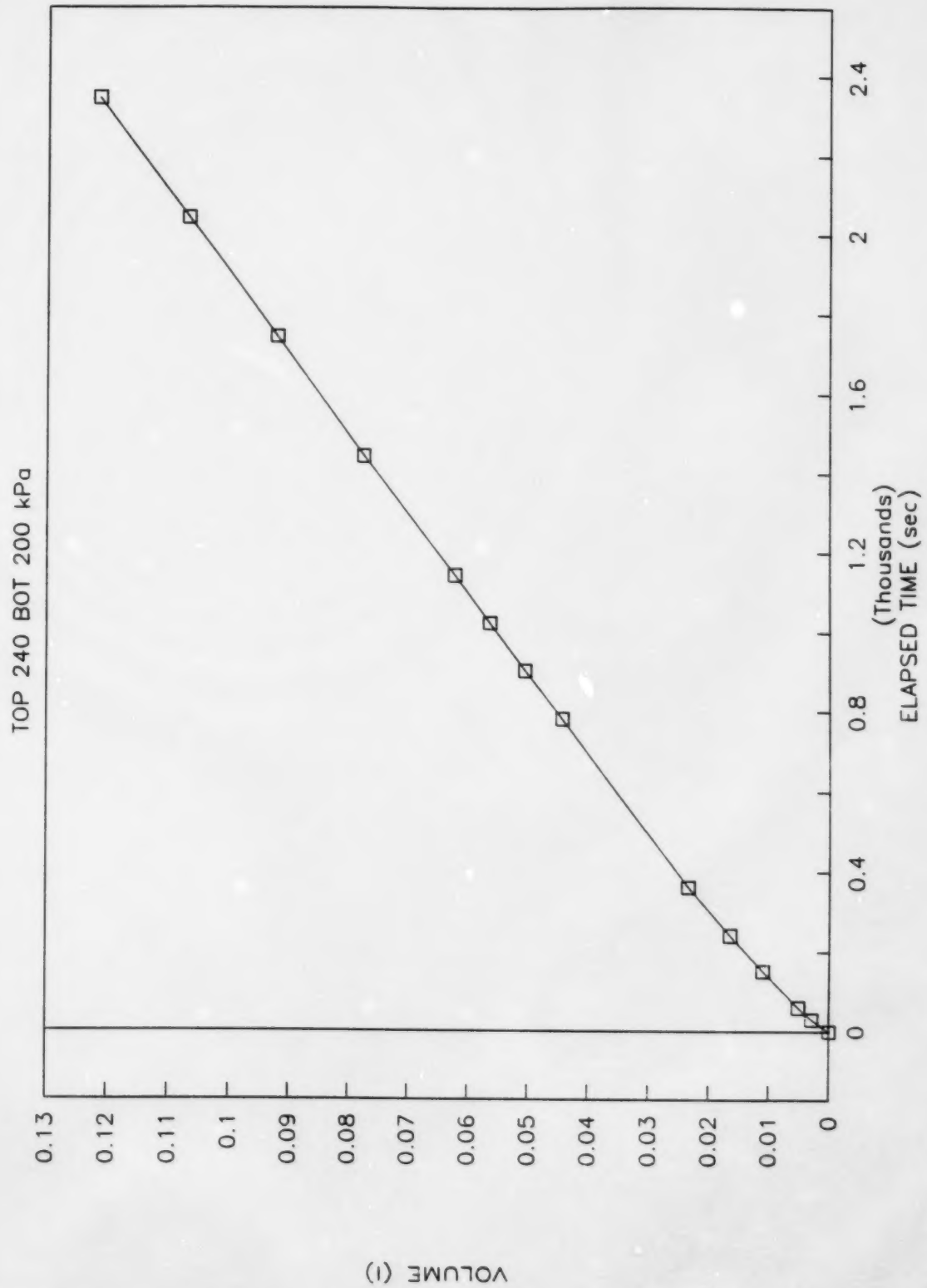

PROJECT No. 912-2055 DRAWN RR REVIEWED KMK DATE APR 92

Golder Associates

PROJECT No. 912-2055 DRAWN RR REVIEWED KMK DATE APR 92

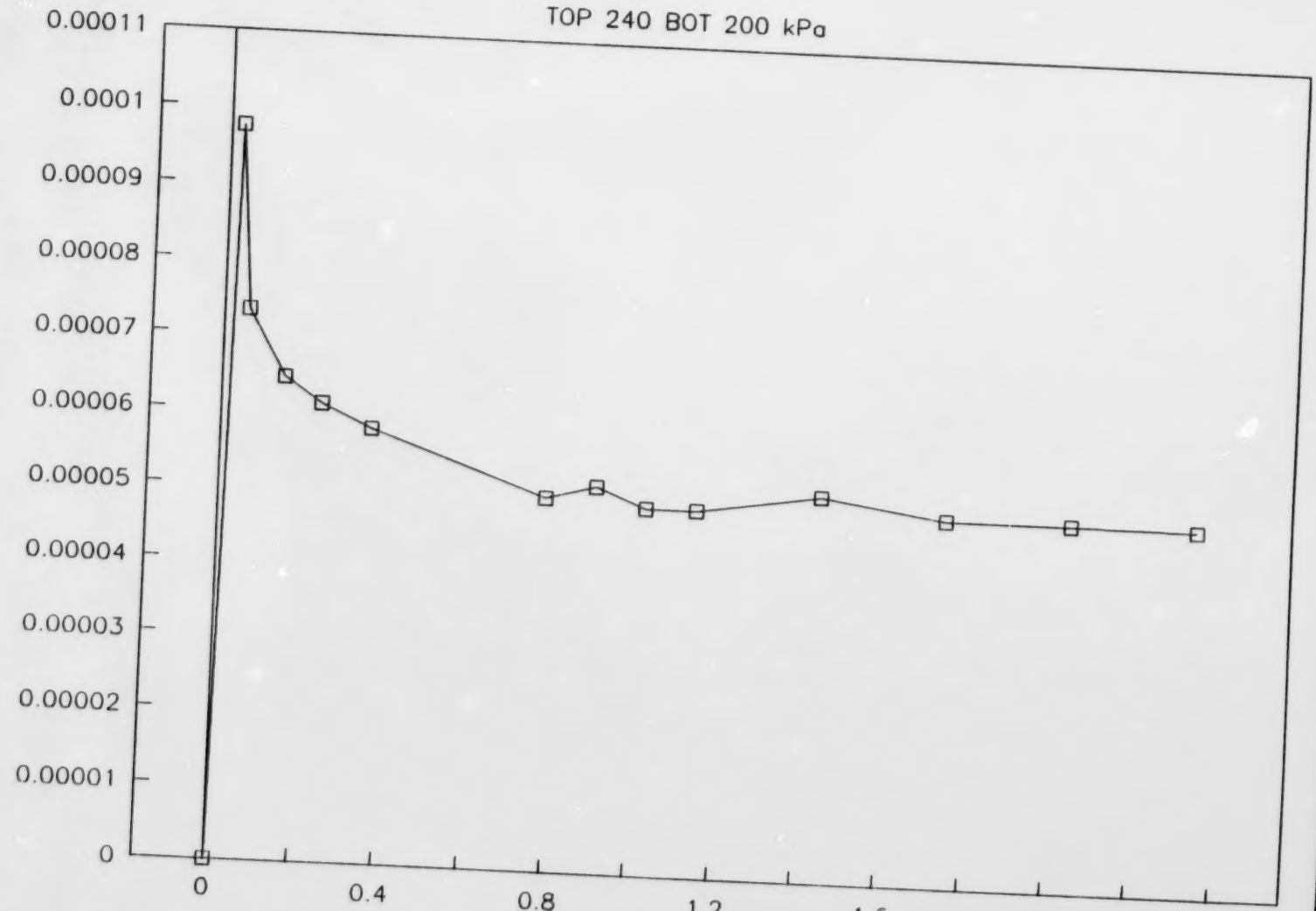

FRACTURE TEST 5 - SUB-FRACTURE INJECTION
V vs time

Figure II-16

Golder Associates

APPENDIX III

STEADY STATE FRACTURE TESTS

FRACTURE TEST 2 - STEADY STATE FRACTURE PIEZOMETRIC READINGS (INJECTION RATE = 0.28 ml/s)

Figure III-1

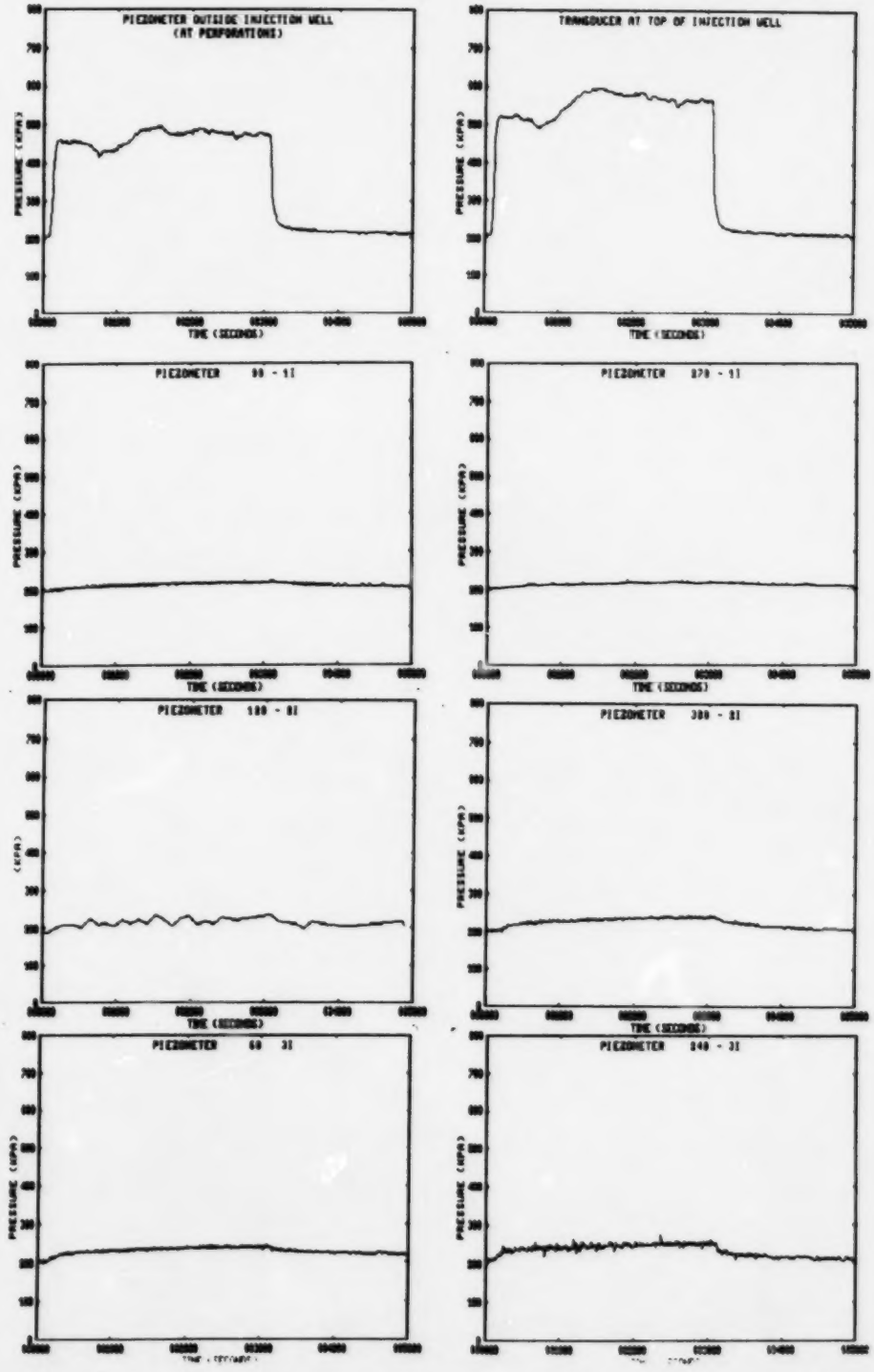
PIEZOMETER OUTSIDE INJECTION WELL (AT PERFORATIONS)
TRANSDUCER AT TOP OF INJECTION WELL
PIEZOMETER 90 - 11
PIEZOMETER 270 - 11
PIEZOMETER 180 - 81
PIEZOMETER 300 - 81
PIEZOMETER 60 - 31
PIEZOMETER 240 - 31
PRESSURE (KPA)
TIME (SECONDS)

PROJECT No. 912-2055 DRAWN RR REVIEWED KMK DATE APR 92

FRACTURE TEST 2 - STEADY STATE FRACTURE PIEZOMETRIC READINGS (INJECTION RATE = 0.40 ml/s)

Figure III-2

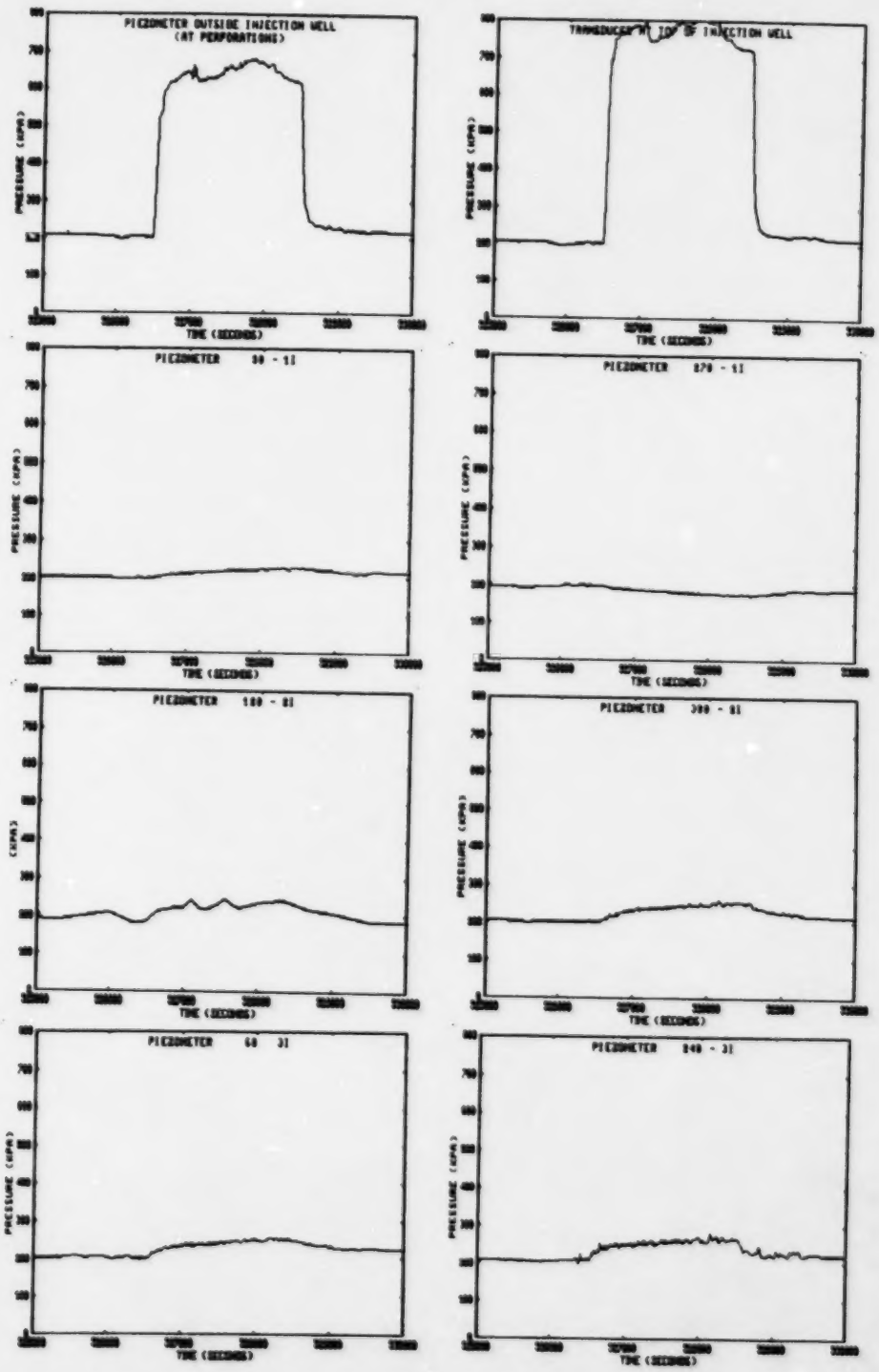

PROJECT No. 912-2055 DRAWN RR REVIEWED KnK DATE APR 92

FRACTURE TEST 2 - STEADY STATE FRACTURE PIEZOMETRIC READINGS (INJECTION RATE = 1.00 ml/s)

Figure III-3

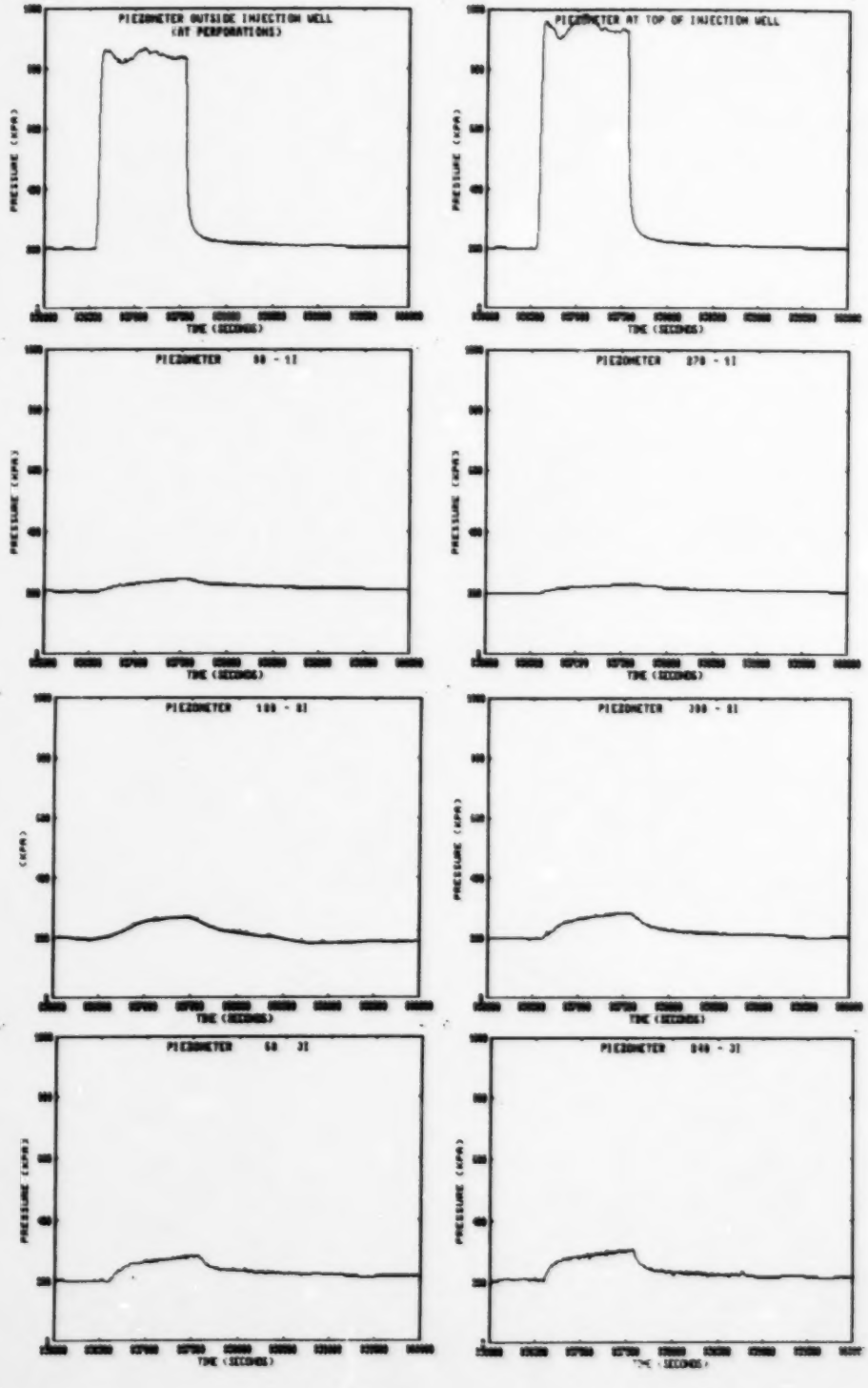
PIEZOMETER OUTSIDE INJECTION WELL (AT PERFORATIONS)
PIEZOMETER AT TOP OF INJECTION WELL
PIEZOMETER 90 - 1I
PIEZOMETER 270 - 1I
PIEZOMETER 180 - 8I
PIEZOMETER 300 - 8I
PIEZOMETER 60 - 3I
PIEZOMETER 840 - 3I
PRESSURE (KPA)
TIME (SECONDS)

PROJECT No. 912-2055 DRAWN RR REVIEWED KMK DATE APR 92

FRACTURE TEST 2 - STEADY STATE FRACTURE PIEZOMETRIC READINGS (INJECTION RATE = 0.25 ml/s)

Figure III-4

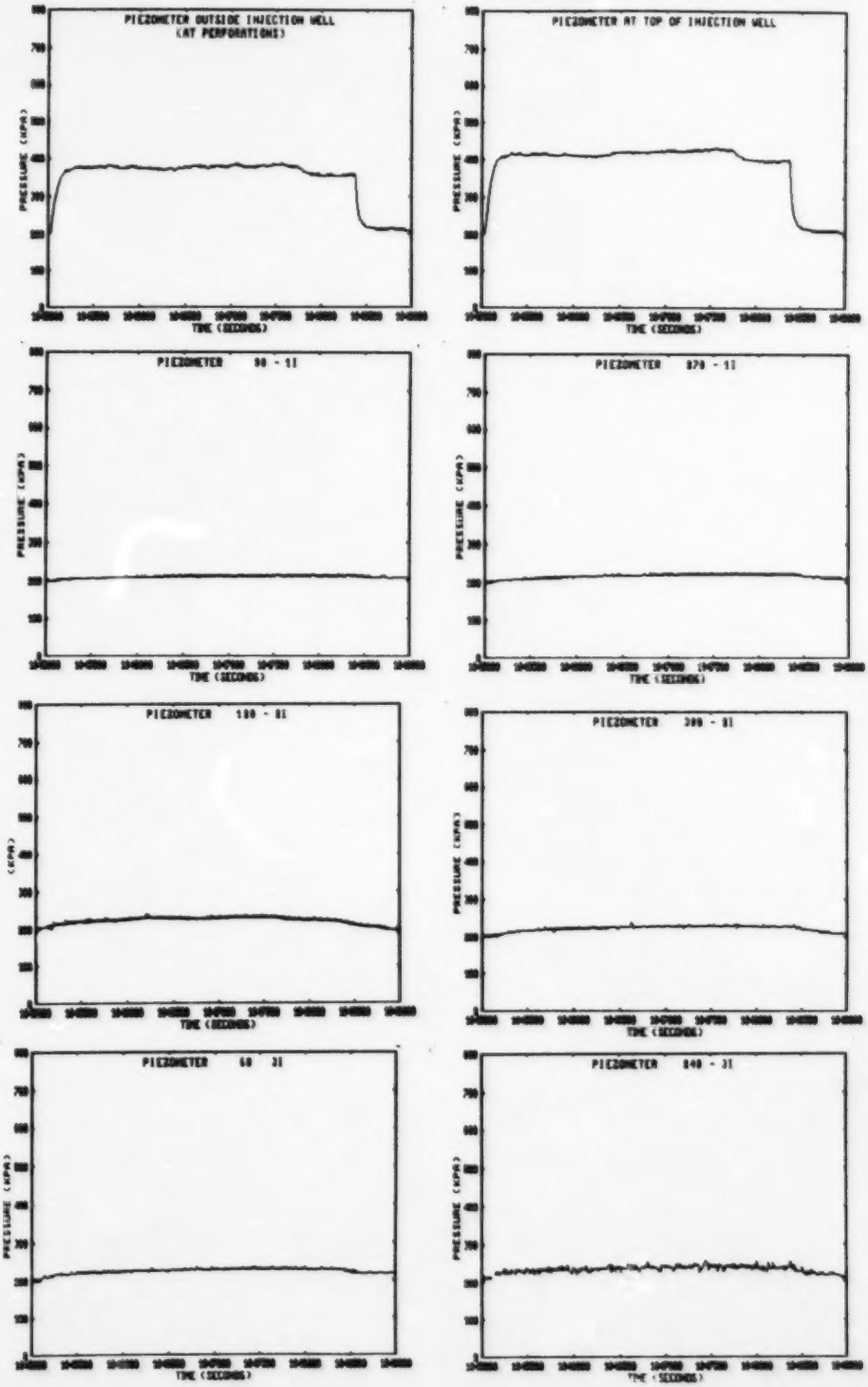

PROJECT No. 912-2055 DRAWN RR REVIEWED KMK DATE APR 92

FRACTURE TEST 3 - STEADY STATE FRACTURE PIEZOMETRIC READINGS (INJECTION RATE = 1.00 ml/s)

Figure III-5

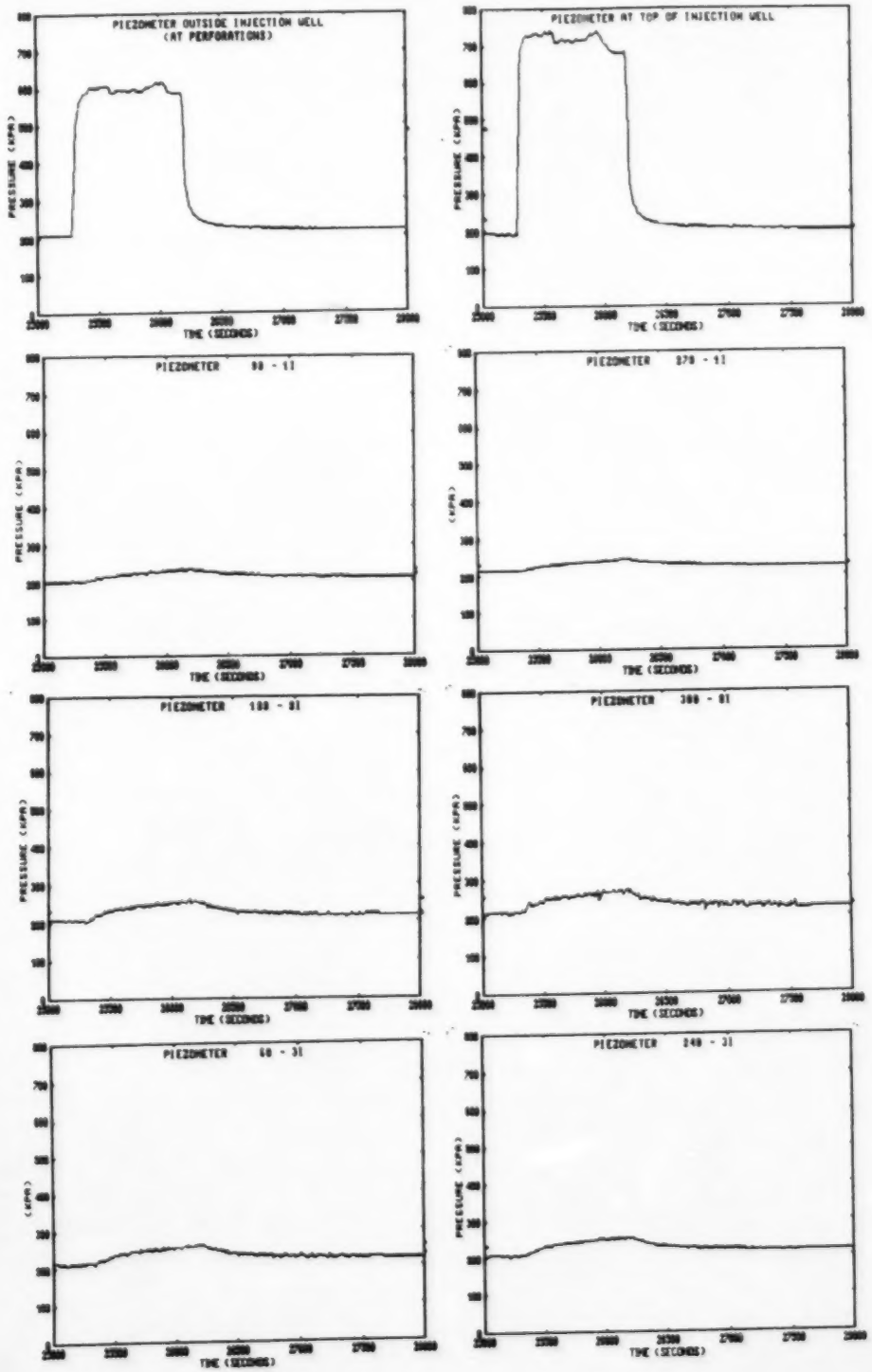
PIEZOMETER OUTSIDE INJECTION WELL (AT PERFORATIONS)
PIEZOMETER AT TOP OF INJECTION WELL
PIEZOMETER 90 - 11
PIEZOMETER 370 - 11
PIEZOMETER 180 - 01
PIEZOMETER 360 - 01
PIEZOMETER 60 - 31
PIEZOMETER 240 - 31
PRESSURE (KPA)
TIME (SECONDS)

PROJECT No. 912-2055 DRAWN RR REVIEWED KHK DATE APR 92

FRACTURE TEST 3 - STEADY STATE FRACTURE PIEZOMETRIC READINGS (INJECTION RATE = 3.0, 10.0, 30.0 and 3.0 ml/s)

Figure III-6

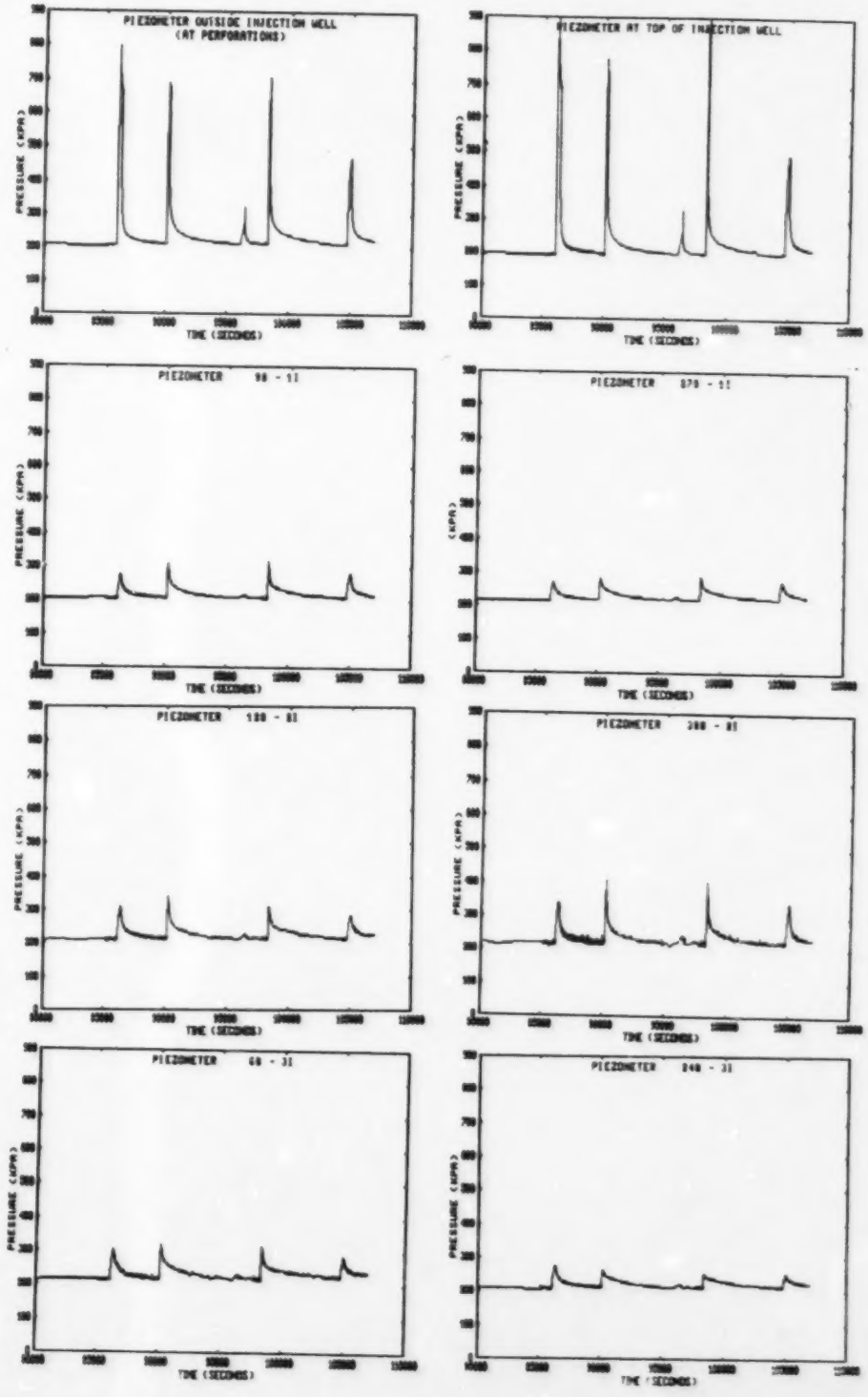
PIEZOMETER OUTSIDE INJECTION WELL (AT PERFORATIONS)
PIEZOMETER AT TOP OF INJECTION WELL
PIEZOMETER 90 - 11
PIEZOMETER 270 - 11
PIEZOMETER 180 - 81
PIEZOMETER 360 - 81
PIEZOMETER 60 - 31
PIEZOMETER 240 - 31
PRESSURE (KPA)
TIME (SECONDS)

PROJECT No. 912-2055 DRAWN RR REVIEWED KHK DATE APR 92

APPENDIX IV

DATA FILE USED IN NUMERICAL SIMULATION

APPENDIX IV

DATA FILE USED IN NUMERICAL SIMULATION

```
*Filename=frac4a.dat
*bring stresses to equilibrium under anisotropic *consolidation
*use axisymmetric + groundwater flow condition
config axi gwflow
grid 50
*strain softening model is used
model ss
*generate outside dimensions of the grid
gen 0.01675,0.01675,1 0.66825,1 0.66825,0
*move the grid so that the injection point is
* 5 cm high
ini y=0.475 i=1,2 j=25
ini y=0.525 i=1,2 j=27
*fix centerline and bottom boundary from movement
fix x i=1 j=1,51
fix y i=1,51 j=1
*apply boundary stresses to sample
apply syy=-400000 j=51
apply sxx=-600000 i=51
ini pp=200000
fix pp
*free drainage boundary at top and bottom boundary
ini pp 0 i=1,51 j=51
fix pp i=1,51 j=51
ini pp 0 i=1,51 j=1
fix pp i=1,51 j=1
ini sat=1
*assign total stresses to all the zones
ini sxx=-600000
ini syy=-400000
*properties of the oil sand
prop den=1485 bulk=27368667 shear=16421200 fric=38
prop coh=0 ten=0 dil=30 ftab=1 dtab=2
table 1 0,38 0.01,30
table 2 0,30 0.01,5
prop por=0.48 perm=3.066e-12
*properties of the glycerin
water den=1330 bulk=333333333
set large
hist
unbal
```

APPENDIX IV (Cont'd)

DATA FILE USED IN NUMERICAL SIMULATION

```
hist gwtime
hist ydisp i=1 j=51
hist ydisp i=25 j=51
hist ydisp i=51 j=51
hist xdisp i=51 j=51
hist xdisp i=51 j=25
hist xdisp i=51 j=1
*monitor pore pressures at various locations
hist pp i=13 j=35
hist pp i=13 j=28
hist pp i=13 j=26
hist pp i=13 j=18
*pore pressure in front of injection point
hist pp i=2 j=26
hist pp i=2 j=29
hist pp i=2 j=23
hist pp i=4 j=26
*pore pressure at the injection point
hist pp i=1 j=25
hist pp i=1 j=26
hist pp i=1 j=27
hist pp i=2 j=25
hist pp i=2 j=27
*pore pressure at level 1 (1/4 radius from center)
hist pp i=13 j=39
*pore pressure at level 2 (1/4 radius from center)
hist pp i=13 j=31
*pore pressure at level 3 (1/4 radius from center)
hist pp i=13 j=21
*set clock time limits to 5000 min
set clock=5000
*set out-of-balance force limit to 80 N
set force=80
*set maximum step to 1000000
set step=1000000
set nmech=1
set ngw=1
*now consolidate the sample and monitor the
*unbalanced nodal force and displacements at the
*boundary
step 3000
```

APPENDIX IV (Cont'd)

DATA FILE USED IN NUMERICAL SIMULATION

```
*save file after consolidation
save frac4a.sav
*reset all displacements to zero before turning
*the flow on at the injection point
ini xdisp=0 ydisp=0
free pp
ini pp 0 i=1,51 j=51
fix pp i=1,51 j=51
ini pp 0 i=1,51 j=1
fix pp i=1,51 j=1
*apply constant flow (in m/s) to the injection point
apply discharge=5.7e-3 i=1 j=25,27
set nmech=200
*step 443 (equivalent to 8.33 sec of flow into the sample)
*each flow step is about 0.0188 sec
step 443
save frac4b.sav
*stop the flow into the sample
apply discharge=0 i=1 j=25,27
set nmech=1
*step 1200 (equivalent to 11.52 sec after flow is stopped)
*each flow step is about 0.0096 sec

*total time = 8.33+11.52 = 19.85 sec
step 1200
save frac4c.sav
*continue monitor pore pressure dissipation
*step 1200 (equivalent to 13.20 sec after last step)
*each flow step is about 0.011 sec
*total time = 19.85+13.20 = 33.05 sec
step 1200
save frac4d.sav
*end of data file
```